UNIVERSITEIT VAN PRETORIA
UNIVERSITY OF PRETORIA
YUNIBESITHI YA PRETORIA

In vitro influence of nutrient deprivation and papaverine exposure in MCF-7 and MDA-MB-231 breast cancer cell lines

by

Michael Christopher Stark

Dissertation submitted in fulfilment of the requirements for the degree

Master of Science

in

Human Physiology

Department of Physiology

School of Medicine

Faculty of Health Sciences,

University of Pretoria

Supervisor: Dr M.H. Visagie (University of Pretoria)

Co-supervisor: Prof Y. Lee (Harvard Medical School)

Co-supervisor and Head of Department: Prof A.M. Joubert (University of Pretoria)

February 2025

Abstract

Breast cancer treatment in South Africa is constrained by limited access to affordable targeted therapies, highlighting the urgent need for cost-effective solutions within the public health sector. Fasting, a free and accessible intervention, shows promise in reducing tumorigenic metabolism and chemotherapy side effects; however, the efficacy is frequently reduced by metabolic plasticity, where metabolic activity shifts from glycolysis to oxidative phosphorylation (OXPHOS) in order to resist nutrient deprivation (ND). Various studies have demonstrated that nutrient-deprived breast tumorigenic cells exhibit increased dependence on OXPHOS for optimal proliferation through augmented mitochondrial complex I expression, highlighting a notable metabolic vulnerability that could potentially be targeted by combining fasting with a mitochondrial complex I inhibitor. Papaverine (PPV), a repurposed mitochondrial complex I inhibitor, was selected for this study due to its low cost, established safety, and accessibility in South Africa. However, the combination of physiological ND and PPV remains to be elucidated. Thus, the aim of this study was to investigate the combined effects of fasting-mimetic glucose and glutamine deprivation and PPV exposure, on proliferation, morphology, cell cycle progression, oxidative stress, superoxide dismutase (SOD) activity, mitochondrial membrane potential ($\Delta\Psi M$), and the activity of 5′ adenosine monophosphate–activated protein kinase (AMPK) and mammalian target of rapamycin (mTOR) in metabolically distinct breast tumorigenic cells. This study used two breast cancer cell lines: OXPHOS-dependent MCF-7 (luminal, hormone receptor–positive) and glycolysis-dependent MDA-MB-231 (basal, triple-negative). The results obtained demonstrate that ND significantly enhanced the antiproliferative effects of PPV in both MCF-7 and MDA-MB-231 cells. Neither PPV nor ND alone significantly inhibited cell proliferation, indicating that ND sensitizes tumorigenic cells to PPV-mediated mitochondrial complex I inhibition. Morphologically, exposure to ND and PPV significantly increased the number of cells exhibiting enlarged morphology and cell protrusions. Furthermore, cell cycle analysis revealed that exposure to ND and PPV did not affect cell cycle progression but did alter reactive oxygen species (ROS) generation, specifically reducing superoxide (O_2^-) generation and increasing hydrogen peroxide (H_2O_2) production, potentially independent of SOD activity. Assessment of $\Delta\Psi M$ revealed cell line–specific responses to ND and PPV exposure, with significant depolarization observed in MCF-7 cells and hyperpolarization in MDA-MB-231 cells. Moreover, in MDA-MB-231 cells, ND and PPV exposure led to the activation of AMPK and the inhibition of mTORC1. These findings suggest that combining ND and PPV targets critical biochemical pathways and molecular markers in breast tumorigenic cells, offering a potentially cost-effective and accessible therapeutic approach for resource-limited settings while aligning with Sustainable Development Goal 3 to promote global health and well-being. Although the combination of fasting and PPV shows promise, further *in vivo* preclinical research is required.

Keywords: breast cancer, fasting, metabolic plasticity, mitochondrial complex I, papaverine

Table of contents

List of abbreviations

4EBP	Eukaryote initiation factor 4E-binding protein
α-KG	α-ketoglutarate
AKAP1	A-kinase anchoring protein 1
AKT	Protein kinase B
AMP	Adenosine monophosphate
AMPK	5' Adenosine monophosphate protein-activated kinase
AMPKα1	AMP-activated catalytic subunit alpha 1
p-AMPKα1	Phosphorylated-AMP-activated catalytic subunit alpha 1
ANOVA	Analysis of variance
ASCT2	Alanine-serine-cysteine transporter subtype 2
ASR	Age standardized rate
ATG	Autophagy-related protein
ATP	Adenosine triphosphate
BSA	Bovine serum albumin
CCCP	Carbonyl cyanide *m*-chlorophenylhydrazone
CI	Confidence intervals
CS	Citrate synthase
CTR	Control complete growth medium
DCF	2,7-dichlorofluorescein
DCFDA	2,7-dichlorofluoresceindiacetate
df	Degrees of freedom
DHE	Dihydroethidium
DMEM	Dulbecco's minimum essential medium
DMSO	Dimethyl sulfoxide
DNA	Deoxyribonucleic acid
DRP1	Dynamin-related protein 1
DSR	Differential stress resistance
DSS	Differential stress sensitization
EAA	Essential amino acid
ELISA	Enzyme-linked immunosorbent assay
ER	Estrogen receptor
ETC	Electron transport chain
$FADH_2$	Dihydroflavin-adenine dinucleotide

FCS	Fetal calf serum
FDA	Food and Drug Administration
FITC	Fluorescein isothiocyanate
Fru-2,6-P_2	Fructose-2,6-bisphosphatase
GAP	GTPase-activating protein
GCL	Glutamate-cysteine ligase
GDH	Glutamate dehydrogenase
GLS1	Kidney-type glutaminase
GLS2	Liver-type glutaminase
GLUT	Glucose transporter
GSH	Glutathione
GSS	Glutathione synthetase
GTP	Guanosine-5'-triphosphate
HER2	Human epidermal growth factor receptor-2
HIF	Hypoxia-inducible factor
HK	Hexokinase
HRP	Horseradish peroxidase
IC_{50}	Half-maximal inhibitory concentration
IGF-1	Insulin-like growth factor 1
IGF-1R	Insulin-like growth factor 1 receptor
JC-1	5’,6,6’-Tetrachloro-1,1’,3,3’-tetraethylbenzimidazolylcarbocyanine
LDH	Lactate dehydrogenase
LKB1	Liver kinase B1
LMICs	Low- and middle-income countries
MAPK	Mitogen-activated protein kinase
MCF-7	Michigan cancer foundation-7
MCT	Monocarboxylate transporter
MDA-MB-231	M.D. Anderson metastatic breast cancer-231
mTOR	Mammalian target of rapamycin
mTORC1	Mammalian target of rapamycin complex 1
p-mTORC1	Phosphorylated-mammalian target of rapamycin complex 1
mTORC2	Mammalian target of rapamycin complex 2
MYC	Myelocytomatosis proto-oncogene
NAD	Nicotinamide adenine dinucleotide
NADPH	Nicotinamide adenine dinucleotide phosphate hydrogen

NADH	Nicotinamide adenine dinucleotide hydrogen
NEAA	Nonessential amino acid
NHF	Non-tumorigenic human fibroblast
ND	Nutrient deprivation
ND1	Nutrient deprivation medium 1
ND2	Nutrient deprivation medium 2
OXPHOS	Oxidative phosphorylation
PBS	Phosphate-buffered saline
PDE-10A	Phosphodiesterase-10A
PDH	Pyruvate dehydrogenase
PE	Phycoerythrin
PDK	3-Phosphoinositide-dependent protein kinase
PFK-1	Phosphofructokinase-1
PGI	Phosphoglucose isomerase
PI3K	Phosphoinositide 3-kinase
PIKK	PI3K family-related protein kinase
PIP2	Phosphatidylinositol-3,4-bisphosphate
PIP3	Phosphatidylinositol-3,4,5-triphosphate
PlasDIC	Polarization-optical transmitted light differential interference contrast
PKM2	Pyruvate kinase M2
PPP	Pentose phosphate pathway
PPV	Papaverine
PR	Progesterone receptor
PTEN	Phosphatase and tensin homologue
Ras	Rat sarcoma
Raf	Rapidly accelerated fibrosarcoma
Raptor	Regulatory-associated protein of mTOR
Rheb	Ras homology enriched in brain
RNA	Ribonucleic acid
RNAi	RNA interference
RNAse A	Ribonuclease A
ROS	Reactive oxygen species
RT	Room temperature
S473	Serine residue 473
S487	Serine residue 487

S1345	Serine residue 1345
S2448	Serine residue 2448
S6K1	Ribosomal protein S6 kinase 1
S939	Serine residue 939
SA	South Africa
SAHPRA	South African Health Products Regulatory Authority
SDS	Sodium dodecyl sulphate
SLC7A11	Solute carrier family 7 member 11
SOD	Superoxide dismutase
T172	Threonine residue 172
T308	Threonine residue 308
T1227	Threonine residue 1227
T1462	Threonine residue 1462
TCA	Tricarboxylic acid
TF	Transcription factor
TIGAR	TP53-induced glycolysis and apoptosis regulator
TMB	3,3',5,5'-tetramethylbenzidine
TSC2	Tuberous sclerosis complex 2
ULK1	Uncoordinated-51-like kinase 1
USA	United States of America
VT	Vehicle-treated
WHO	World Health Organization
xCT	Cystine/glutamate antiporter
XO	Xanthine oxidase

List of figures

List of tables

1. Background

Cancer is one of the leading causes of mortality worldwide, accounting for 9.7 million deaths annually (1). Approximately 70% of these cancer-related deaths occur in low- and middle-income countries (LMICs), with the highest percentage reported in sub-Saharan Africa (2). This stark disparity underscores the significant differences in cancer outcomes between high-income regions and LMICs (2). For instance, clear contrasts exist between South Africa (SA) and the United States of America (USA), where breast-, prostate-, and lung cancer account for the highest incidence and mortality age-standardized rates (ASR) in each country's population (**Figure 1A**) (1,3). Global Cancer Observatory analyses reveal a two-fold higher incidence ASR in the USA compared to SA, but the mortality ASR is higher in SA, with a 2.8-fold greater mortality-to-incidence ASR ratio compared to the USA (**Figure 1B and 1C**) (1).

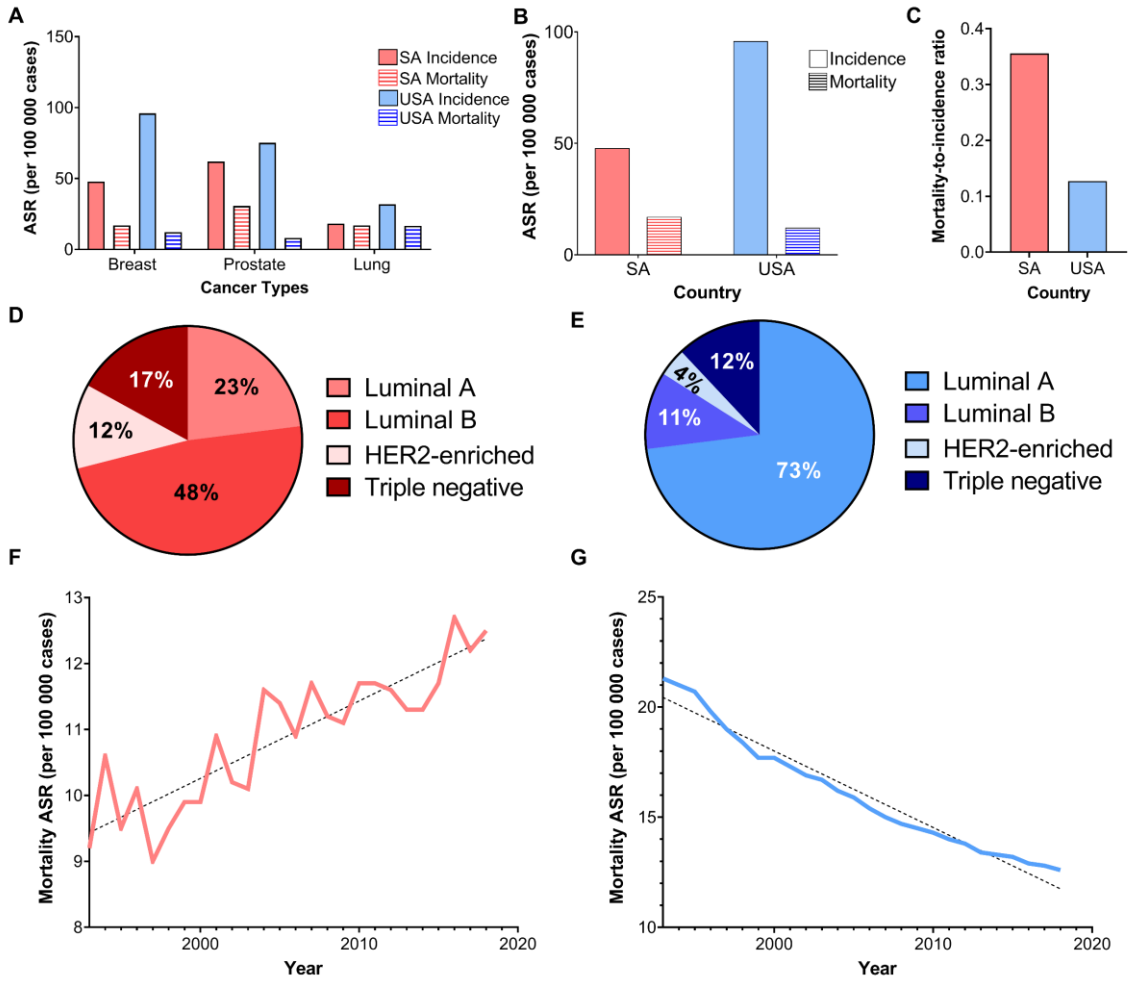

Figure 1. *Breast cancer statistics for SA and the USA were obtained from the Global Cancer Observatory database (Lyon, France) (1,3). (A) Incidence and mortality ASR (world) for breast, prostate, and lung cancer per 100,000 individuals (ages 0-85+) in 2022. (B) Breast cancer incidence and mortality ASR (world) per 100,000 individuals in 2022. (C) Mortality-to-incidence ASR ratio for breast cancer in 2022. Subtype distribution in SA (D) and the USA (E). Mortality ASR (world) trends in SA (F) and the USA (G) from 1993 to 2018. Charts created by MC Stark using GraphPad Prism 8 (GraphPad Software, San Diego, CA, USA).*

Recent studies by the World Health Organization (WHO) have revealed notable differences in breast cancer outcomes between SA and the USA (4). In SA, the five-year survival rate for breast cancer is 40%, compared to 90% in the USA, highlighting significant inequalities in healthcare access and differences in the prevalence of breast cancer subtypes (4). However, not only does limited access to healthcare contribute to the high mortality rate in South Africa, but another important factor to consider is that breast cancer patients in South Africa are often diagnosed at a more advanced stage, which likely contributes to the higher mortality rates (4). Breast cancer intrinsic subtypes are biologically distinct entities, characterized by specific gene expression patterns of the estrogen receptor (ER), progesterone receptor (PR) and human epidermal growth factor receptor-2 (HER2) (5–7). The most widely accepted subtypes are luminal A, luminal B, HER2-enriched, and basal-like. The luminal A breast cancer types are ER+, and/or PR+ and HER2-, the luminal B breast cancer types are ER+, and/or PR+ and HER2 (+/-), HER2-enriched are ER-, PR- and HER2+, and the basal-like or triple negative breast cancer (TNBC) are ER-, PR- and HER2- (6,7). The prevalence of breast cancer subtypes differ substantially between SA and the USA, where the most prevalent breast cancer subtype is luminal B (48% of all breast cancer diagnoses) in SA and luminal A (73% of all breast cancer diagnoses) in USA (**Figure 1D and 1E**) (8,9). In addition, SA has a higher relative prevalence of TNBC and HER2-enriched subtypes compared to the USA, accounting for 17% and 12% of all breast cancer diagnoses in SA, respectively (8,9).

While significant advancements have been made in the screening and diagnosis of breast cancer in SA, the accessibility to targeted therapeutics with high clinical efficacy is severely limited, consequently culminating in poor survival rates of breast cancer patients (2). The prohibitively high cost of these therapies results in a significant socioeconomic burden to uninsured breast cancer patients (2). Within SA, approximately 16% of the population is insured and has access to the private healthcare system providing patients with ground-breaking breast cancer therapies (10,11). Thus, more than 84% of the South African population (40 million people) are dependent on conventional chemotherapies (e.g., doxorubicin, paclitaxel, and cyclophosphamide), which often have negative side effects, including alopecia, neutropenia, and gastrointestinal disturbances due to their lack of selectivity for breast tumorigenic cells (11,12). Despite commendable efforts by governmental agencies and the South African Health Products Regulatory Authority (SAHPRA) to improve the financial accessibility of therapies, health insurance schemes have continued to fall short in reaching the intended population over the past 20 years (13). The increase in uninsured patients in SA highlights a potential attributor to the major increase in breast cancer mortality rates observed in SA within the last 20 years (**Figure 1F**). Conversely, in the USA, where more than 92% of the population possesses medical insurance, there has been a significant decrease in breast cancer mortality rates, potentially owing to the increased accessibility of targeted breast cancer therapeutics (**Figure 1G**) (14). Thus, there is an urgent unmet need for low-cost integrative therapies, which minimize side effects and can be simply integrated into the current breast cancer treatment arsenal in SA.

1.1. Metabolic reprogramming and metabolic inhibitors for cancer therapy

The ability of tumorigenic cells to actively reprogram carbon metabolism to support rapid proliferation has gained widespread recognition, establishing it as a defining hallmark of cancer (**Figure 2**) (15–17). Metabolic reprogramming is a dynamic process that has been identified as a consequence of mutations in oncogenes and tumor suppressor genes and can lead to significant alterations in metabolic enzymatic activities (18,19). Mutations in phosphoinositide 3-kinase (PI3K), myelocytomatosis proto-oncogene (Myc), p53 and phosphatase and tensin homologue (PTEN) lead to perturbations in various intracellular signalling pathways, including the PI3K/protein kinase B (AKT)/ mammalian targeted of rapamycin (mTOR) and rat sarcoma (Ras)/rapidly accelerated fibrosarcoma (Raf)/mitogen-activated protein kinase (MAPK) pathways (17–19).

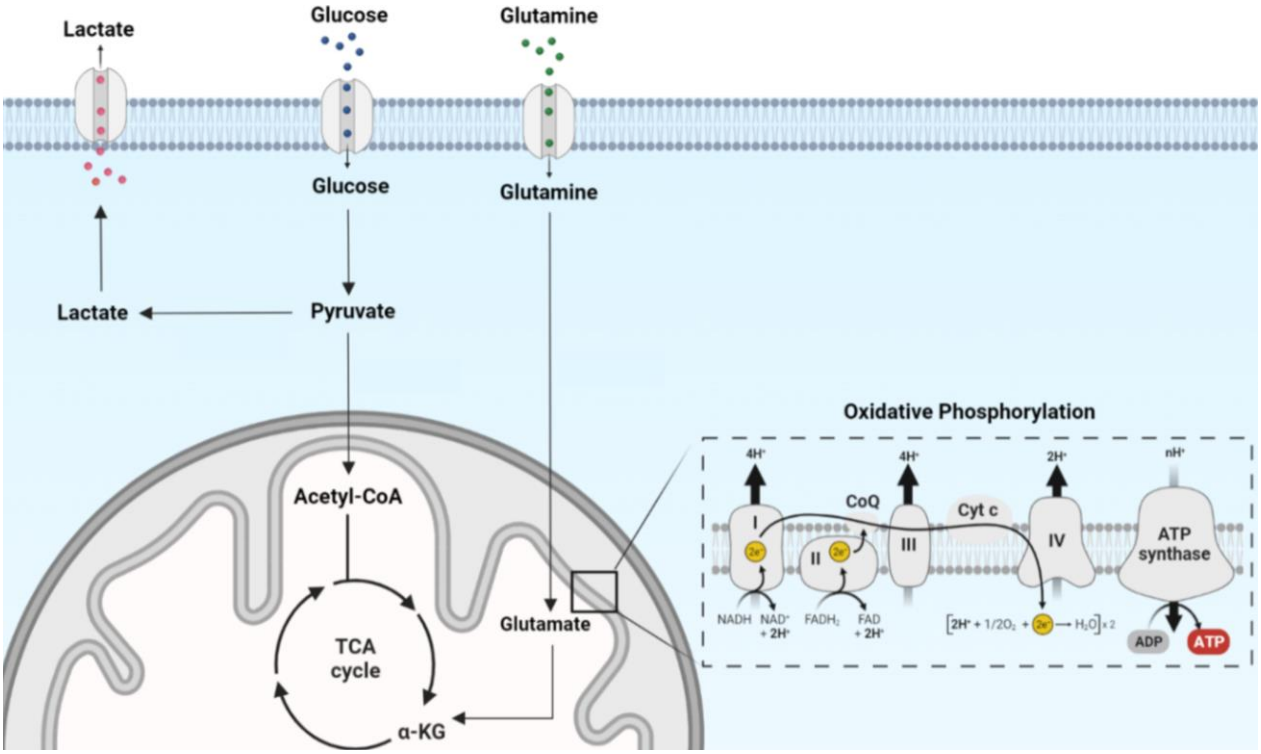

Figure 2. *Summarized representation illustrating glucose and glutamine cellular metabolism. Within the TCA cycle, nicotinamide adenine dinucleotide hydrogen (NADH) and dihydroflavine-adenine dinucleotide (FADH2) are produced, which are essential electron donors needed in OXPHOS (20). During OXPHOS, NADH and FADH2 deposit two electrons into the electron transport chain (ETC) at complexes I and II, respectively (20,21). Diagram designed and created by MC Stark using BioRender® (Toronto, Canada).*

The activation of PI3K triggers downstream activation of AKT and mTOR, which subsequently facilitates the stabilization of hypoxia-inducible factor (HIF) (**Figure 3**) (22–24). AKT increases glycolytic rates by upregulating expression and membrane translocation of glucose transporters (GLUTs) and phosphorylation of key glycolytic enzymes, including hexokinase (HK) and phosphofructokinase-1 (PFK-1) (24–26). Furthermore, mTOR further augments glycolysis through the induction of HIF-1, a transcription factor (TF) that increases the expression of glucose transporter 1 (GLUT1) (27). In addition, HIF-1 activates pyruvate

dehydrogenase kinase (PDK), which subsequently inhibits pyruvate dehydrogenase (PDH) (28,29). Consequently, the inhibition of PDH impedes the entry of pyruvate into the tricarboxylic acid (TCA) cycle, thereby decreasing the rate of oxidative phosphorylation (OXPHOS) and favouring glycolysis for adenosine triphosphate (ATP) production (29,30). The oncogenic TF, Myc, also upregulates the transcription of various glycolytic enzymes, including GLUT1, lactate dehydrogenase (LDH) and PDK-1 (30–32). However, Myc has an additional function of upregulating glutamine metabolism by increasing the expression of mitochondrial glutaminase (GLS), which converts glutamine to glutamate (33). Finally, p53, a key tumor suppressor, inhibits glycolysis by increasing the expression of TP53-induced glycolysis and apoptosis regulator (TIGAR) (34). TIGAR inactivates fructose-2,6-bisphosphatase (Fru-2,6-P_2), leading to a decreased rate of glycolysis (34). Additionally, p53 activates PTEN, which inhibits the PI3K/AKT/mTOR pathway leading to decreased glycolytic activity (35). Since p53 is frequently mutated in breast cancer, its inhibitory effects on glycolysis are absent resulting in excessive glycolytic rates (30, 36).

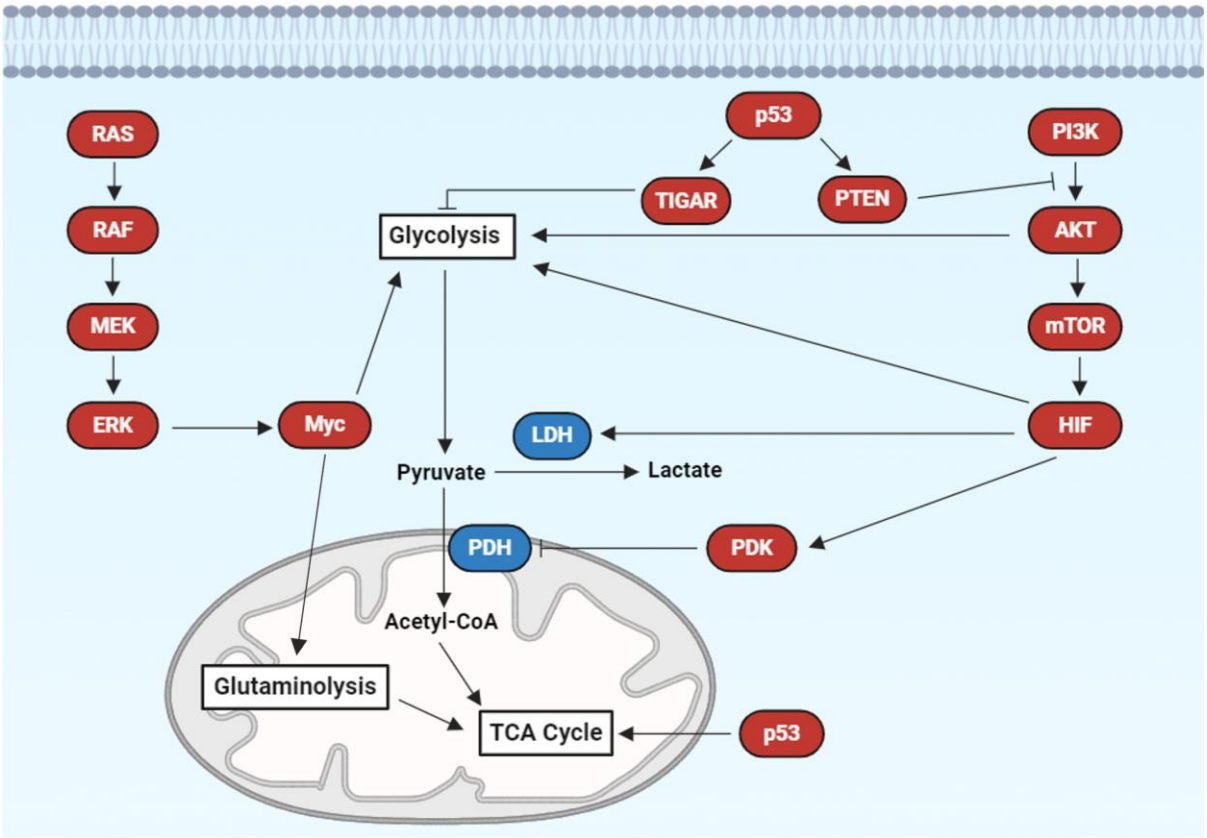

Figure 3. *Signalling pathways involved in tumorigenic cell metabolism. Disruptions in p53 and the hyperactivation of PI3K leads to increased rates of glycolysis mediated though AKT, mTOR and HIF signalling (35). Ras/Raf/MAPK signalling leads to the activation of Myc, which transcribes various genes involved in glycolysis and glutaminolysis (31). Diagram designed and created by MC Stark using BioRender® (Toronto, Canada).*

Although metabolic reprogramming is known to result from genetic mutations, it is multifaceted, also stemming from various perturbations at the epigenomic, transcriptomic, and metabolomic levels (19). All of these

factors collectively contribute to maintaining the hyperproliferative nature of tumorigenic cells by modifying multiple metabolic pathways, particularly glycolysis, glutaminolysis, and OXPHOS (19,37). In addition, recent research has demonstrated a connection between metabolic reprogramming and the development of resistance to various chemotherapies and radiation therapies (30,38,39). Thus, given the crucial role that metabolic reprogramming plays in tumorigenesis, a deeper understanding of the primary carbon sources that sustain the bioenergetic (ATP production and consumption), biosynthetic, and redox demands of tumorigenic cells is required (15,40). Overall, this knowledge may reveal novel metabolic- and biochemical vulnerabilities that can potentially be targeted for more effective cancer treatment.

Glucose is the main carbon source for ATP synthesis in the body and is essential for cell survival and proliferation (41,42). Multiple tumorigenic cell types reprogram glucose metabolism from the TCA cycle and OXPHOS to favour aerobic glycolysis, where pyruvate is converted into lactate even in the presence of oxygen (43,44). This phenomenon was first discovered in 1924 by Otto Heinrich Warburg and was later called the Warburg effect (45–47). Tumorigenic cells prefer aerobic glycolysis since this process rapidly produces ATP and various glycolytic intermediates, which are diverted into secondary biosynthetic pathways that produce key macromolecule building blocks, including cofactors, nucleotides, lipids, and amino acids (16,48,49). Although aerobic glycolysis is capable of rapidly producing ATP, it does so in an inefficient manner (2 ATP per glucose) when compared to mitochondrial ATP synthesis (36 ATP) (16,50). To circumvent the 18-fold decrease in ATP production compared to OXPHOS, tumorigenic cells increase glycolytic flux by upregulating GLUT1 and additional rate-limiting enzymes, including HK and PFK-1 (16). Warburg speculated that the increased rates of aerobic glycolysis were a consequence of functional defects in the mitochondria (51,52). However, recent discoveries have challenged this notion since a wide range of tumorigenic cell types have demonstrated the ability to switch their metabolism to OXPHOS during periods of biogenetic stress (53,54).

Due to the heightened reliance of tumorigenic cells on aerobic glycolysis, numerous researchers have focused on the impact of glucose deprivation on breast tumorigenic cells with differing metabolic phenotypes (18,53,55–57). Furthermore, literature indicates that luminal A MCF-7 breast tumorigenic cells rely significantly more on OXPHOS for ATP production, whereas basal triple negative MBA-MD-231 breast cells predominantly depend on aerobic glycolysis (**Figure 4**) (58,59). Glucose deprivation in both the MCF-7 and MDA-MB-231 cell lines result in decreased proliferation, reduced metastasis and inhibition of anchorage-independent colony formation, primarily due to decreased ATP and reduced macromolecule production (60). Furthermore, glucose deprivation disrupts glycolysis and the pentose phosphate pathway (PPP), which consequently results in the depletion of nicotinamide adenine dinucleotide phosphate hydrogen (NADPH), leading to redox imbalances and reactive oxygen species (ROS) production (60–63). Nonetheless, breast tumorigenic cells have demonstrated the ability to acquire resistance to glucose deprivation by reverting metabolism back to OXPHOS in order to obtain sufficient ATP and replenish macromolecule intermediates

(53,64,65). Previous *in vitro* Seahorse XF analysis revealed that glucose-deprived MDA-MB-231 cells experience an approximate 40% increase in the rate of mitochondrial respiration (66). Moreover, a main anaplerotic pathway enabling the transition to mitochondrial metabolism involves the upregulation of pyruvate carboxylase, which converts pyruvate into oxaloacetate, a key TCA intermediate (64,67,68). However, the primary anaplerotic pathway enabling resistance to the bioenergetic, biosynthetic and redox stress initiated by glucose deprivation is glutaminolysis (64,69,70).

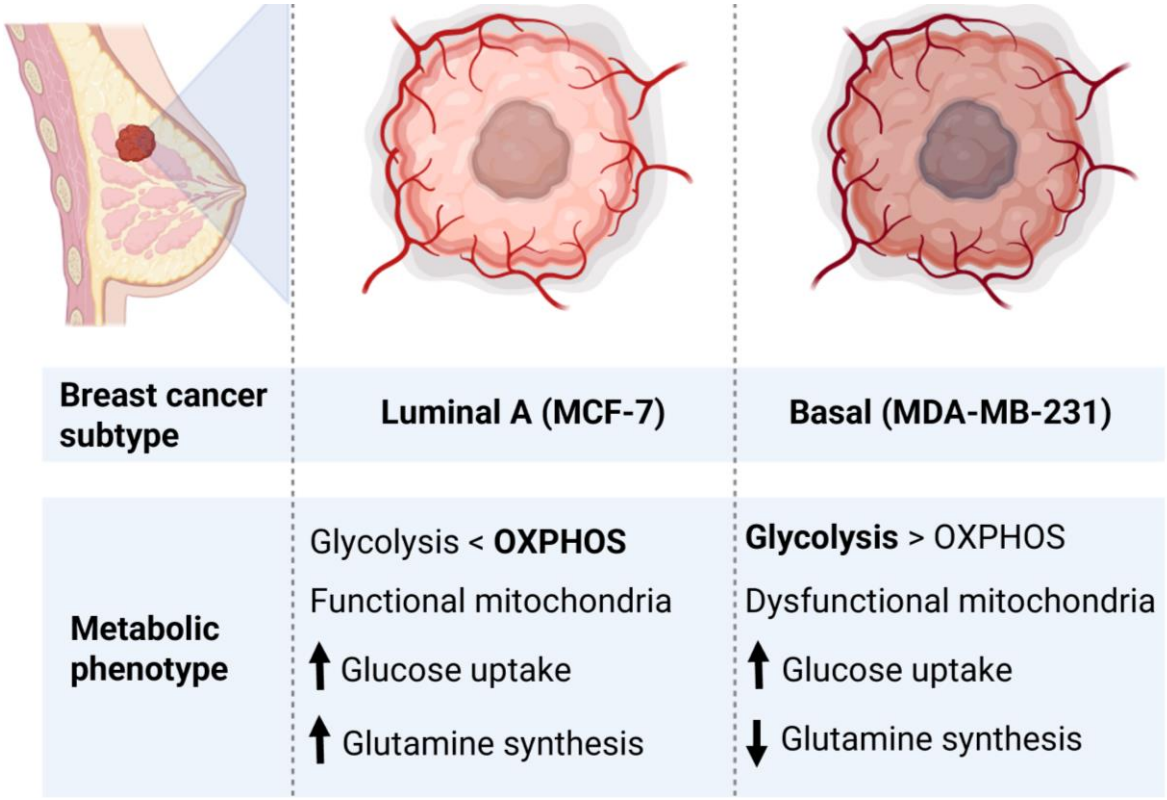

Figure 4. *Metabolic phenotypes of luminal A (MCF-7) and basal (MDA-MB-231) cells. MCF-7 cells favour OXPHOS for ATP production, whereas MBA-MD-231 cells favour aerobic glycolysis, potentially owing to the presence of functional and dysfunctional mitochondria, respectively (58,59). Both cell lines exhibit increased glucose uptake; however, de novo glutamine synthesis differs between these cell lines (58). Diagram designed and created by MC Stark using BioRender® (Toronto, Canada).*

Glutamine is another carbon source that plays a crucial role in sustaining the rapid growth and proliferation of breast tumorigenic cells (64,71). Glutamine is a non-essential amino acid (NEAA) and is the most abundant amino acid in the body, accounting for 30% to 35% of all nitrogen transported in the blood (72,73). Despite glutamine being a NEAA that cells can produce *de novo*, most tumorigenic cells are dependent on exogenous glutamine supply, where the rate of glutamine uptake exceeds that of glutamine biosynthesis (71,74,75). Overall, the heightened reliance of tumorigenic cells on exogenous glutamine has led to glutamine being recognized as an essential amino acid (EAA) for tumorigenic metabolism (76). Glutamine plays a major role in maintaining cellular bioenergetics, where it is metabolized through glutaminolysis, which initially involves the conversion of glutamine to glutamate in the mitochondria (20,64). This conversion of glutamine to

glutamate is mediated by two forms of glutaminase, namely kidney-type glutaminase (GLS1) and liver-type glutaminase (GLS2) (77,78). Thereafter, glutamate is further converted into α-ketoglutarate (α-KG), an important intermediate in the TCA cycle, through the action of glutamate dehydrogenase (GDH), which simultaneously reduces $NADP^+$ to NADPH (20,79). In addition to serving as a carbon source for the TCA cycle, glutamine also serves as a nitrogen source for the biosynthesis of nucleotides, NEAAs (alanine, aspartate, and serine) and glutathione (GSH), an antioxidant vital for maintaining ROS homeostasis (64,71). Furthermore, the production of glutathione involves the conversion of glutamine to glutamate, succeeded by the ligation of glutamate and cysteine by glutamate-cysteine ligase (GCL) (80). Subsequently, glutathione synthetase (GSS) incorporates glycine into ligated glutamate-cysteine, resulting in the formation of GSH (80,81).

Owing to the versatile role of glutamine in tumorigenic cell metabolism, extensive research has been conducted to investigate the effects of glutamine deprivation on breast tumorigenic cells (64,82). In both MCF-7 and MDA-MB-231 cells, glutamine metabolism is significantly increased in addition to being essential for tumor growth and migration (83,84). Glutamine deprivation ranging from 24-96 hours results in antiproliferative effects and induces cell death in both MCF-7 and MDA-MB-231 cells in a time-dependent manner (82). Furthermore, glutamine deprivation results in cell cycle arrest and an increase in ROS production in both MCF-7 and MDA-MB-231 cell lines (82). A more prominent antiproliferative effect was observed in MCF-7 cells, suggesting that luminal breast tumorigenic cells are more dependent on glutamine metabolism (82). Nevertheless, similar to the response observed in glucose deprivation, glutamine-deprived tumorigenic cells also exhibit the utilization of the compensatory anaplerotic pathway involving pyruvate carboxylase (64). Ultimately, the metabolic plasticity of tumorigenic cells promotes resistance to deprivation of either glucose or glutamine individually by enhancing the utilization of the alternative nutrient (64). Hence, this phenomenon presents an enticing metabolic vulnerability that could be targeted pharmacologically by simultaneously inhibiting upregulated glycolytic and glutaminolysis enzymes to overcome metabolic adaptability (85,86).

Targeting tumorigenic cell metabolism has been proposed as a promising therapeutic strategy and may provide a potential advantage in precision medicine, where combinational strategies and novel compounds targeting particular biochemical pathways can be designed based on multiomic data (85). Previous transcriptomic analyses have demonstrated that messenger RNA (mRNA) expression of solute carrier family 2 member 1 (*SLC2A1*), the gene which encodes GLUT1, is significantly ($P < 0.0001$) elevated in TNBC compared to ER positive- and HER2-enriched breast tumors (87). The identification of increased dependence on GLUT1 in TNBC cells led to the development of small-molecule inhibitors, particularly BAY-876 and STF-31 (**Figure 5**) (85,87,88). Both have demonstrated the ability to impair the growth of patient-derived xenograft TNBC tumors exhibiting increased glycolytic activity and low OXPHOS rates; however, further research is needed to demonstrate their clinical efficacy (87).

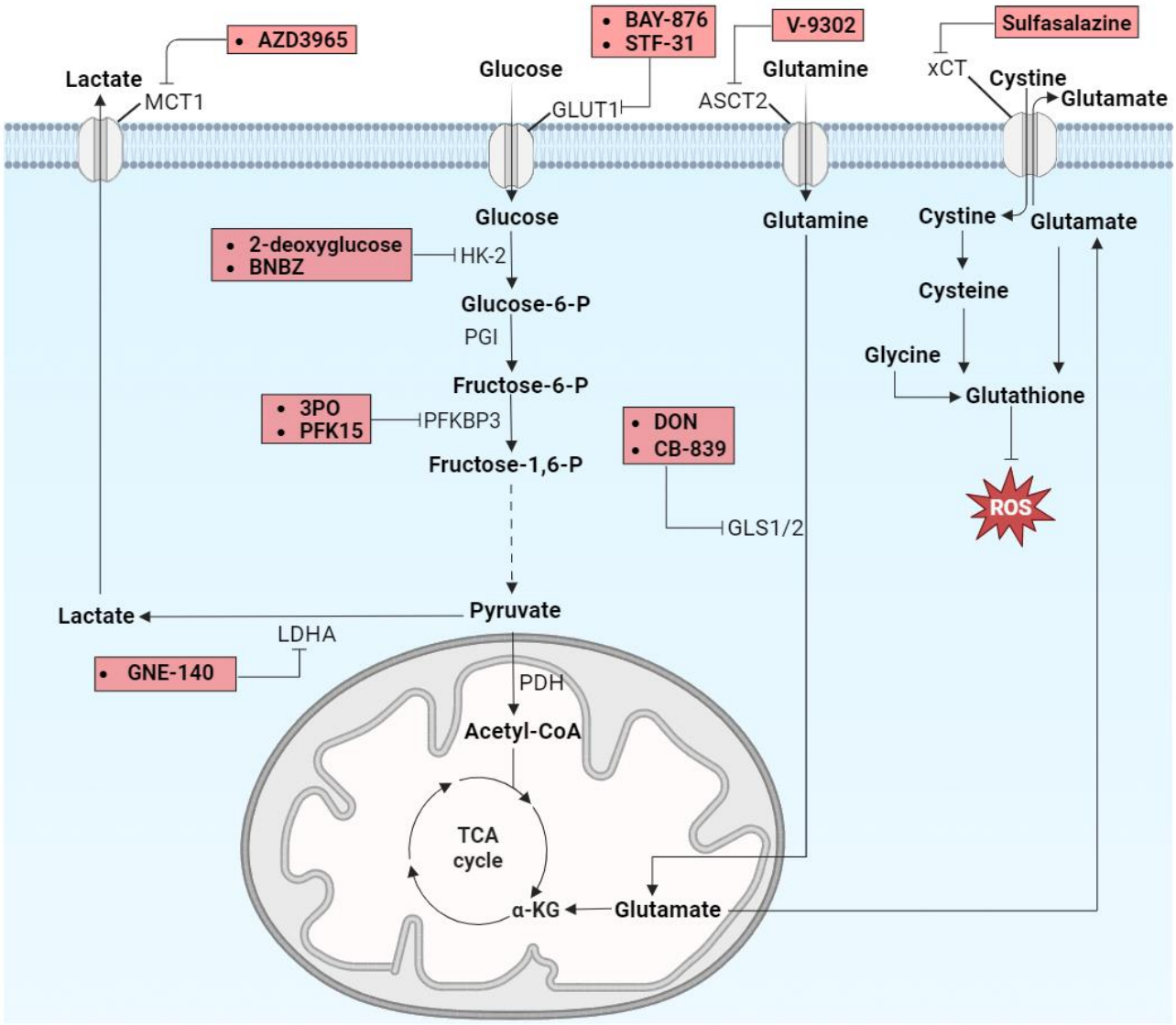

Figure 5. *Inhibitors of glucose and glutamine metabolism under development. Multiple transporters, particularly GLUT1, monocarboxylate transporter (MCT), Alanine-serine-cysteine transporter subtype 2 (ASCT2), and cystine/glutamate antiporter (xCT), are overexpressed in tumorigenic cells (85). Additionally, the increased expression of HK, PFK-1, LDH, GLS1/2 has also been noted in tumorigenic cells (16,85). Hence, various inhibitors (shown in red), most of which are still in preclinical development, are being investigated (85). Diagrams designed and created by MC Stark using BioRender® (Toronto, Canada).*

The increased expression of intracellular glycolytic enzymes, including HK-2, 6-phosphofructo-2-kinase/fructose-2,6-bisphosphatase-3 (PFKFB3), and LDH, which is associated with higher metastatic potential and lower breast cancer survival rates, has driven the development of several inhibitors (89–91). Most notably, 2-deoxy-D-glucose (2DG), a glucose analogue, demonstrated a significant decrease in tumor progression *in vivo*, but in clinical trials, proved to have undesirable side effects and limited efficacy, owing to on-target off-tumor toxicity (85,92). This prompted the development of an additional HK2 inhibitor, benitrobenrazide (BNBZ), designed to minimize toxicity and improve therapeutic outcomes (93). BNBZ, administered at 150 mg/kg, effectively inhibits tumor growth in pancreatic and colon cancer mouse models

by 63.4% and 66.2%, respectively (93). However, further research is needed to evaluate its efficacy in breast cancer models (93). Moreover, owing to the increased expression of PFKFB3 in breast tumors, two novel inhibitors have been developed, namely (2E)-3-pyridin-3-yl-1-pyridin-4-ylprop-2-en-1-one (3PO) and 1-(4-pyridinyl)-3-(2-quinolinyl)-2-propen-1-one (PFK15) (85,94,95). Both compounds, 3PO and PFK15, have exhibited potent inhibitory effects on cell migration and proliferation in TNBC (MDA-MB-231) cells and suppress tumor growth *in vivo* with minimal side effects (94,95). In addition, recent studies have shown regulating lactate production and secretion may be a promising approach to mitigate breast cancer growth and tumor microenvironment (TME) remodelling (96). LDHA has been identified as a potential target to decrease pyruvate-to-lactate conversion, leading to the generation of (R)-3-((2-chlorophenyl)thio)-4-hydroxy-6-(4-morpholinophenyl)-6 (GNE-140) (85,97). However, due to the robust metabolic adaptability of tumorigenic cells, GNE-140 has not yielded significant inhibitory effects on tumor growth (97). Nonetheless, targeting lactate secretion through monocarboxylate transporter 1 (MCT1) blockade has elicited favourable outcomes *in vivo*, owing to intracellular acidification of tumorigenic cells and a reduction in angiogenesis due to decreased lactate accumulation in the TME (98). Among MCT1 inhibitors, AZD3965, a first-in-class inhibitor that underwent a phase I clinical trials (NCT01791595) for patients with advanced solid tumors including colorectal and lung cancer, renal and cardiotoxicity, highlighting the lack of selectivity for tumorigenic cells (99,100).

The elevated rates of glutaminolysis observed in breast tumorigenic cells have prompted investigations into the underlying molecular mechanisms (64). Literature indicates that the expression of alanine-serine-cysteine transporter subtype 2 (ASCT2), a glutamine transporter, is elevated in high-risk breast cancer subtypes, including TNBC, highlighting a potential target for therapeutic intervention (101). A competitive ASCT2 antagonist, 2-amino-4-bis(aryloxy benzyl)aminobutanoic acid (V-9302), has been shown to reduce tumor volume by 23% in TNBC mouse models and sensitize breast tumors to anti-programmed cell death protein 1 (PD-1) immune checkpoint inhibitor therapy (102,103). However, no clinical trials have been conducted to date. An additional transporter of potential therapeutic targeting value for breast cancer is the cystine/glutamate antiporter (xCT), which imports cystine for GSH biosynthesis and antioxidant defence (104). Recent analyses have demonstrated that solute carrier family 7 member 11 *(SLC7A11)*, the gene encoding xCT, exhibits differential expression in breast cancer subtypes (105). The mRNA expression of *SLC7A11* is significantly elevated in TNBC ($P < 0.001$) and luminal B tumors ($P = 0.02$), with copy number gains observed in HER2+ cancers ($P = 0.01$). Furthermore, ER-negative and TNBC subtypes show the highest protein expression, underscoring xCT's potential role in breast cancer progression (105). These findings led to the repurposing of sulfasalazine, an anti-rheumatic drug that has been shown to be an effective xCT inhibitor and has demonstrated promising suppression of TNBC growth through GSH depletion, leading to the induction of ferroptosis (106). Furthermore, targeting GLS1 and GLS2 has been proposed an effective breast

cancer therapeutic strategy, resulting in the establishment of 6-diazo-5-oxo-norleucine (DON) and telaglenastat (107–109). However, the therapeutic potential of both of these compounds have been hampered due to poor clinical outcomes and toxicity in clinical trials (85,107–109). The use of DON in breast cancer clinical studies has been reported since the 1950s; however, due to only 11% of patients exhibiting a partial response and high rates of adverse events (>80% of patients), its investigation for breast cancer treatment was discontinued (107–109). Additionally, telaglenastat has been investigated in phase 2 clinical trials (NCT03428217) in combination with cabozantinib for advanced renal cell carcinoma, but it did not improve progression-free survival (110). Nonetheless, despite the development of various glucose- and glutamine metabolic inhibitors, their use has been constrained by unfavourable side effects, which are largely due to the lack of specificity for tumorigenic cells (85,111). Moreover, considering that these inhibitors are currently in the developmental stage, a process that demands substantial resources and significant financial investment, it is probable that the pricing of these therapies will be high, rendering them inaccessible to breast cancer patients within LMICs (85,112). Therefore, there is an unmet need to identify new cost-effective strategies with improved safety profiles that can simultaneously downregulate glucose- and glutamine metabolism.

1.2. Fasting and metabolic plasticity

Fasting has emerged as a promising practice to decrease blood glucose- and glutamine concentrations, leading to downregulated glycolytic- and glutaminolytic flux (113,114). Furthermore, fasting for a 12-hour period results in a significant reduction in both blood glucose- and glutamine levels. Glucose concentrations typically decrease to approximately 3.9-5.6 mM/L, while glutamine concentrations vary between 0.5-0.8 mM/L (115,116). To circumvent the reduction in blood glucose concentrations, various homeostatic processes are induced, particularly glycogenolysis, gluconeogenesis and ketogenesis in the liver and lipolysis in adipose tissues, which lead to the release of glucose and ketone bodies into the blood stream (**Figure 6A**) (114,117). An *in vitro* study investigating the effects of glucose and glutamine deprivation at physiological concentrations demonstrated a decrease in cell proliferation and the induction of apoptosis in MDA-MB-231 cells (18). The study further revealed that even short-term (2–6 hours) physiological glutamine and glucose deprivation resulted in decreased cell density, rounded cells, and apoptosis induction through ROS generation and mitochondrial dysfunction, which are associated with bioenergetic, biosynthetic, and redox stress (18). Additionally, TNBC cells responded more prominently to glutamine and glucose deprivation compared to cervical tumorigenic cells, due to their highly glycolytic nature (18). Furthermore, *in vivo* studies in mice bearing subcutaneous breast cancer (4T1) showed that two cycles of short-term fasting can be as effective as chemotherapeutic intervention with cyclophosphamide or doxorubicin in delaying the progression of breast cancer (113,118). Moreover, fasting also increased the toxicity of doxorubicin (DXR) against breast 4T1 cells while enhancing the ability of non-tumorigenic cells to withstand the toxic chemotherapeutic effects, a phenomenon known as differential stress resistance (DSR) (**Figure 6B**) (113, 119).

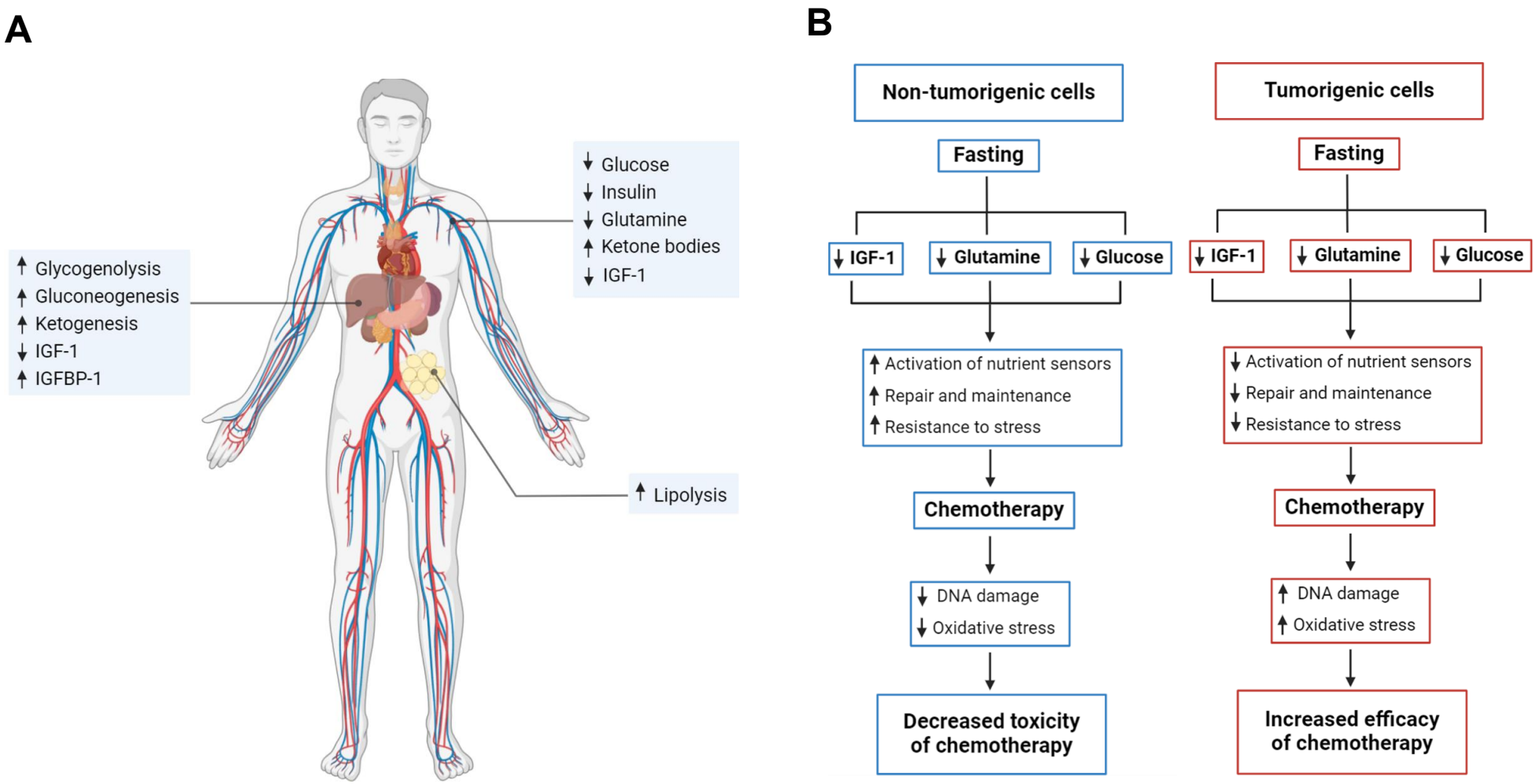

Figure 6. *Fasting's physiological effects and molecular mechanisms in cancer. (A) Summarized diagrammatic representation of the physiological effects of fasting After 8 hours of fasting, the liver increases glycogenolysis, gluconeogenesis, ketogenesis, and IGFBP-1 secretion, while decreasing IGF-1 secretion (113–117). IGFBP-1 also binds to circulating IGF-1, impeding its binding to IGF-1R (113,119). Additionally, fasting increases lipolysis (resulting in higher circulating ketone bodies and fatty acids) and decreases glucose, insulin, and glutamine concentrations (113–117). (B) Schematic overview of the differential effects exerted by fasting on non-tumorigenic (differential stress resistance) versus tumorigenic cells (differential stress sensitization). Diagrams designed and created by MC Stark using BioRender® (Toronto, Canada) and Microsoft PowerPoint 2021 (Redmond, Washington, USA).*

The principle of DSR has been partially validated in clinical trials, as demonstrated in a pilot study involving 13 women with early-stage luminal-like breast cancer (Stage II/III) (120). This study evaluated the efficacy and safety of fasting for 24 hours before and after receiving a (neo)-adjuvant combinational therapy known as TAC, which comprises docetaxel (Taxotere), doxorubicin (Adriamycin), and cyclophosphamide (120). One week post-exposure to TAC, the fasting group exhibited significantly higher mean thrombocyte ($P = 0.00007$) and erythrocyte ($P = 0.007$) counts compared to the TAC treatment only group. The data obtained confirmed that fasting is safe and results in reduced haematological toxicities compared to those who adhered to standard nutritional guidelines. Similarly, a clinical study (NCT00936364) evaluated the safety and feasibility of fasting combined with platinum-based chemotherapy in patients with various cancers, including breast, prostate, and ovarian cancer (121). Participants fasted for 24, 48, or 72 hours, and fasting-related side effects were limited to grade 2 or lower, primarily fatigue, headache, and dizziness. The comet assay, a sensitive method for detecting nuclear deoxyribonucleic acid (DNA) damage in individual eukaryotic cells, revealed reduced DNA damage in leukocytes from subjects who fasted for 48 hours or more (121). These findings further support the reduction in haematological toxicity associated with fasting. However, fasting for 48 hours is not ideal for patients with pre-existing nutritional deficiencies or low body mass index (BMI), as extended fasting could exacerbate muscle loss, worsen nutritional deficits, and increase the risk of complications such as hypoglycaemia and weakened immunity (122). Thus, a 24-hour fasting period may offer a safer alternative for such patients. Nonetheless, this study was conducted on a small cohort (n = 20) and focused solely on chemotherapy-induced side effects without evaluating therapeutic outcomes (121). Therefore, larger studies are needed to validate these findings and explore the therapeutic potential of fasting in combination with chemotherapy.

While fasting has been shown to decrease blood glucose and glutamine concentrations, which may contribute to a reduction in chemotherapy-induced side effects observed in clinical studies and reduced tumor growth *in vivo*, additional factors, such as lowered levels of insulin like growth factor 1 (IGF1), may also play a significant role (119, 123,124). For instance, a clinical trial (NCT00936364) conducted in cancer patients demonstrated that IGF-1 levels decreased by 30%, 33%, and 8% in the 24-, 48-, and 72-hour fasting cohorts, respectively (121). IGF-1 is known to be associated with breast cancer progression through the activation of the PI3K/AKT/mTOR signalling pathway (123,124). Thus, the inhibition of tumor growth mediated by fasting in preclinical studies could be attributed to the inhibition of mTOR, a key regulator of cell growth and proliferation (125,126). The protein, mTOR, is a 289-kDa serine/threonine protein kinase belonging to the PI3K family of related protein kinases (PIKKs) and is composed of two multi-subunit complexes, namely, mTOR complex 1 (mTORC1) and mTOR complex 2 (mTORC2) (127,128). While both complexes respond to IGF-1 signalling, only mTORC1 is influenced by nutrient availability, in particular glucose- and glutamine levels (129,130). High nutrient availability and PI3K-mediated growth factor signalling both activate

mTORC1, which subsequently promotes ribosomal biogenesis and protein synthesis while inhibiting autophagy (**Figure 7**) (131,132).

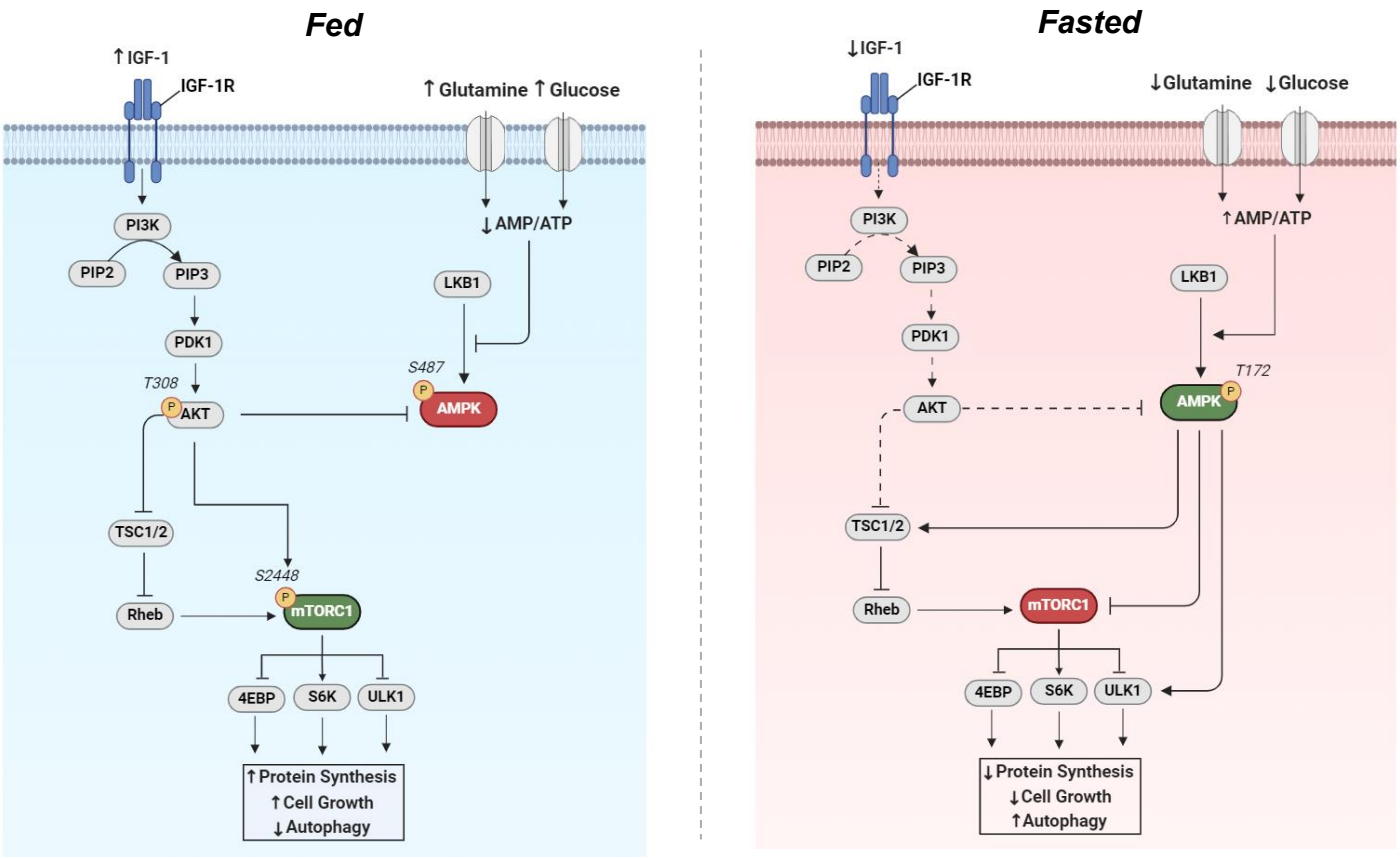

Figure 7. *Interplay of AMPK and mTOR cell signalling pathways in fed and fasted states. In the fed state the PI3K/AKT/mTOR pathway is activated and AMPK signalling is inhibited, where in the fasted state PI3K signalling is dampened and AMPK is activated due to an increased AMP/ATP ratio leading to the inhibition of mTORC1 (131,132). mTORC1 serves an inhibitor eukaryote initiation factor 4E-binding protein (4EBP) and uncoordinated-51-like kinase 1 (ULK1) and activator ribosomal protein S6 kinase 1 (S6K1) (132). Diagrams designed and created by MC Stark using BioRender® (Toronto, Canada).*

Once activated by the binding of IGF-1 to its respective receptor (IGF-1R), PI3K facilitates the conversion of phosphatidylinositol-3,4-bisphosphate (PIP2) to phosphatidylinositol-3,4,5-triphosphate (PIP3) (133,134). Thereafter, PIP3 activates PDK-1, which in turn activates AKT through phosphorylation at threonine residue 308 (T308) in the activation loop (135,136). Activated AKT indirectly stimulates mTORC1 through its inhibitory effects on tuberous sclerosis complex 2 (TSC2), which functions as an inhibitor of Ras homology enriched in brain (Rheb), an activator of mTORC1 (128,137). Although, AKT has also demonstrated the ability to directly activate mTORC1 through phosphorylation at serine residue 2448 (S2448), a critical step for mTORC1 activation and is frequently utilized as an indicator of mTORC1 activity (138). Moreover, the connection between heightened glucose and glutamine levels and the activation of mTORC1 has been associated with the suppression of 5'-adenosine monophosphate-activated protein kinase (AMPK), which acts as an inhibitor of mTORC1 (139–142).

The primary function of AMPK is its role as a cellular energy sensor, activated in response to low ATP levels, signalled by an increased AMP-to-ATP ratio (140,143). Conditions presenting with high glucose- and glutamine concentrations results in AMPK inhibition due to a reduced AMP/ATP ratio, subsequently leading to the disruption of its suppressive impact on mTORC1 (144,145). Additionally, in response to PI3K-mediated growth factor signalling, AKT inhibits AMPK activity by phosphorylating the catalytic α1 subunit (AMPKα1) at serine residue 487 (S487) (146). This phosphorylation hinders the phosphorylation of threonine residue 172 (T172) by liver kinase B1 (LKB1), a critical step necessary for the activation of AMPK (147,148). Therefore, the decreased proliferation and survival of tumorigenic cells after fasting can possibly be attributed to the inhibition of mTORC1 by AMPK (114,149). The decreased glycolytic- and glutaminolytic flux caused by fasting results in a significant reduction in ATP production, thereby leading to an elevated AMP/ATP ratio (150). In response to this metabolic stress, LKB1 phosphorylates AMPK at T172, facilitating its activation (147). Additionally, the decline in IGF-1-related signalling leads to diminished AKT activation, resulting in decreased S487 phosphorylation, contributing to a more pronounced elevation of T172 phosphorylation (134,146,147). Subsequently, activated AMPK inhibits mTORC1 directly by phosphorylating the regulatory-associated protein of mTOR (Raptor) and indirectly by phosphorylating TSC2 on threonine residue 1227 (T1227) and serine residue 1345 (S1345), improving TSC2's capacity to inhibit Rheb and thus mTORC1 activation (147,151,152). This sequence of events leads to the suppression of mTORC1 signalling, resulting in the activation of 4EBP and ULK1, in addition to the inhibition of S6K1 (131,132,153). This ultimately leads to a decrease in protein synthesis and growth, accompanied by an increase in autophagy, which is further induced through the direct activation of ULK1 by AMPK (153,154). Autophagy is an intracellular catabolic process by which cytoplasmic material constituents (organelles and proteins) are engulfed by autophagosomes and further degraded upon fusion with lysosomes (155,156). This phenomenon is referred to as macroautophagy and is extensively acknowledged as a mechanism that mitigates bioenergetic stress in nutrient-deprived tumorigenic cells (157,158). Nevertheless, while autophagy offers a pro-survival mechanism against ND, it has also been recognized as a potential target for the induction of cell death mediated through excessive autophagy-induced cell death (ACD), occurring in an apoptosis-independent manner (159).

Despite the potential of fasting to impede cell growth and proliferation, metabolic plasticity confers resistance to tumorigenic cells during glucose- and glutamine deprivation by reverting metabolism back to OXPHOS, thus ensuring an adequate ATP supply (**Figure 8**) (39,53,54,64). This resistance stems from the heightened expression of two key anaplerotic enzymes responsible for replenishing the TCA cycle, namely, GLS and pyruvate carboxylase, as previously discussed. However, recent *in vivo* studies have demonstrated that a prominent adaptive mechanism employed by nutrient-deprived TNBC cells is the upregulation of mitochondrial complex I expression and activity, an enzyme essential for OXPHOS (53). Mitochondrial complex I is a crucial component of the ETC, where it plays a pivotal role by oxidizing NADH to nicotinamide

adenine dinucleotide (NAD+) while simultaneously transferring two electrons to ubiquinone (160,161). The electron transfer is coupled with the translocation of four protons across the mitochondrial membrane (160,161). Ultimately, this process contributes to the generation of the proton-motive force necessary to drive ATP production through OXPHOS (161). Moreover, a study that utilized RNA interference (RNAi) revealed that breast tumorigenic cells cultured in nutrient-deprived conditions exhibited increased dependence on OXPHOS for optimal proliferation through augmented mitochondrial complex I expression, thereby highlighting a notable metabolic vulnerability (162). Thus, an integrated therapeutic approach combining ND and mitochondrial complex I inhibition emerges as a promising avenue for therapeutic exploration, with the potential to induce substantial bioenergetic stress and ultimately reduce breast cancer progression

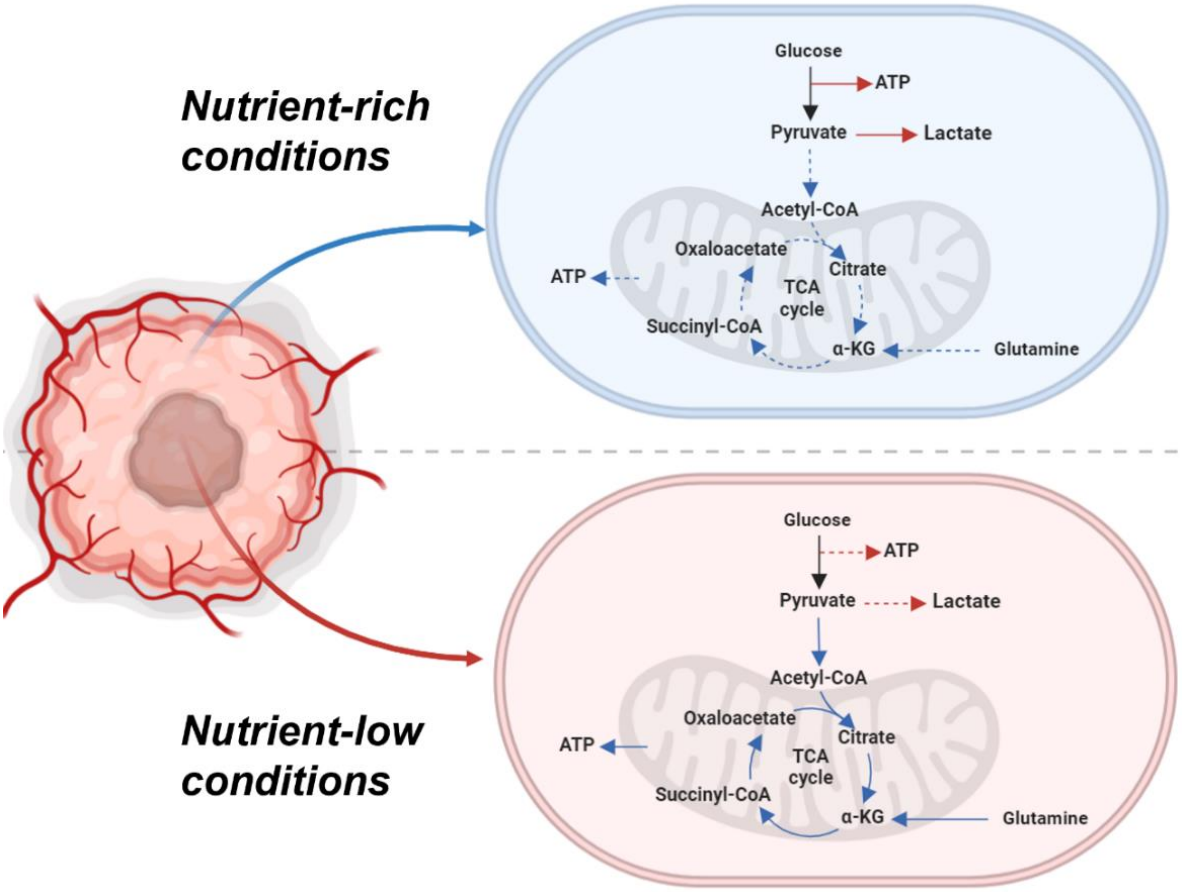

Figure 8. *Metabolic plasticity in tumorigenic cells. Metabolic plasticity induced by ND in breast tumorigenic cells involves an adaptive resistance mechanism, where tumorigenic cells shift from glycolysis to OXPHOS (39,53,54,64). This shift is primarily mediated by increased activity of mitochondrial complex I (53). In nutrient-rich conditions, tumorigenic cells favour aerobic glycolysis (solid red arrows) for ATP production and reduce mitochondrial metabolism (dashed blue arrows)(39,53,54,64). However, under nutrient-deprived conditions, there is a major shift to mitochondrial metabolism, prioritizing pyruvate entry into the TCA cycle (solid blue arrows) and reducing lactate production (dashed red arrows) (39,53,54,64). Consequently, the heightened dependence of nutrient-deprived tumorigenic cells on OXPHOS presents a metabolic vulnerability that could be exploited for hypersensitization to complex I inhibitors. Diagrams designed and created by MC Stark using BioRender® (Toronto, Canada).*

1.3. Mitochondrial complex I inhibitors

The recognition of the elevated dependence of nutrient-deprived tumorigenic cells on OXPHOS has prompted the development of numerous novel mitochondrial complex I inhibitors, many of which have entered clinical trials (163–167). A potent mitochondrial complex I inhibitor, IACS-010759, demonstrated promising antitumor efficacy in acute myeloid leukemia (AML) xenograft models, reducing tumor growth by approximately 80% after 15 days of daily oral administration (5–10 mg/kg), and subsequently entered two phase I clinical trials for breast cancer (NCT03291938) and refractory AML (NCT02882321) (**Table 1**) (166–168). However, due to dose-related toxicities including lactic acidosis and peripheral neuropathy the drug was discontinued from further development (167). Furthermore, a recently developed biguanide mitochondrial complex I inhibitor, IM156, entered a phase I clinical trial (NCT03272256) for advanced refractory solid tumors, including breast cancer (169,170). This was the first-in-human dose-escalation study to determine a recommended phase II oral dose (800 mg daily) for a mitochondrial complex I inhibitor. However, notable side effects, including severe nausea and elevated plasma lactate levels, were observed, and further research is needed to evaluate its therapeutic efficacy.

Table 1: New and repurposed small molecules exhibiting mitochondrial complex I inhibitory properties.

Inhibitor	Structure	Development phase	References
IACS-010759	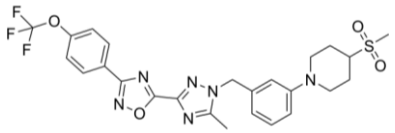	Phase 1 (NCT03291938 and NCT02882321)	(166–168)
IM156	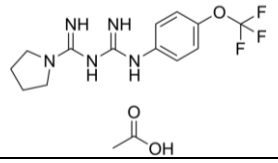	Phase I (NCT03272256)	(169,170)
Mubritinib	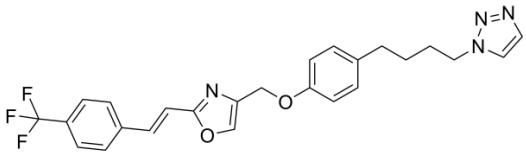	Phase 1 (NCT00034281)	(164,171)
Phenformin	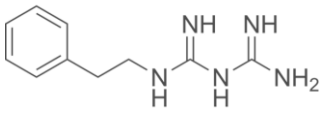	FDA approved for diabetes but discontinued in 1970s	(164, 172)
Metformin	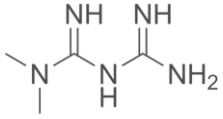	SAHPRA approved for diabetes Phase 3 (NCT01101438)	(164, 173–175)
Papaverine	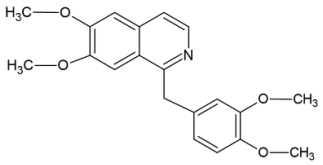	SAHPRA approved for cerebral vasospasm Phase 1 (NCT03824327)	(176–178)

The high incidence of adverse events associated with IACS-010759 and IM156 may result from their insufficient selectivity for tumorigenic cells, leading to on-target off-tumor toxicity in non-tumorigenic cells. The excessive inhibition of mitochondrial respiration leads to a pronounced shift towards glycolysis, resulting in elevated lactate production and consequently, lactic acidosis (164, 167). The increased risk of lactic acidosis is not unique to IACS-010759 and IM156 but has also been demonstrated in other highly potent mitochondrial complex I inhibitors, including mubritinib, and particularly phenformin (164,171,172). Phenformin, a previously FDA-approved diabetes drug, was withdrawn from the US market in 1977 due to the high risk of inducing lactic acidosis (172). Accordingly, it is necessary to identify mitochondrial complex I inhibitors that exhibit moderate inhibitory effects and possess superior, well-established safety profiles to fully exploit the increased reliance of nutrient-deprived tumorigenic cells on OXPHOS for therapeutic intervention (65,164,167). Ideally, such mitochondrial complex I inhibitors should be low-cost and widely accessible within public hospitals in South Africa.

Drug repurposing (DR) emerges as highly advantageous strategy for the identification of mitochondrial complex I inhibitors currently in use within current South African medical system. Economically, repurposing drugs circumvents the extensive costs associated with early-stage research and development, preclinical testing, and the initial phases of clinical trials of new mitochondrial complex I inhibitor therapeutic modalities, and thus the time-to-market is significantly increased (179,180). Currently, the most studied mitochondrial complex I inhibitor is metformin (MET), a diabetes drug approved by the SAHPRA that has undergone extensive international clinical research (173,174). Several studies have demonstrated that the combination of ND and MET profoundly disrupts the metabolism and growth of tumorigenic cells (53,65,181,182). However, MET only exerted antiproliferative effects on nutrient-deprived tumorigenic cells but not those propagated in high-nutrient conditions (53,65,182). This observation emphasizes that inducing a metabolic shift to OXPHOS, accomplished by means of ND, notably sensitizes tumorigenic cells to mitochondrial complex I inhibition. Despite MET being the subject of investigation in more than 300 clinical trials for cancer, the results of most of these investigations have been conflicting since MET has not demonstrated a significant improvement in overall survival rates (182). Furthermore, a phase 3 randomized clinical trial (NCT01101438) demonstrated that the addition of MET to standard neoadjuvant chemotherapy (drugs not specified) did not significantly improve invasive disease–free survival compared to the placebo group (P = 0.93) (183). The recognition that fasting can be used to sensitize breast tumorigenic cells to MET has now led researchers at the M.D. Anderson Cancer Centre to initiate a Phase 2 clinical trial (NCT05023967) investigating the effect of nightly fasting and MET in women with stage I/II breast cancer (184). However, MET requires substantial concentrations (IC_{50}~20 mM) to effectively inhibit mitochondrial complex I activity, which far exceeds the plasma concentrations achievable in patients (185,186). Patients receiving doses of 250 to 2550 mg/day, commonly used in cancer clinical trials, exhibited MET plasma concentrations of 5 to 20 µM, potentially

explaining its limited therapeutic efficacy (187–190). Therefore, to fully take advantage of the metabolic vulnerabilities of nutrient-deprived breast tumorigenic cells, it is imperative to continue exploring alternative small molecules that can effectively inhibit mitochondrial complex I at clinically relevant concentrations.

1.4. Papaverine

Papaverine (PPV), a SAHPRA-approved small-molecule therapy for the treatment of cerebral vasospasm, has recently been discovered to be an effective mitochondrial complex I inhibitor (178). PPV is a non-narcotic ergot alkaloid that was first isolated from *Papaver Somniferum* in 1848 and has been routinely used in the clinic as a vasodilator due its ability to inhibit phosphodiesterase-10A (PDE10A) (177,191). Compared to MET, which necessitates 24 hours and millimolar concentrations to inhibit mitochondrial complex I, PPV demonstrates superior inhibitory effects at a 200-fold lower concentration (100 µM), achieving moderate inhibition of mitochondrial complex I within 30 min (176,178). Furthermore, similar to MET, PPV is also cost-effective and is frequently used in the public health care sector in SA. Notably, PPV has been extensively used as a therapeutic agent for over a century with a well-documented safety profile (177). The most common adverse event associated with long-term PPV use is injection site fibrosis, further emphasizing its safety (178). These attributes make PPV an appealing alternative for mitochondrial complex I inhibition. *In vivo* studies have shown that even when administered at intravenous and intramuscular SAHPRA-approved doses (2 mg/kg), PPV effectively inhibits mitochondrial complex I, leading to a significant increased tumor oxygenation in hypoxic tumors models, thus potentially enhancing the efficacy of radiotherapy (176,178). These findings have pioneered a new field of study in metabolic radiosensitization and have led to a clinical trial (NCT05136846), which is currently recruiting patients to investigate the combination of PPV and chemoradiation for the treatment of stage II-III non-small cell lung cancer. However, prior *in vivo* studies conducted before this trial did not demonstrate a reduction in tumor volume when PPV was administered as a monotherapy in TNBC (EO771) xenograft mice (178). The absence of tumor growth inhibition could be attributed to the mice being fed ad libitum, leading to tumorigenic cells that did not exhibit the heightened reliance on increased mitochondrial complex I activity typically observed in nutrient-deprived tumorigenic cells. Thus, to fully exploit PPV's mitochondrial complex I inhibitory effects, it is imperative to first induce metabolic plasticity in tumorigenic cells to favour OXPHOS, possibly through fasting-mediated ND, thereby hypersensitizing tumorigenic cells to PPV.

Recent high-throughput screening analyses of 7000 compounds aimed at identifying candidates that can exacerbate the antiproliferative effects of glucose deprivation in luminal breast tumorigenic cells (MCF-7) revealed that PPV exhibited optimal effects and selectively induced apoptosis in glucose-deprived MCF-7 cells; however, these effects were not observed in MCF-7 cells cultured in high glucose concentrations (192). Thus, this finding underscores the potential of leveraging PPV in conjunction with ND as a comprehensive

therapeutic strategy. However, the combinational effects of glucose- and glutamine deprivation at physiological fasting levels, along with PPV in metabolically distinct breast tumorigenic cells have not been explored to date. Therefore, this present study aimed to investigate the effects of physiological glucose- and glutamine deprivation and PPV (hereafter referred to as ND + PPV) on OXPHOS-dependent (MCF-7) and glycolysis-dependent (MDA-MB-231) cell lines. Firstly, the effects of ND + PPV were investigated on the proliferation, cell morphology, and cell cycle progression in both cell lines to determine the extent of growth inhibition, morphological changes, and alterations in cell cycle dynamics induced by the combined treatment. Furthermore, given that OXPHOS is the primary mitochondrial metabolic pathway targeted in this study, the effects of ND + PPV were assessed on ROS production (specifically superoxide [O_2^-] and hydrogen peroxide [H_2O_2]), superoxide dismutase (SOD) activity, and mitochondrial membrane potential. Given that previous literature has demonstrated that the AMPK/mTOR axis is markedly altered in response to ND or mitochondrial complex I inhibition, the effects of ND combined with PPV were investigated on two key phosphorylation sites, namely mTORC1 S2448 and AMPKα1 S487. Overall, the comprehensive examination of the cellular processes included in this current study may provide critical biomolecular insights into the impact of ND + PPV on different breast cancer metabolic subtypes. Additionally, this study can further aid in understanding how adaptive metabolic plasticity responses induced by ND create metabolic vulnerabilities in breast tumorigenic cells, which can be exploited by using mitochondrial complex I inhibitors such as PPV. Lastly, the data obtained can potentially uncover additional metabolic vulnerabilities and biochemical determinants that may lead to the development of novel targeted small-molecule therapies. However, the potential impact of this study extends beyond these findings; it holds promise in contributing to the ongoing efforts to enhance the affordability, accessibility, and efficacy of targeted therapies for breast cancer patients in SA and other sub-Saharan African countries. Furthermore, since PPV is an extensively utilized SAHPRA-approved therapeutic widely accessible in the South African public health sector, with well-studied pharmacokinetic and safety profiles, clinical trials can be accelerated, resulting in a substantial reduction in time and cost. As a consequence, the translational potential of this research project is maximized, offering promising prospects for the advancement of fasting and PPV as a potential therapeutic option for financially constrained breast cancer patients.

2. Aim

The aim of this research project was to investigate the effect of physiological ND and PPV exposure in MCF-7 and MDA-MB-231 cell lines.

3. Objectives

The objectives of this study were as follows:

1. To determine the effect of ND + PPV on the proliferation of MCF-7 and MDA-MB-231 cell lines by means of spectrophotometry (crystal violet staining).

2. To determine the effect of ND + PPV on the two-dimensional (2D) morphology of MCF-7 and MDA-MB-231 cell lines by means of light microscopy.

3. To determine the effect of ND + PPV on the three-dimensional (3D) morphology of MCF-7 and MDA-MB-231 cell lines by means of polarization-optical transmitted light differential interference contrast microscopy (PlasDIC).

4. To determine the effect of ND + PPV on cell cycle progression and cell death induction in MCF-7 and MDA-MB-231 cell lines by means of flow cytometry (propidium iodide staining).

5. To determine the effect of ND + PPV on O_2^- production in MCF-7 and MDA-MB-231 cell lines by means of fluorescent microscopy (dihydroethidium [DHE] staining)

6. To determine the effect of ND + PPV on H_2O_2 production in MCF-7 and MDA-MB-231 cell lines by means of fluorescent microscopy (2,7-dichlorofluoresceindiacetate [DCFDA] staining)

7. To determine the effect of ND + PPV on SOD activity in MCF-7 and MDA-MB-231 cell lines by means of spectrophotometry.

8. To determine the effect of ND + PPV on mitochondrial membrane potential in MCF-7 and MDA-MB-231 cell lines by means of flow cytometry (MitoProbe™ JC-1 assay).

9. To determine the effect of ND + PPV on the expression of S487 phosphorylated AMPKα1 in MCF-7 and MDA-MB-231 cell lines by means of spectrophotometry (enzyme-linked immunosorbent assay [ELISA]).

10. To determine the effect of ND + PPV on the expression of S2448 phosphorylated mTORC1 in MCF-7 and MDA-MB-231 cell lines by means of flow cytometry.

4. Materials and Methods

4.1. Materials

4.1.1. Cell lines

MCF-7 is a luminal subtype A human breast tumorigenic cell line that is positive for estrogen receptor (ER), progesterone receptors (PR), and glucocorticoid receptors and negative for human epidermal growth factor receptor-2 (HER2) (82,183,194). This cell line was obtained from the American Type Culture Collection (Manassas, Virginia, USA). MDA-MB-231 is a basal human breast tumorigenic cell line negative for ER, PR, and HER2 receptors (82,193). This cell line was retrieved from a metastatic adenocarcinoma site and was obtained from the American Type Culture Collection (Manassas, Virginia, USA). Both MCF-7 and MDA-MB-231 cells were cultured in Dulbecco's minimum essential medium (DMEM) supplemented with fetal calf serum (FCS) (56°C, 30 min), 100 U/mL penicillin G, 100 mg/mL streptomycin and amphotericin B (250 mg/L) (Capricorn Scientific [Ebsdorfergrund, Hessen, Germany]). Cells were propagated in 75 cm^2 and/or 25 cm^2 tissue culture flasks and incubated at 37°C and 5% CO_2 atmospheric conditions.

4.1.2. Reagents

All reagents were purchased from Merck & Co., Inc. (Darmstadt, Germany) unless otherwise stated. The following reagents, including FCS, antibiotic/antimycotic solution (100X), and DMEM, were purchased from Capricorn Scientific (Ebsdorfergrund, Hessen, Germany). (8R,13S,14S,17S)-2-ethyl-13-methyl-7,8,9,11,12,13,14,15,16,17decahydro-6H-cyclopenta [a]phenanthrane-3,17-diylbis-sulphamate (EMBS) was supplied by iThemba Labs (Cape Town, Western Cape, SA). PPV was acquired from Merck & Co., Inc. (New Jersey, USA) in powdered form and was dissolved in dimethyl sulfoxide (DMSO) at a concentration of 50 mM. Vehicle-treated (VT) cells were propagated in complete growth medium with equal volumes of DMSO as PPV-treated cells, where the final dilution of the DMSO did not exceed 0.3% (v/v). The superoxide dismutase (SOD) activity assay kit was purchased from Merck & Co., Inc. (New Jersey, USA). The Mitoprobe™ JC-1 assay kit and anti-S2448 mTORC1 antibodies were supplied by Thermo Fisher Scientific Co. (Waltham, Massachusetts, USA). Lastly, the Phospho-AMPKα1 (Ser487) ELISA kit was purchased from RayBiotech, Inc. (Norcross, Georgia, USA).

4.1.3. Physiological nutrient deprivation media

This study utilized two ND media, formulated to closely simulate typical physiological glucose- and glutamine serum concentrations, which are validated based on previous research (18,195). Nutrient deprivation medium 1 (ND1) contained 6.0 mM glucose and 0.6 mM glutamine, and nutrient deprivation medium 2 (ND2) contained 3.5 mM glucose and 0.6 mM glutamine. The negative control for all experiments included cells propagated in complete growth medium (CTR) supplemented with 25.52 mM glucose and 4.00 mM

glutamine. This served as a baseline for direct comparison by establishing a reference point for cellular behaviour under optimal nutritional/growth conditions. Moreover, two additional negative controls were utilized: first, cells exposed to ND1 and ND2 only for 24 hours, and second, cells exposed to PPV only for 24 hours. These controls aided in determining if changes in the experimental groups resulted from the combined effects of ND and PPV exposure rather than from ND or PPV alone. Lastly, all experimental media were supplemented with FCS (56°C, 30 min), 100 U/mL penicillin G, 100 mg/mL streptomycin and amphotericin B (250 mg/L) (Capricorn Scientific [Ebsdorfergrund, Hessen, Germany]).

4.2. Methods

4.2.1. Cell proliferation: crystal violet staining (spectrophotometry)

The crystal violet staining assay was used to determine the effect of ND + PPV on cell proliferation. Crystal violet is a purple triphenylmethane cation dye that allows for the quantification of cell number by intercalating between DNA bases, where the number of cells cultured in a monolayer is directly proportional to the intensity of crystal violet staining (196). The absorbance of crystal violet is determined using a spectrophotometer at a wavelength of 570 nm (197).

MCF-7 and MDA-MB-231 cells were seeded at 5000 cells per well in a 96-well plate. Cells were incubated for 24 hours to allow for cell attachment in a humidified atmosphere at 37°C and 5% CO_2. Cells were washed with phosphate buffer saline (PBS) thrice and then exposed to the two ND media. Thereafter, the cells were incubated in a humidified atmosphere at 37°C and 5% CO_2 for 24 hours, as previous research has shown that this is the optimal time needed to induce a starvation response in tumorigenic cells while having minimal effects on cell viability (18). Subsequently, cells were exposed to PPV (50-200 µM) for 24 hours since previous *in vitro* studies have demonstrated that PPV exhibited optimal antiproliferative effects in breast tumorigenic cell lines at this concentration range and exposure period (196). The positive control for this experiment included cells exposed to 0.2% sodium dodecyl sulphate (SDS), as previous research has demonstrated that SDS results in a significant decrease in cell numbers (196). After 24 hours, the medium was discarded, and the cells were fixed using 1% glutaraldehyde (100 µL) for 15 min at room temperature (RT). Glutaraldehyde was discarded, and cells were stained using 0.1% crystal violet (100 µL). The plate was incubated at RT for 30 min. Excess crystal violet was discarded and the plate was submersed under running water and left to dry overnight. Crystal violet was solubilized by adding 0.2% Triton X-100 (100 µL) to the wells, and the plate was incubated at RT overnight. The absorbance was determined at 570 nm using an EPOCH Microplate Reader (Biotek Instruments, Inc. (Winooski, Vermont, USA) (198). The data obtained was analysed using Microsoft Excel 2020 (Microsoft Corporation, Washington, USA) and GraphPad Prism 8 software (GraphPad Software, San Diego, California, USA).

4.2.2. Cell morphology: 2D and 3D morphological analysis (light microscopy)

4.2.2.1. Semi-quantitative cell morphological analysis (light microscopy)

To determine and quantify the morphological changes induced by ND + PPV, light microscopy was utilized. MCF-7 and MDA-MB-231 cells were seeded in a 24-well plate with 20,000 cells per well. The plates were incubated for 24 hours to allow for cell attachment in a humidified atmosphere at 37°C and 5% CO_2. Cells were washed with PBS thrice and then exposed to the two ND media. Subsequently, the cells were incubated for 24 hours in a humidified atmosphere at 37°C and 5% CO_2, then exposed to PPV (100 µM) for another 24 hours. This concentration was used for all subsequent experiments since it demonstrated optimal antiproliferative effects and has demonstrated to effectively inhibit mitochondrial complex I in breast tumorigenic cell lines (178). The positive control included cells exposed to 0.4 µM EMBS for 48 hours since past literature has demonstrated that EMBS significantly increases cells demonstrating aberrant morphology at this concentration and exposure period (196). Thereafter, an Axiovert 40 CFL microscope (Zeiss, Oberkochen, Germany) was used to capture images at 20X magnification. The morphology of 100 cells was examined using the Carl Zeiss™ AxioVision Rel. 4.8 software (Zeiss, Oberkochen, Germany), where the number of cells demonstrating aberrant and no aberrant morphology was recorded for each sample thrice. Finally, the data obtained was analysed using Microsoft Excel 2020 (Redmond, Washington, USA) and GraphPad Prism 8 software (GraphPad Software, San Diego, California, USA).

4.2.2.2. Polarization-optical transmitted light differential interference contrast microscopy

To evaluate the 3D morphological changes induced by ND + PPV, PlasDIC was utilized. PlasDIC is a contrast microscopy technique capable of capturing high-quality 3D images of the morphology of cells and cell clusters (198). Furthermore, PlasDIC uses non-polarized light to illuminate cells, which results in superior quality high-contrast images (198).

MCF-7 and MDA-MB-231 cells were seeded in a 24-well plate with 20,000 cells per well. The plates were incubated for 24 hours to allow for cell attachment in a humidified atmosphere at 37°C and 5% CO_2. Cells were washed with PBS thrice and then exposed to the two ND media. Cells were incubated for 24 hours in a humidified atmosphere at 37°C and 5% CO_2. Subsequently, the cells were exposed to PPV (100 µM) for 24 hours. The positive control included cells exposed to 0.4 µM EMBS for 48 hours since previous studies have demonstrated that EMBS at this concentration and exposure period significantly increase cells demonstrating aberrant morphology (196). Finally, the 3D morphology of the cells were captured at 40X magnification using an Axiovert 40 CFL microscope (Zeiss, Oberkochen, Germany).

4.2.3. Cell cycle progression and cell death-induction: propidium iodide staining (flow cytometry)

The effects of ND + PPV on cell cycle progression and cell death induction was investigated by means of propidium iodide staining and flow cytometry. Propidium iodide is a red fluorescent nuclear and chromosomal intercalating counterstain that allows for the quantification of DNA correlating to the stages of the cell cycle during cell division (199). In addition, this assay can be used to indicate the induction of cell death, as cells in the sub-G_1 phase possess fragmented DNA, reflecting the DNA endonucleolytic cleavage that occurs during cell death processes (e.g. apoptosis) (200).

MCF-7 and MDA-MB-231 cells were seeded at 500,000 cells per T25 cm^2 flask and left for 24 hours to allow for attachment in a humidified atmosphere at 37°C and 5% CO_2. Cells were washed with PBS thrice and then exposed to the two ND media. Cells were incubated for 24 hours in a humidified atmosphere at 37°C and 5% CO_2. Subsequently, the cells were exposed to PPV (100 µM) for 24 hours. The positive control included cells exposed to 0.4 µM EMBS since previous research has demonstrated that EMBS exposure results in a significant increase in cells occupying the sub-G_1 phase and induces a G_2/M block (196). After 24 hours, the cells were trypsinized and resuspended in 2 mL of growth medium. Cells were then centrifuged (300 x *g*, 5 min) and the supernatant was removed and discarded. Cells were then resuspended in ice-cold PBS (200 µL) containing 0.1% FCS. Ice-cold 70% ethanol (4 mL) was then added in a dropwise manner, and cells were stored at 4°C for 24 hours. Cells were centrifuged (300 x *g*, 5 min), and the supernatant was removed. Cells were then resuspended in 1 mL of PBS containing propidium iodide (40 µg/mL), ribonuclease A (RNase) (100 µg/mL) and Triton X-100 (0.1%) and samples were incubated at 37°C for 45 min. Finally, propidium iodide fluorescence was be measured using a Cytoflex® flow cytometer (Beckman Coulter, Inc. [Brea, California, USA]) available from the Institute of Cellular and Molecular Medicine, Department of Immunology, University of Pretoria, South Africa. A total of 10,000 events were recorded per condition, and data from cell debris (particles smaller than apoptotic bodies) and clumps of two or more cells were removed from further analysis. Cell cycle distributions were then calculate using Kaluza analysis software from Beckman Coulter, Inc. (Brea, California, USA) by assigning relative DNA content per cell to sub-G_1-, G_1, S- and G_2M fractions. Lastly, the data obtained was be further analysed using Microsoft Excel 2020 (Redmond, Washington, USA) and GraphPad Prism 8 software (GraphPad Software, San Diego, California, USA).

4.2.4. Oxidative stress: O_2^- and H_2O_2 using DHE and DCFDA staining (fluorescent microscopy)

4.2.4.1. O_2^- production using DHE staining (fluorescent microscopy)

Fluorescent microscopy was used to determine the effects of ND + PPV on the production of O_2^- by means of DHE staining. DHE is rapidly taken up by cells and is oxidized by O_2^- to produce fluorescent 2-hydroethidine cations, which can be detected at excitation and emission wavelengths of 535 nm and 610 nm, respectively (201).

MCF-7 and MDA-MB-231 cells were seeded in 24-well plates at a density of 20,000 cells per well and incubated for 24 hours in a humified atmosphere at 37°C and 5% CO_2 to allow for attachment. Cells were washed with PBS thrice and then exposed to the two ND media. Cells were incubated for 24 hours in a humidified atmosphere at 37°C and 5% CO_2. Cells were exposed to PPV (100 µM) for 24 hours. The positive control included cells exposed to 0.4 µM EMBS for 48 hours, as previous *in vitro* studies have demonstrated that EMBS at this concentration and exposure period significantly increases O_2^- production in tumorigenic cells (202). Cells were then washed with PBS and stained for 45 min using 10 µM DHE at 37°C and 5% CO_2. Thereafter, the cells were washed with 500 µL of PBS, and an additional 500 µL of PBS was added to each well. Images of DHE-stained (red) cells was captured using a Zeiss Axiovert CFL40 microscope, Zeiss Axiovert MRm monochrome camera (Zeiss, Oberkochen, Germany) and Zeiss filter 15. The fluorescence intensity of at least 100 cells per condition was analyzed using ImageJ software (National Institutes of Health, Bethesda, Maryland, USA). Finally, all data obtained was further analysed using Microsoft Excel 2020 (Redmond, Washington, USA) and GraphPad Prism 8 software (GraphPad Software, San Diego, California, USA).

4.2.4.2. H_2O_2 production using DCFDA staining (fluorescent microscopy)

Fluorescent microscopy was used to determine the effects of ND + PPV on H_2O_2 production by means of DCFDA staining. DCFDA is a non-fluorescent probe that is oxidized by H_2O_2 to yield 2,7-dichlorofluorescein (DCF), a fluorescent derivative that can be detected with maximum excitation and emission wavelengths of 485 nm and 530 nm, respectively (203–205).

MCF-7 and MDA-MB-231 cells were seeded in 24-well plates at a density of 20,000 cells per well and incubated for 24 hours in a humified atmosphere at 37°C and 5% CO_2 to allow for attachment. Cells were washed with PBS thrice and then exposed to the two ND media. Cells were incubated for 24 hours in a humidified atmosphere at 37°C and 5% CO_2. Thereafter, the cells were exposed to PPV (100 µM) for 24 hours. The positive control included cells exposed to 0.4 µM EMBS for 48 hours since previous literature has demonstrated that EMBS at this concentration and exposure period significantly increases H_2O_2 production in tumorigenic cells (206). Cells were then washed with PBS (1 mL) and incubated with 20 µM DCFDA for 20 min at 37°C and 5% CO_2. Next, the cells were washed with PBS (500 µL), after which an additional 500 µL of PBS was added to each well. Finally, a Zeiss Axiovert CFL40 microscope, Zeiss Axiovert MRm monochrome camera (Zeiss, Oberkochen, Germany) and Zeiss filter 9 used to capture images of DCFDA-stained (green) cells. The fluorescence intensity of at least 100 cells was determined using ImageJ software developed by the National Institutes of Health (Bethesda, Maryland, USA). The data obtained was further analyzed using Microsoft Excel 2020 (Redmond, Washington, USA) and GraphPad Prism 8 software (GraphPad Software, San Diego, California, USA).

4.2.5. SOD activity (spectrophotometry)

To determine the effect of ND + PPV on SOD activity, a SOD activity determination kit from Merck & Co., Inc. (New Jersey, USA) was used. Superoxide dismutase's (SODs) are a group of metalloenzymes which serve as the first line of defence against oxidative damage induced by ROS. These proteins catalyze the dismutation of O_2^- into molecular oxygen and H_2O_2 (207).

MCF-7 and MDA-MB-231 cells were seeded in T25 cm^2 flasks at a density of 1,000,000 cells and incubated in a humidified atmosphere for 24 hours at 37°C and 5% CO_2. Cells were washed with PBS thrice and then exposed to the two ND media. Cells were incubated for 24 hours in a humidified atmosphere at 37°C and 5% CO_2. Cells were exposed to PPV (100 µM) for 24 hours. The positive control consisted of cells exposed to the O_2^- scavenger, 6 mM tiron for 48 hours, as previous *in vitro* studies have demonstrated that tiron at this concentration and exposure period results in significant decreases in SOD activity (208). Subsequently, cells were then trypsinized and lysed through freeze–thaw cycles, alternating between ice and RT for four repetitions of 10 min each. The lysates were then centrifuged (14 000 x *g*, 10 min) at 4ºC, and the supernatant was collected, transferred to a sterile microcentrifuge tube, and samples were kept on ice. Next, 20 µL of sample solution, WST working solution (200 µL), dilution buffer (20 µL), and enzyme working solution (200 µL) were added to each well of a 96-well plate, and relevant blanks were added according to the manufacturer's instructions. After mixing, the samples were incubated for 20 min at 37°C, followed by absorbance measurement at 450 nm using an EPOCH Microplate Reader (Biotek Instruments, Inc., Winooski, Vermont, USA). Finally, all data obtained was further analysed using Microsoft Excel 2020 (Redmond, Washington, USA) and GraphPad Prism 8 software (GraphPad Software, San Diego, California, USA).

4.2.6. Mitochondrial membrane potential: JC-1 staining (flow cytometry)

The effect of ND + PPV on mitochondrial membrane potential (ΔψM) was investigated using the MitoProbe™ 5',6,6'-tetrachloro-1,1',3,3'-tetraethylbenzimidazolylcarbocyanine iodide (JC-1) assay. JC-1 is a cationic dye used in flow cytometry to determine mitochondrial polarization (209). This dye aggregates and fluoresces an orange–red color in non-compromised cells with a polarized ΔψM; however, in compromised cells possessing a depolarized ΔψM, the dye does not aggregate and emits green fluorescence (209). Thus, the effects of ND and PPV exposure on ΔψM can be determined by obtaining the ratio of red/green fluorescence.

MCF-7 and MDA-MB-231 cells were seeded in T25 cm^2 flasks at a density of 500,000 cells per flask and incubated for 24 hours in a humified atmosphere at 37°C and 5% CO_2 to allow for attachment. Cells were washed with PBS thrice and then exposed to the two ND media. Cells were incubated for 24 hours in a humidified atmosphere at 37°C and 5% CO_2. Subsequently, the cells were exposed to PPV (100 µM) for 24 hours. Cells were then trypsinized, centrifuged (300 x *g*, 5 min) and resuspended in 2 mL complete growth medium. The positive control consisted of cells exposed to 50 mM carbonyl cyanide m-

chlorophenylhydrazone (CCCP) for 5 min at 37°C with 5% CO_2. The samples were then stained with 200 µM JC-1 (10 µL) and incubated for 30 min at 37°C with 5% CO_2. Samples were centrifuged (300 x *g*, 5 min), and the supernatant was discarded. The cells were then resuspended and washed in 2 mL of PBS, followed by another round of centrifugation (300 x *g*, 5 min) and subsequent removal of the supernatant. Next, 500 µL of PBS was added, and the fluorescence intensity emitted from each sample was determined using a Cytoflex® flow cytometer (Beckman Coulter, Inc. [Brea, California, USA]) available from the Institute of Cellular and Molecular Medicine, Department of Immunology, University of Pretoria, South Africa. A total of 10,000 events was recorded per condition, and data from cell debris were removed from further analysis. Finally, the samples was analyzed using Kaluza analysis software from Beckman Coulter (Brea, California, USA). All data obtained was further analysed using Microsoft Excel 2020 (Redmond, Washington, USA) and GraphPad Prism 8 software (GraphPad Software, San Diego, California, USA).

4.2.7. AMPK and mTORC1 signalling: p-AMPKα1 (S487) and p-mTORC1 (S2448) expression

4.2.7.1. p-AMPKα1 (S487) expression (enzyme-linked immunosorbent assay)

The impact of ND + PPV on AMPK activity was assessed using sandwich ELISA. In nutrient-rich conditions, the catalytic α1 subunit of AMPK is phosphorylated at S487 by AKT, resulting in the inhibition of AMPK activity (146). Furthermore, the inhibitory effects initiated by S487 phosphorylation are due to the hindrance of T172 phosphorylation by LKB1, a crucial step for AMPK activation (147,148). Hence, the phosphorylation of the inhibitory site S487 on AMPKα1 functioned as an indicator of AMPK activity.

MCF-7 and MDA-MB-231 cells were seeded in T25 cm^2 flasks at a density of 500,000 cells per flask and incubated for 24 hours in a humified atmosphere at 37°C and 5% CO_2 to allow for attachment. Cells were washed with PBS thrice and then exposed to the two ND media. Cells were incubated for 24 hours in a humidified atmosphere at 37°C and 5% CO_2. Subsequently, the cells were exposed to PPV (100 µM) for 24 hours. Cells were trypsinized and resuspended in 2 mL complete growth medium. Thereafter, the cells were centrifuged (300 x *g*, 5 min), and the supernatant was be removed. The cells were then be washed once with PBS (1 mL), followed by centrifugation (300 x *g*, 5 min)), and the supernatant was removed. Cell lysate buffer (250 µL) was used to resuspend the pellet, and the lysates were incubated with gentle shaking at 4°C for 30 min. The lysates were centrifuged (20,000 x *g*, 10 min, 4°C), and the supernatant was transferred to a new microcentrifuge tube and the samples were kept on ice. Next, 100 µL of sample was added to each well of the microplate (coated with anti-pan-AMPKα1) and was incubated with gentle shaking at RT for 2.5 hours. The solution was then discarded and washed 4 times with 1X Wash Solution (provided by the supplier). Thereafter, 100 µL of the primary anti-phospho-AMPKa1 (S487) antibody was added to each well and incubated for 1 hour at RT with gentle shaking, followed by an additional washing step as mentioned above. Subsequently, 100 µL of the prepared horseradish peroxidase (HRP)-conjugated secondary antibody was added to each well

and incubated for 1 hour at RT with gentle shaking, followed by an additional washing step. Next, 3,3',5,5'-tetramethylbenzidine (TMB) one-step substrate reagent (100 µL) was added to each well and incubated for 30 min at RT in the dark with gentle shaking. Finally, stop solution (50 µL) was added to each well, and the absorbance was be measured at 450 nm using an EPOCH Microplate Reader (Biotek Instruments, Inc. [Winooski, Vermont, USA]). The data obtained was analysed using Microsoft Excel 2020 (Microsoft Corporation, Washington, USA) and GraphPad Prism 8 software (GraphPad Software, San Diego, California, USA).

4.2.7.2. p-mTORC1 (S2448) expression (flow cytometry)

The effects of ND + PPV on mTORC1 activity were assessed by quantifying the expression of S2448-phosphorylated mTORC1 using flow cytometry. Phosphorylation of mTORC1 at S2448, a key site regulated by the upstream PI3K/AKT signaling pathway, is a reliable indicator of its activation. Multiple studies have shown that p-mTORC1 (S2448) expression strongly correlates with mTORC1 activity, and it was therefore used in this study to assess mTORC1 activity (138,210,211).

MCF-7 and MDA-MB-231 cells were seeded in T25 cm^2 flasks at a density of 500,000 cells per flask and incubated for 24 hours in a humified atmosphere at 37°C and 5% CO_2 to allow for attachment. Cells were washed with PBS thrice and then exposed to the two ND media. Cells were incubated for 24 hours in a humidified atmosphere at 37°C and 5% CO_2. Subsequently, the cells were exposed to PPV (100 µM) for 24 hours. Cells were then trypsinized and resuspended in 2 mL DMEM, followed by centrifugation (300 x *g*, 5 min). The supernatant was discarded, and the pellet was resuspended in 1 mL of PBS containing 4% formaldehyde and incubated on ice for 20 min. Subsequently, the cells were centrifuged (300 x *g*, 5 min), and the supernatant was discarded. The cells were then resuspended with PBS (1 mL), followed by centrifugation (300 x *g*, 5 min), removal of the supernatant, and resuspension in 1 mL of PBS containing 0.2% Triton X-100 and 1% bovine serum albumin (BSA). This was followed by a 20 min incubation period on ice and thereafter, the cells were centrifuged (300 x *g*, 5 min) and the supernatant was discarded. Next, the pellet was resuspended with PBS containing 1% BSA (1 mL), followed by centrifugation (300 x *g*, 5 min), removal of the supernatant, and resuspension with 100 µL of PBS containing 5% phycoerythrin (PE)-cyanine7 anti-phospho-mTOR (S2448) antibody. The samples were incubated for 30 min in the dark on ice. Subsequently, the cells were centrifuged (300 x *g*, 5 min), and the supernatant was removed. The pellet was then resuspended with PBS containing 1% BSA (1 mL), followed by centrifugation (300 x *g*, 5 min), removal of the supernatant, and resuspension in 500 µL of PBS. Finally, the fluorescence intensity emitted from each sample was measured using a Cytoflex® flow cytometer (Beckman Coulter, Inc. [Brea, California, USA]) available from the Institute of Cellular and Molecular Medicine, Department of Immunology, University of Pretoria, South Africa. A total of 10,000 events was recorded per condition, and data from cell debris was removed from further analysis.

Finally, the samples were analyzed using Kaluza analysis software from Beckman Coulter (Brea, California, USA). All data obtained was further analysed using Microsoft Excel 2020 (Redmond, Washington, USA) and GraphPad Prism 8 software (GraphPad Software, San Diego, California, USA).

4.2.8. Statistical considerations

Quantitative data was obtained from spectrophotometry (cell proliferation, SOD activity and phospho-AMPKα1 (S487) expression) and flow cytometry (cell cycle progression, mitochondrial membrane potential and phospho-mTORC1 (S2448) expression). Flow cytometry analysis involved at least 10,000 events, was conducted three times, and was analyzed using the Kaluza analysis software from Beckman Coulter, Inc. (Brea, California, USA). Furthermore, semi-quantitative and qualitative data was obtained from light microscopy (cell morphological changes) and fluorescent microscopy (O_2^- and H_2O_2 production). For fluorescent microscopy, the fluorescent intensity of at least 100 cells was evaluated per condition using the ImageJ software developed by the National Institutes of Health (Bethesda, Maryland, USA). For cell morphology analysis, the morphology of 100 cells per condition was evaluated, and the number of cells with aberrant morphological changes was recorded for each sample. Three independent experiments were conducted for each technique, and the mean and standard deviation (SD) were calculated. The data are displayed in bar charts and are presented as the means ± SDs. Statistical analysis for significance was performed using a one-way analysis of variance (ANOVA) test at a 0.05 level of significance (P-value < 0.05) with GraphPad Prism 8 software (GraphPad Software, San Diego, California, USA). Moreover, P values are represented in all graphs as follows: * ($P < 0.05$), ** ($P < 0.01$), *** ($P < 0.001$), and **** ($P < 0.0001$) compared to CTR (0 µM PPV); # ($P < 0.05$), ## ($P < 0.01$), and ### ($P < 0.001$) compared to ND1 (0 µM PPV); *x* ($P < 0.05$), *xx* ($P < 0.01$), *xxx* ($P < 0.001$), and *xxxx* ($P < 0.0001$) compared to ND2 (0 µM PPV).

5. Results

5.1. Cell proliferation: Crystal violet staining (spectrophotometry)

To determine the effects of ND + PPV on the proliferation of MCF-7 and MDA-MB-231 cell lines, the crystal violet staining assay was utilized. The crystal violet staining technique was selected over conventional resazurin assays since it provides a reliable measure of cell viability that is not confounded by the potential metabolic changes induced by ND + PPV on mitochondrial respiration (212). This is corroborated by previous studies investigating ND and mitochondrial complex I inhibition, which demonstrated that resazurin assays do not correlate with actual cell numbers; thus, more direct quantification methods, like crystal violet staining, are needed (181). Notably, this assay is cost-effective and simple, incorporating three steps: glutaraldehyde fixation, crystal violet staining, and solubilization using Triton X-100. For this assay, three different growth media (CTR, ND1, and ND2) and a PPV concentration range of 50-200 µM were utilized, since previous

studies demonstrated that PPV within this range exhibits optimal antiproliferative effects in breast tumorigenic cell lines (196).

Due to metabolic plasticity, which allows tumorigenic cells to enhance or sustain proliferation under bioenergetic stress and makes them hypersensitive to mitochondrial complex I inhibitors like PPV, the optimal duration of ND needed to induce a starvation-like proliferative response in both cell lines was evaluated. Three time points (6, 24 and 36 hours) were utilized and selected based on their frequent use in clinical trials without causing severe adverse effects or significant weight loss (213). The proliferation of MCF-7 cells decreased at 6 hours in both ND1 and ND2 by 8% ($P < 0.001$) and 13% ($P < 0.01$) compared to CTR medium, respectively (**Figure 9A**). Although compared to the respective 6-hour marks, propagation in ND1 and ND2 for 24 hours resulted in an increase by 13% and 6% ($P < 0.05$), respectively, indicating a starvation-like proliferative response. Similarly, in the MDA-MB-231 cell line, 6 hour propagation in ND1 and ND2 decreased proliferation by 3% and 18.3% ($P < 0.01$) compared to CTR medium, respectively (**Figure 9B**). Compared to the cells propagated in CTR medium, 24 hours of propagation in ND1 and ND2 resulted in decreases in proliferation by 17.3% ($P < 0.0001$) and 21.7% ($P < 0.01$), respectively. Although, compared to the 6-hour mark, 24 hours of propagation in ND2 did not result in a significant change in proliferation ($P = 0.5$) and instead led to a slight plateau. However, both cell lines demonstrated a significant decrease in proliferation when propagated in ND1 and ND2 for 36 hours. MCF-7 cells cultured in ND1 and ND2 for 36 hours resulted in a 27% ($P < 0.05$) and 36% ($P < 0.01$) decrease in proliferation compared to CTR medium, respectively. Likewise, MDA-MB-231 cells propagated in ND1 and ND2 for 36 hours exhibited a 44% ($P < 0.01$) and 33% ($P < 0.01$) decrease in proliferation compared CTR medium, respectively. Together, these results demonstrate that a 36-hour propagation in ND media leads to excessive decreases in cell proliferation, rendering it unsuitable for PPV sensitivity testing. Moreover, since propagation in ND1 and ND2 led to increased and/or sustained proliferation, indicating starvation-like proliferative responses in both cell lines, all subsequent experiments subjected the cells to 24 hours of ND prior to PPV exposure.

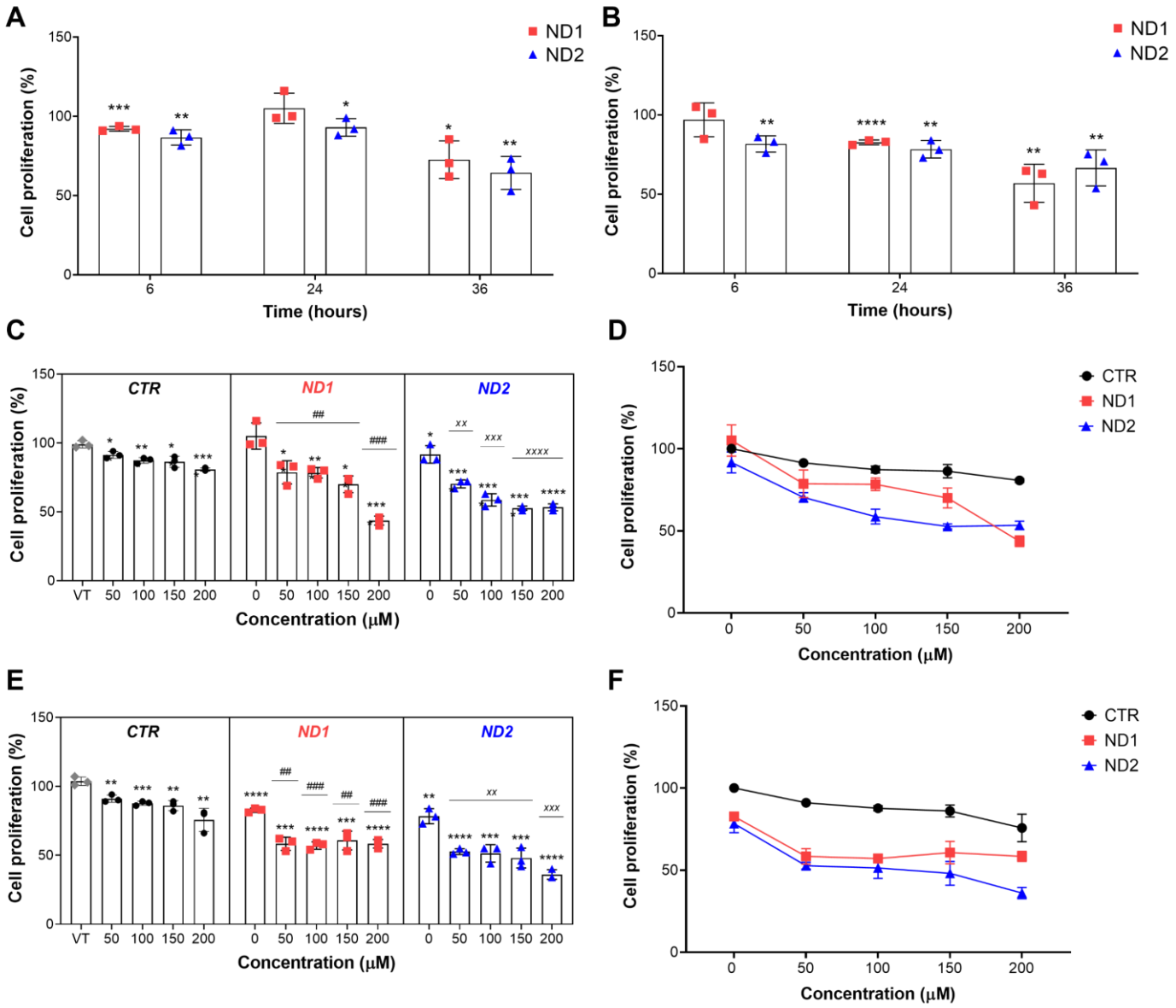

Figure 9. *Effects of ND + PPV on the proliferation of MCF-7 and MDA-MB-231 cells. (A & B) Proliferation of MCF-7 (A) and MDA-MB-231 (B) cells propagated in ND1 (red square data points) and ND2 (blue triangle data points) for various durations (6, 24, and 26 hours), as assessed through crystal violet staining. (C & D) Proliferation of MCF-7 cells propagated in CTR (black circle data points), ND1 and ND2 for 24 hours, followed by exposure to PPV (50 - 200 μM) for 24 hours. Vehicle-treated (VT) cells are represented as bars with grey diamond data points. (E & F) Proliferation of MDA-MB-231 cells propagated in CTR, ND1 and ND2 for 24 hours, followed by exposure to PPV (50 - 200 μM) for 24 hours. The absorbance values for all the experimental conditions were measured against CTR (0 μM PPV) to determine the relative cell proliferation. Data are presented as the means ± SDs of three independent experiments, with statistical significance calculated using a one-way ANOVA. P values are represented as detailed in the statistical considerations section.*

Next, the combination of ND and PPV exposure was evaluated, with cells cultured in both types of ND media or CTR medium for 24 hours, followed by exposure to PPV (50-200 μM) for an additional 24 hours. Previous *in vitro* studies have demonstrated that this concentration range and exposure period yield optimal antiproliferative effects in breast tumorigenic cell lines (196). Both MCF-7 cells (**Figure 9C and 9D**) and

MDA-MB-231 cells (**Figure 9E and 9F**) displayed significantly increased sensitivity to PPV after ND. In the MCF-7 cell line, propagation in CTR medium followed by exposure to 50 µM, 100 µM, 150 µM, and 200 µM PPV resulted in statistically significant decreases in proliferation to 91%, 87%, 86%, and 81% relative to CTR (0 µM PPV), respectively. However, propagation in ND1 and ND2 resulted in a significant sensitization effect, markedly enhancing the antiproliferative effects of PPV. Propagation in ND1 followed by exposure to 50 µM, 100 µM, 150 µM, and 200 µM PPV resulted in statistically significant decreases in proliferation to 79%, 78%, 70%, and 43% relative CTR (0 µM PPV), respectively. The most prominent starvation-mediated sensitization effect in the MCF-7 cell line was observed when cells were cultured in ND2 prior to PPV exposure, resulting in a statistically significant ($P < 0.0001$) decrease in proliferation to 70%, 59%, 53%, and 53% when exposed to 50 µM, 100 µM, 150 µM, and 200 µM PPV, respectively. Corresponding antiproliferative trends were observed in the MDA-MB-231 cell line, where cells cultured in CTR medium and exposed to 50 µM, 100 µM, 150 µM, and 200 µM PPV had statistically significant decreases in proliferation to 91%, 88%, 86% and 76% relative CTR (0 µM PPV), respectively. Furthermore, when compared to the MCF-7 cell line, MDA-MB-231 cells exhibited more prominent sensitization to PPV following propagation in ND1 and ND2. For instance, when cultured in ND1 and exposed to 50 µM, 100 µM, 150 µM, and 200 µM PPV, proliferation decreased to 58%, 57%, 61% and 58% relative to CTR (0 µM PPV), respectively. Similar to the MCF-7 cell line, propagation in ND2 resulted in the greatest starvation-mediated sensitization effect to PPV, with exposure to 50 µM, 100 µM, 150 µM, and 200 µM PPV statistically significantly decreasing proliferation to 53%, 51%, 48% and 36%, respectively. Importantly, in both cell lines, VT-treated cells did not exhibit any statistically significant changes in proliferation compared to CTR (0 µM PPV). The proliferation of MCF-7 cells decreased to 99%, and the MDA-MB-231 cell line increased to 104%, relative to CTR (0 µM PPV).

Thus, these results demonstrate that ND sensitizes both OXPHOS-dependent MCF-7 cells and glycolytic-dependent MDA-MB-231 cells. The antiproliferative effects were observed with increased potency at lower glucose- and glutamine concentrations, particularly in the ND2 condition. These effects were especially evident in the MDA-MB-231 cell line, where ND2 + PPV yielded the most prominent antiproliferative effects. Thus, the degree of sensitization to PPV appears to depend on the concentrations of both glucose and glutamine, as well as the metabolic phenotype of the cell line. Overall, the data indicates that combining ND and PPV yielded significantly greater antiproliferative effects compared either ND or PPV alone. Finally, considering that a recent study demonstrated that 100 µM PPV significantly inhibits mitochondrial complex I in breast tumorigenic cell lines, resulting in a major reduction in oxygen consumption, a critical indicator of mitochondrial activity, this concentration was chosen for further investigation (178). Moreover, the slight plateau observed after exposure to 100 µM PPV further validated the utilization of this concentration for all subsequent experiments.

5.2. Cell morphology: 2D and 3D morphological analysis (light microscopy)

Due to the decrease in proliferation in both cell lines following exposure to ND + PPV, it was essential to investigate the morphological changes to further elucidate the effects of this combinational therapy on cell structure. This was achieved through the utilization of 2D and 3D (PlasDIC) light microscopy methods, which aided in the detailed examination of the prevalence and nature of aberrant morphological changes induced by ND + PPV. A semi-quantitative analysis was conducted on 2D microscopy images, examining the morphology of 100 cells and recording the number of cells exhibiting aberrant morphologies, including rounded morphology (RM), shrunken rounded morphology (SRM), cellular protrusions (CP), and enlarged morphology (EM). Each sample was analyzed in triplicate. These morphological changes were selected as indicators of cellular stress, cell death, and metabolic perturbations based on previous literature (214).

In the MCF-7 cell line, CTR + PPV significantly increased the prevalence of cells demonstrating SRM, CP and EM by 4.3% ($P < 0.01$), 17.7% ($P < 0.001$) and 4% ($P < 0.01$) compared to the CTR (0 µM PPV), respectively (**Figure 10A and 10B**). Although, increases in the number of cells demonstrating these morphological changes were also noted when propagated in ND1 and ND2 only. Propagation in ND1 only led to a statistically significant increase in cells demonstrating SRM by 2.3% ($P < 0.05$), CP by 9.7% ($P < 0.01$), and EM by 2% ($P < 0.05$) compared to CTR (0 µM PPV), respectively (**Figure 10C**). Similarly, propagation in ND2 only, led to a statistically significant increase in cells demonstrating SRM, CP and EM by 3.7% ($P < 0.05$), 15.3% ($P < 0.01$) and 9.3% ($P < 0.05$), respectively (**Figure 10D**). However, the most significant increase in aberrant morphological changes was observed after MCF-7 cells were exposed to ND + PPV. Propagation in ND1 followed by exposure to 100 µM PPV resulted in statistically significant increase in SRM, CP and EM by 4% ($P < 0.01$), 14% ($P < 0.01$) and 14.3% ($P < 0.001$) when compared to CTR (0 µM PPV), respectively. In comparison to ND1, the only statistically significant change observed in aberrant morphologies when exposed to ND1 + PPV was in cells demonstrating EM, where there was a significant increase of 12% ($P < 0.001$). The most pronounced increase in the prevalence of these aberrant morphologies was observed in ND2 + PPV group, where propagation in ND2 followed by exposure to 100 µM PPV resulted in a statistically significant ($P < 0.01$) increase in RM, SRM, CP and EM by 7.3%, 7%, 16.7% and 13.7% compared to CTR (0 µM PPV), respectively. Unexpectedly, compared to ND2, the only statistically significant change in cells exposed to ND2 + PPV was a 7% increase in cells demonstrating RM ($P < 0.01$). Lastly, VT MCF-7 cells did not exhibit any statistically significant changes in RM, SRM, CP and EM with only a 2%, 1%, 2% and 0% change compared to CTR (0 µM PPV), respectively.

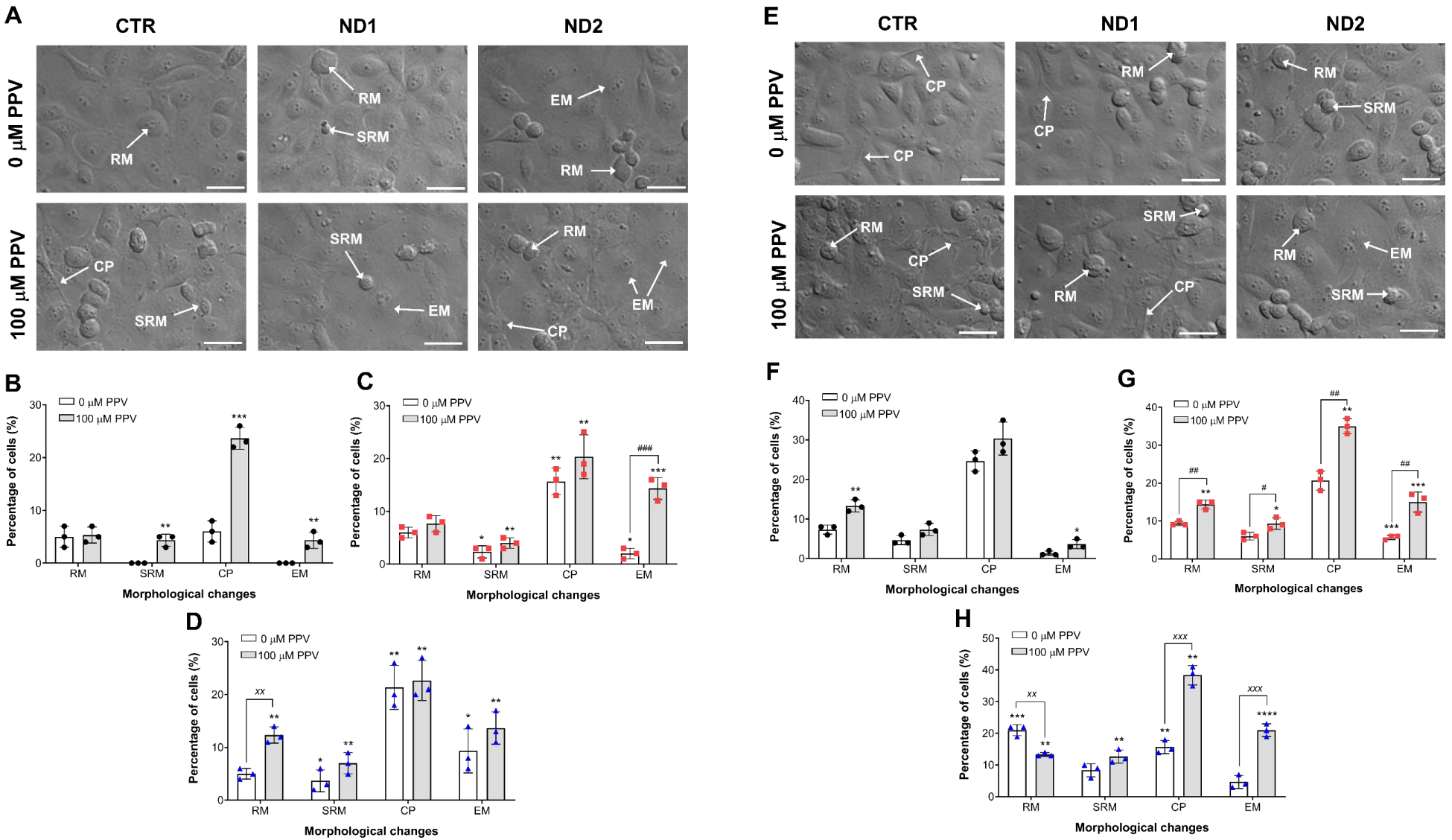

Figure 10. *Morphological changes induced by ND + PPV (100 µM) in MCF-7 and MDA-MB-231 cells. (A) 3D morphology of MCF-7 cells under different experimental conditions; scale bars = 40 µm. (B-D) Percentage of MCF-7 cells exhibiting aberrant morphological changes in the CTR (B), ND1 (C) and ND2 (D) experimental groups. (E) 3D morphology of MDA-MB-231 cells under different experimental conditions; scale bars = 40 µm. (F-H) Percentage of MDA-MB-231 cells exhibiting aberrant morphological changes in the CTR (F), ND1 (G) and ND2 (H) experimental groups. Data are presented as the means ± SDs of three independent experiments, with statistical significance calculated using a one-way ANOVA. P values are represented as detailed in the statistical considerations section.*

In the MDA-MB-231 cell line, the prevalence of aberrant morphologies differed from what observed in the MCF-7 cell line. Cells exposed to CTR + PPV resulted in a statistically significant increase in the prevalence of cells demonstrating RM by 6% ($P < 0.01$) and EM by 2.3% ($P < 0.05$) compared to CTR (0 µM PPV) (**Figure 10E and 10F**). After MDA-MB-231 cells were propagated in ND1 and ND2, there was a decrease in the number of cells exhibiting CP by 4% and 9% ($P < 0.01$) compared to CTR (0 µM PPV) (**Figure 10G and 10H**). However, when exposed to ND1 + PPV and ND2 + PPV, there was a significant increase in cells exhibiting CP by 10.3% ($P < 0.01$) and 13.7% ($P < 0.01$) compared to CTR (0 µM PPV), respectively. When compared to their respective ND controls, cells exposed to ND1 + PPV showed a 14.3% increase ($P < 0.01$) compared to ND1 (0 µM PPV) , and cells exposed to ND2 + PPV showed a significant increase of 22.7% ($P < 0.001$) compared to ND2 (0 µM PPV). Another notable morphological difference compared to the MCF-7 cell line, was the pronounced and significant increase in cells demonstrating EM following ND + PPV. Propagation in ND1 and ND2 alone resulted in an increase in cells demonstrating EM, by 4.3% ($P < 0.01$) and 2.3% compared to CTR (0 µM PPV), respectively. However, there was a prominent statistically significant increase in cells demonstrating EM by 13.7% ($P < 0.001$) in ND1 + PPV and 19.7% ($P < 0.0001$) in ND2 + PPV compared to CTR (0 µM PPV). These results were also statistically significant compared to the ND controls, where exposure to ND1 + PPV resulted in a 9.3% increase ($P < 0.01$) compared to ND1 (0 µM PPV), and exposure to ND2 + PPV resulted in a 16% increase ($P < 0.001$) compared to ND2 (0 µM PPV). Moreover, differences in cells demonstrating RM was observed between ND1 and ND2 groups, where ND1 alone did not yield any significant changes in cells exhibiting RM, but when combined with PPV had a statistically significant ($P < 0.01$) by 7% compared to CTR (0 µM PPV). Conversely, when compared to CTR (0 µM PPV), ND2 resulted in the greatest statistically significant ($P < 0.001$) increase in cell demonstrating RM by 13.6%, but when combined with PPV had a decrease by 7.7% ($P < 0.01$) compared to ND2 (0 µM PPV). Lastly, there were increases in the prevalence of cells demonstrating SRM after exposure to ND1 + PPV by 4.7% ($P < 0.05$) and ND2 + PPV by 8% ($P < 0.01$) compared to the CTR group (0 µM PPV). Overall, these results demonstrate that ND + PPV exerts differential effects on the prevalence of aberrant morphologies in both cell lines, with EM being the most conspicuous change. This increase in cells demonstrating EM was most notably observed in the glycolytic MDA-MB-231 cell line, especially under lower glucose and glutamine conditions (ND2). Finally, VT MDA-MB-231 cells did not exhibit any statistically significant changes in RM, SRM, CP and EM with only a 0.3%, 1%, 2.3% and 1.7% change compared to CTR (0 µM PPV), respectively.

5.3. Cell cycle progression and cell death-induction: Propidium iodide staining (flow cytometry)

Given that ND + PPV induced significant reductions in the proliferation of both MCF-7 and MDA-MB-231 cell lines accompanied with aberrant morphological observations, further analysis was conducted to determine whether these antiproliferative effects were due to cell cycle arrest or the induction of cell death. This was

achieved through the utilization of ethanol fixation, Triton X-100 mediated membrane permeabilization, propidium iodide staining and flow cytometry. Propidium iodide is ideal for analyzing cell cycle progression since it is a fluorogenic compound that intercalates with DNA, enabling accurate quantification of cellular DNA content, which is critical for distinguishing between the different cell cycle phases (G_1, S and G_2/M) (215). Thus, this technique allows for the determination of the percentage and distribution of cells in each phase of the cell cycle through flow cytometric analysis. Furthermore, this assay is valuable tool for assessing cell death induction, particularly apoptosis, as cells in the sub-G_1 phase are characterized by reduced DNA content, a hallmark of DNA fragmentation (215). This fragmented DNA results from endonucleolytic cleavage, a process that occurs during apoptosis, leading to the appearance of a distinct sub-G_1 population.

In the MCF-7 cell line, exposure to ND + PPV did not induce any significant alterations in cell cycle progression, except for a statistically significant increase in the percentage of cells occupying the S phase to 13.9% ($P < 0.05$) when exposed to ND2 + PPV (**Figure 11A and 11B**) However, propagation in ND1 and ND2 alone, also resulted in a statistically significant ($P < 0.01$) increase in cells occupying the S phase to 16.2% and 16.7%, respectively. Contrarily, exposure to CTR + PPV led to a decrease in cells occupying the S-phase to 6% ($P < 0.05$). Additionally, only insignificant changes in the percentage of cells within the sub-G_1 phase were noted when cells were exposed to ND1 alone and in combination with PPV, with increases of 0.28% and 0.26% compared to CTR (0 µM PPV), respectively. Furthermore, the most prominent increase in cells occupying the sub-G_1 phase was observed after propagation in ND2, increasing by 1.44% ($P < 0.001$) compared to the CTR (0 µM PPV) (**Figure 11C**). ND2 + PPV led to an increase of 1.1% ($P < 0.01$), which, although significant, was less prominent than the increase observed with ND2 alone, highlighting an intriguing differential response. Similarly, in the MDA-MB-231 cell line, exposure to ND + PPV did not significantly alter cell cycle progression, while propagation in ND medium alone increased the percentage of cells in the S phase (**Figure 11D and 11E**). Propagation in ND1 and ND2 led to an increased prevalence of cells within the S phase to 11.3% ($P < 0.05$) and 13.1% ($P < 0.01$), respectively. In addition, a decrease in the percentage of cells in the G_1 phase to 72.6% ($P < 0.05$) was observed in ND1 alone, but this effect was not observed when combined with PPV or in ND2 alone (**Figure 11F**). The most significant increase in MDA-MB-231 cells in the sub-G1 phase was observed after exposure to CTR + PPV, with an increase of 0.7% ($P < 0.05$) compared to CTR (0 µM PPV). Exposure to ND1 + PPV resulted in an increase in the percentage of cells in the sub-G_1 phase by 0.5% ($P < 0.01$) compared to the CTR (0 µM PPV). Conversely, ND2 + PPV did not significantly change the percentage of cell occupying sub-G_1 compared to the CTR (0 µM PPV). Collectively, these findings suggest that ND + PPV does not induce cell cycle arrest and exerts comparable effects on cell cycle progression in both cell lines. However, ND alone significantly increases the percentage of cells in the S phase in both cell lines. Lastly, differential effects on the percentage of cells in the sub-G1 phase were observed; however, these changes were predominantly insignificant and are unlikely to have biological relevance.

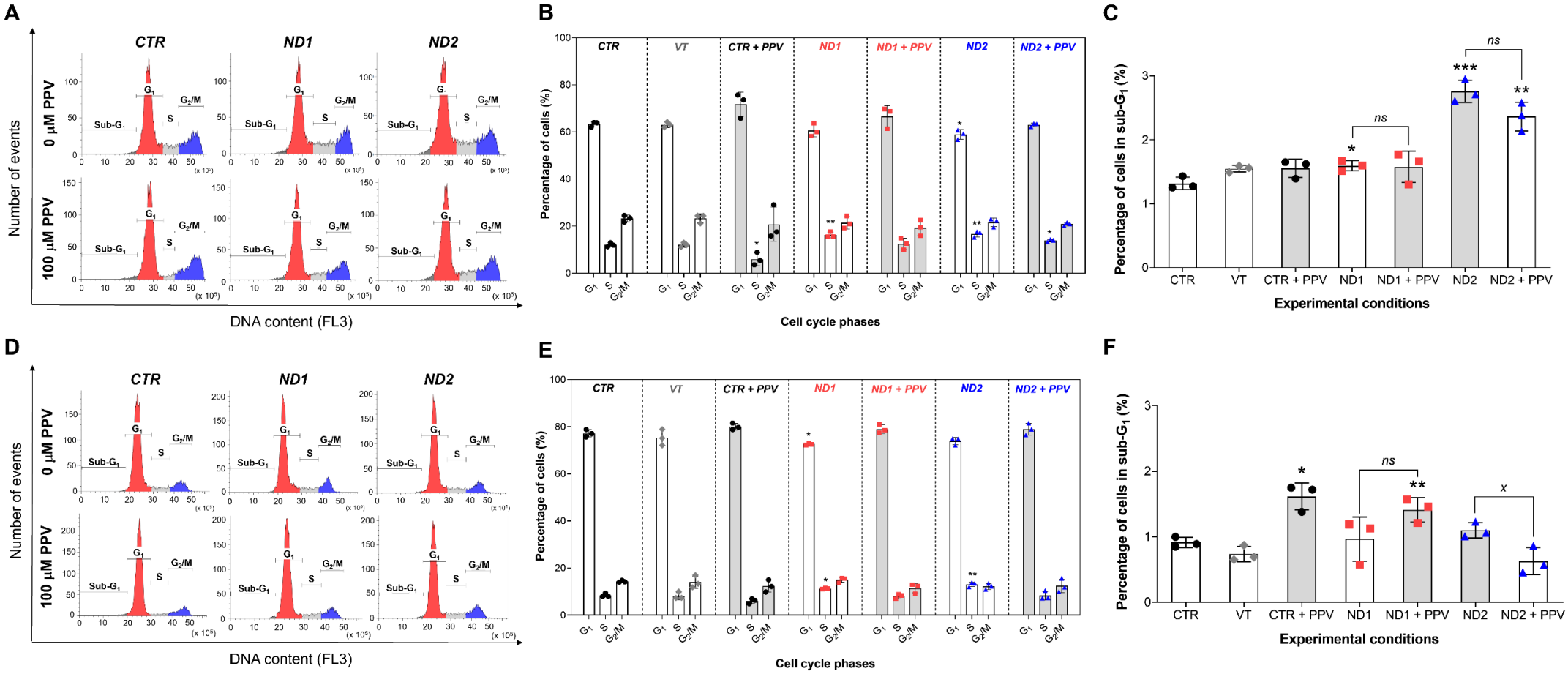

Figure 11. *Cell cycle progression of MCF-7 and MDA-MB-231 cells exposed to by ND + PPV (100 µM). (A) Representative cell cycle fluorescence histograms (FL3) of propidium iodide-stained MCF-7 cells, with sub-G_1, G_1, S, and G_2/M phases indicated in dark grey, red, light grey, and blue, respectively. (B) Percentage of MCF-7 cells occupying G_1, S, and G_2/M phases. (C) Percentage of MCF-7 cells occupying sub-G_1 phase. (D) Representative cell cycle fluorescence histograms (FL3) of propidium iodide-stained MDA-MB-231 cells, with sub-G_1, G_1, S, and G_2/M phases indicated in dark grey, red, light grey, and blue, respectively. (E) Percentage of MDA-MB-231 cells occupying G_1, S, and G_2/M phases in different experimental conditions. (F) Percentage of MDA-MB-231 cells occupying sub-G_1 phase. Data are presented as the means ± SDs of three independent experiments, with statistical significance calculated using a one-way ANOVA. P values are represented as detailed in the statistical considerations section.*

5.4. Oxidative stress: O_2^- and H_2O_2 using DHE and DCFDA staining (fluorescent microscopy)

Given that ND downregulates key metabolic pathways including glycolysis and glutaminolysis, while PPV suppresses OXPHOS via mitochondrial complex I inhibition, the combined effect of ND and PPV on mitochondrial ROS production was assessed (113,114,178). This was achieved by quantifying the levels of O_2^- and H_2O_2 using DHE and DCFDA staining, respectively. Furthermore, O_2^- is one of the primary ROS generated by the mitochondrial electron transport chain, particularly at mitochondrial complex I, making it a useful indicator of oxidative stress and mitochondrial complex I activity (216,217). In addition, H_2O_2, a downstream product of O_2^- dismutation, serves as a stable and diffusible ROS, which can further interact with other molecules to further propagate oxidative damage (218). Therefore, measuring both O_2^- and H_2O_2 provides a comprehensive assessment of mitochondrial ROS production and the potential oxidative stress induced by exposure to ND + PPV. These results may offer valuable insights into the potential mechanisms underlying the antiproliferative effects observed with the combination of ND and PPV, particularly whether these effects are associated with alterations in mitochondrial reactive oxygen species (ROS), specifically O_2^- and H_2O_2. Additionally, this study could shed light on potential alterations in ROS scavenging enzymes, such as superoxide dismutase or catalase, further elucidating the biochemical pathways involved in the observed antiproliferative effects.

In MCF-7 cells, CTR + PPV did not lead to any significant changes in O_2^- production compared to CTR (0 µM PPV) (**Figure 12A and 12B**), while differential effects were observed when cells were propagated in ND mediums alone and in combination with PPV. For instance, compared to the CTR (0 µM PPV), propagation in ND1 resulted in a fold increase in O_2^- production to 1.12 ($P < 0.0001$), while ND2 yielded a fold increase to 1.17 ($P < 0.01$). However, O_2^- production decreased when combined with PPV, with the most notable reduction observed in ND2 + PPV, with a fold decrease to 0.91 ($P < 0.001$) relative to CTR (0 µM PPV), while ND1 + PPV led to a fold decease to 0.94 ($P < 0.01$). In contrast, differential results were observed in H_2O_2 production when exposed to both ND1 and ND2, alone and in combination with PPV (**Figure 12C and 12D**). Compared to CTR (0 µM PPV), propagation in ND1 resulted in a marked fold increase in H_2O_2 production to 1.38 ($P < 0.0001$). However, in combination with PPV, only a slight 1.39-fold increase was observed, exhibiting a non-significant difference between ND1 and ND1 + PPV. Correspondingly, propagation in ND2 alone and in combination with PPV led to statistically significant ($P < 0.001$) increase in H_2O_2 production, with a fold increase to 1.34 and 1.40, compared to CTR (0 µM PPV), respectively. Exposure to CTR + PPV resulted in the least prominent increase in H_2O_2 production, with a fold increase to 1.28 ($P < 0.001$) compared to CTR (0 µM PPV). Importantly, VT MCF-7 cells did not exhibit any statistically significant changes in either O_2^- or H_2O_2 production, showing an insignificant fold increase to 1.02 and 1.03 increase compared to CTR (0 µM PPV), respectively.

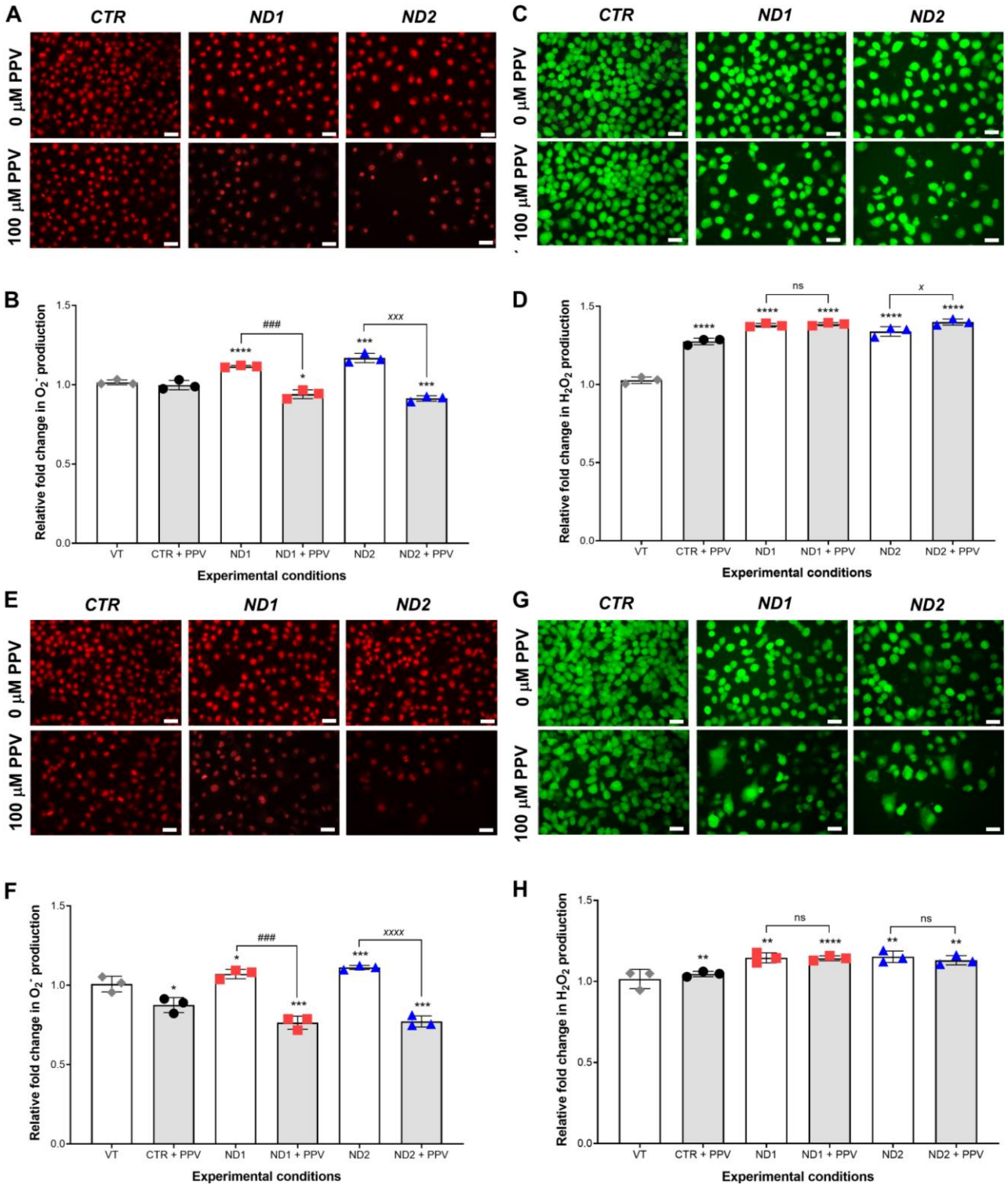

Figure 12. *Relative fold changes in O_2^- and H_2O_2 following ND + PPV (100 µM). (A) Fluorescence micrographs of DHE-stained MCF-7 cells; scale bars = 40 µm. (B) Relative fold changes in O_2^- production in MCF-7 cells. (C) Fluorescence micrographs of DCFDA-stained MCF-7 cells. (D) Relative fold changes in H_2O_2 production in MCF-7 cells. (E) Fluorescence micrographs of DHE-stained MDA-MB-231 cells. (F) Relative fold changes in O_2^- production in MDA-MB-231 cells. (G) Fluorescence micrographs of DCFDA-stained MDA-MB-231 cells (H) Relative fold changes in H_2O_2 production in MDA-MB-231 cells. The mean fluorescence intensity for all conditions was measured against CTR (0 µM PPV) to determine relative fold change values. Data are presented as the means ± SDs of three independent experiments, with statistical significance calculated using a one-way ANOVA. P values are represented as detailed in the statistical considerations section.*

MDA-MB-231 cells exhibited similar alterations in both O_2^- and H_2O_2 production when exposed to ND alone and in combination with PPV, compared to the MCF-7 cell line. Firstly, exposure to CTR + PPV resulted in a fold decrease in O_2^- production to 0.88 ($P < 0.05$) compared to CTR (0 µM PPV) (**Figure 12E and 12F**). Moreover, similar to the MCF-7 cell line, MDA-MB-231 cells propagated in ND1 and ND2 exhibited an upregulation of O_2^- production to 1.07-fold ($P < 0.05$) and 1.12-fold ($P < 0.001$) relative to CTR (0 µM PPV), respectively. Furthermore, upon the combination exposure to PPV, O_2^- production significantly decreased, with ND1 + PPV resulting in a fold decrease to 0.76 ($P < 0.001$) and ND2 + PPV resulting in a fold decrease to 0.77 ($P < 0.001$), compared to CTR (0 µM PPV). However, H_2O_2 production significantly increased in all treatment groups, with the smallest change observed in CTR + PPV with a fold increase to 1.04 ($P < 0.01$) compared to CTR (0 µM PPV) (**Figure 12G and 12H**). Propagation in ND1 alone and in combination with PPV led to statistically significant increases in H_2O_2 production to 1.15 ($P < 0.01$) and 1.14 ($P < 0.0001$), compared to CTR (0 µM PPV), respectively. In addition, compared to CTR (0 µM PPV), propagation in ND2 and in combination with PPV resulted in a fold increase in H_2O_2 production to 1.15 and 1.13, respectively. Notably, no significant changes in H_2O_2 production were observed between ND alone groups and ND + PPV. Finally, VT MDA-MB-231 cells did not exhibit significant changes in either O_2^- or H_2O_2 production compared, with a fold increase to 1.01 and 1.001 compared to CTR (0 µM PPV), respectively.

These findings reveal that ND leads to an increase in O_2^- production in both cell lines, with the most pronounced elevation of O_2^- observed in conditions of lower glucose- and glutamine availability (ND2). Interestingly, when ND is combined with PPV, O_2^- production markedly decreases, exceeding the reduction observed with PPV alone. This effect is more pronounced in the glycolysis-dependent MDA-MB-231 cell line, suggesting a synergistic interaction between ND and PPV in suppressing O_2^- production. In contrast, H_2O_2 production was elevated across all treatment groups in both cell lines, with insignificant changes observed in the ND-treated groups, both alone and in combination with PPV. The greatest increase in H_2O_2 production was seen in the OXPHOS-dependent MCF-7 cell line, indicating that the metabolic profile of each cell line influences its ROS production response. Finally, to further understand the mechanism underlying the decrease in O_2^- but the increase in H_2O_2 following ND + PPV, it is essential to determine how this combination affects mitochondrial SOD activity.

5.5. SOD activity (spectrophotometry)

The ROS scavenging system includes SOD, catalase (CAT), glutathione peroxidase (GPx), peroxiredoxin (PRx), and thioredoxin (TRx) (219) (**Figure 13A**). In the mitochondria, SOD catalyzes the dismutation of O_2^- into H_2O_2 and O_2, which are further converted to H_2O and O_2 by CAT or peroxidases (220). Given that ND + PPV led to a decrease in O_2^- along with an increase in H_2O_2, the influence of SOD activity was further investigated. The determination of SOD activity was conducted using the SOD Activity Determination Kit

(Sigma–Aldrich), which utilizes WST-1, water-soluble tetrazolium salt that produces a soluble formazan dye upon reduction by O_2^- (**Figure 13B**). The amount of formazan generated is linearly related to xanthine oxidase (XO) activity, which is inhibited by SOD. Thus, by measuring the extent of this inhibition through colorimetry, the SOD inhibition rate (%) can be determined, which directly correlates with SOD activity. Lastly, as the absorbance at 450 nm directly correlates with the concentration of O_2^-, SOD activity can be quantified by assessing the reduction in colour intensity at this wavelength.

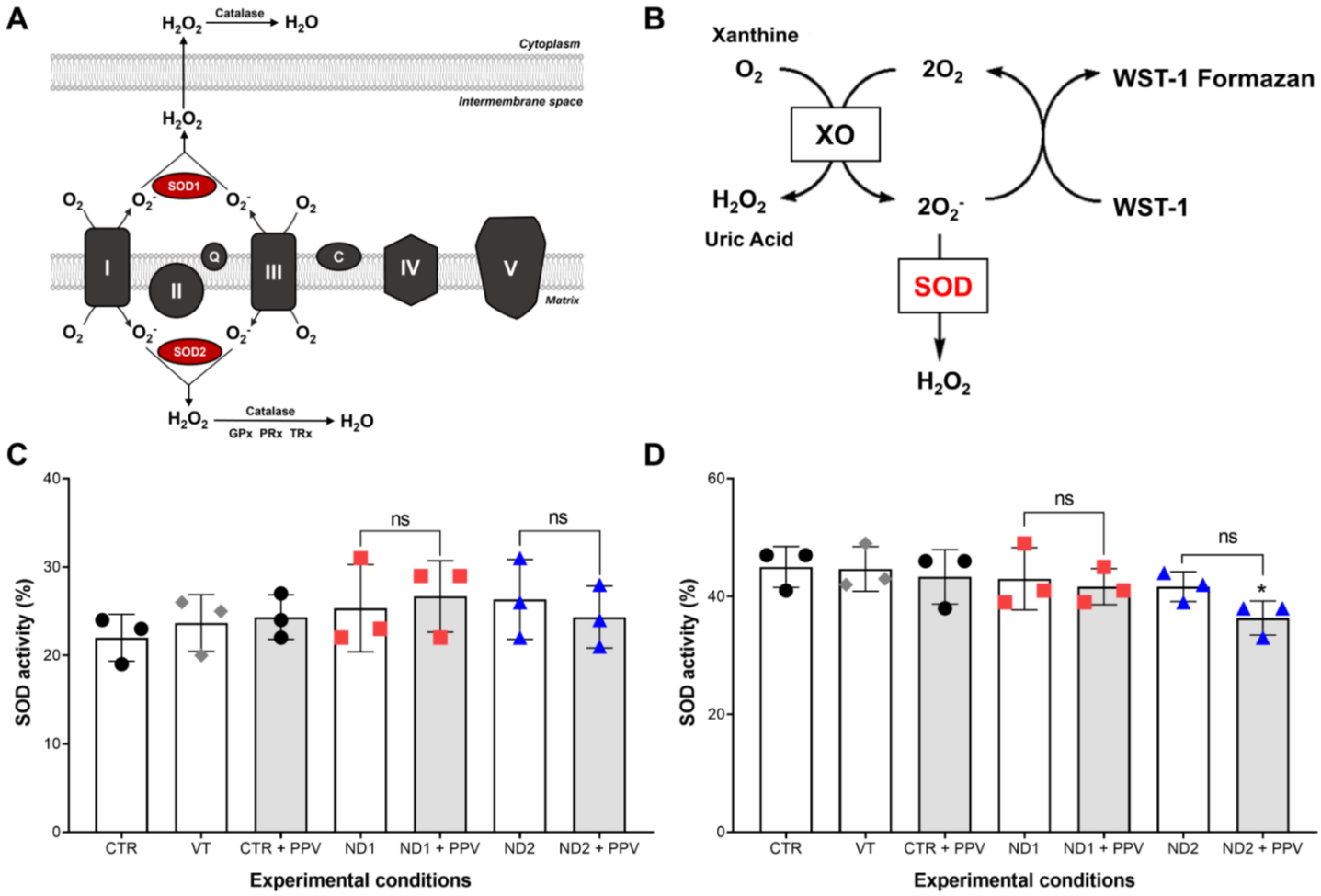

Figure 13. *Impact of ND + PPV (100 µM) on SOD activity in MCF-7 and MDA-MB-231 cells. (A) Mitochondrial ROS scavenging system. Respiratory chain complexes I and III (black) generate O_2^-, which is further converted to H_2O_2 by the SOD system, involving SOD1 an SOD2 within the mitochondrial intermembrane space and matrix, respectively. (B) The SOD activity assay uses WST-1 to produce a formazan dye upon O_2^- reduction. SOD activity is be quantified by assessing the reduction in colour intensity at 450 nm. (C) SOD activity within MCF-7 cells exposed to different experimental conditions. (D) SOD activity within MDA-MB-231 cells exposed to different experimental conditions. Data are presented as the means ± SDs of three independent experiments, with statistical significance calculated using a one-way ANOVA. P values are represented as detailed in the statistical considerations section.*

Despite the decrease in O_2^- and increase in H_2O_2, which are typically associated with enhanced SOD activity, no prominent changes in SOD activity were detected following ND + PPV in either the MCF-7 or MDA-MB-

231 cell lines. In MCF-7 cells, CTR + PPV did not significantly alter SOD activity levels, and similarly, ND1 and ND2, either alone or combined with PPV, showed no significant changes in SOD activity compared to CTR (0 µM PPV) (**Figure 13C**). Additionally, the changes ND1 + PPV and ND2 + PPV exerted on SOD activity were not statistically significant when compared to the respective ND medium controls. Similar results were observed in the MDA-MB-231 cell line, where CTR + PPV, ND1, ND2, and ND1 + PPV did not result in a statistically significant alteration in SOD activity compared to CTR (0 µM PPV) (**Figure 13D**). However, a significant decrease ($P < 0.05$) was observed only in the ND2 + PPV group, with SOD activity decreasing by 8.7% compared to CTR (0 µM PPV). Together, VT MCF-7 and MDA-MB-231 cells exhibited insignificant changes in SOD activity compared CTR (0 µM PPV).

These results demonstrated that ND + PPV does not alter SOD activity, particularly in MCF-7 cells. However, the only significant change in SOD activity was detected in MDA-MB-231 cells, where ND2 + PPV reduced activity. However, this finding does not explain the concurrent decrease in O_2^- and increase in H_2O_2 as noted in the ROS production assays. Therefore, this data suggests that the differential effects of ND + PPV on O_2^- and H_2O_2 in both cell lines are likely due to an alternative mechanism, potentially involving disruption in the ETC, mediated through PPV's mitochondrial complex I inhibitory effects.

5.6. Mitochondrial membrane potential: JC-1 staining (flow cytometry)

The potential disruption in the ETC mediated by ND + PPV was investigated by assessing the effects on mitochondrial membrane potential ($\Delta\psi M$) using the JC-1 staining assay. JC-1 dye exhibits potential-dependent accumulation in mitochondria, where at a lower $\Delta\psi M$, JC-1 remains in its monomeric form, emitting green fluorescence at 529 nm (**Figure 14A**) (209, 221). Conversely, at an elevated $\Delta\psi M$, JC-1 forms red fluorescent aggregates and accumulates within the mitochondria, emitting fluorescence at 590 nm (209, 221). Consequently, mitochondrial polarization can be assessed by measuring the red/green fluorescence intensity ratio, where a lower ratio indicates depolarization and a higher ratio indicates hyperpolarization. In the MCF-7 cell line, exposure to CTR + PPV resulted in a marked decrease in JC-1 red fluorescence intensity, as indicated by the two-parameter (dual-colour fluorescence) density plot (**Figure 14B**). Consequently, the decrease in JC-1 aggregates led to a significant fold reduction in the red/green ratio to 0.26 ($P < 0.001$) relative to CTR (0 µM PPV) (**Figure 14C**). However, propagation in ND1 and ND2 did not result in a significant fold change in the red/green ratio. In contrast, the addition of PPV to ND resulted in the most prominent decrease in the red/green ratio, with ND1 + PPV and ND2 + PPV resulting in statistically significant ($P < 0.0001$) fold decreases to 0.11 and 0.12 relative to CTR (0 µM PPV), respectively. The red/green ratio changes observed in ND1 + PPV and ND2 + PPV were not statistically significant when compared to the respective ND medium controls.

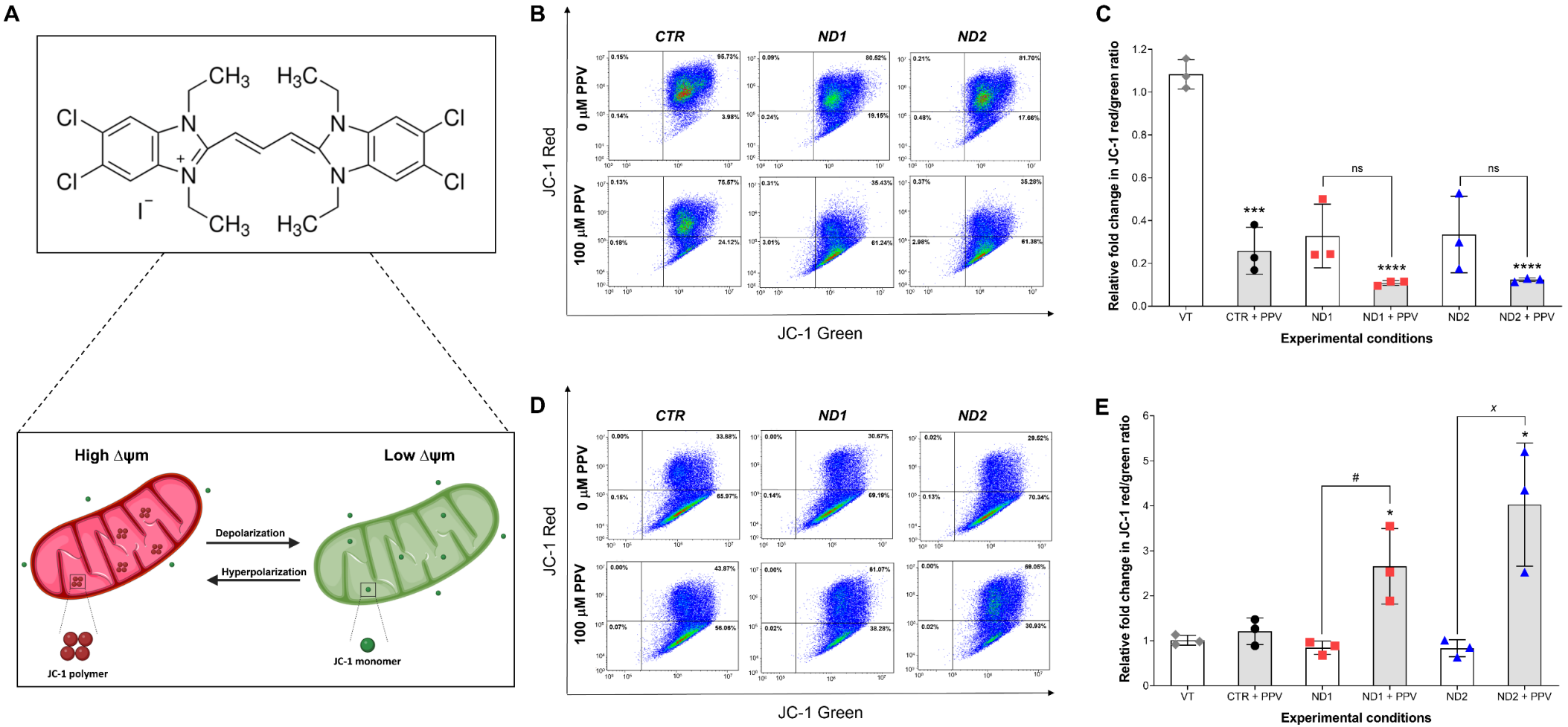

Figure 14. *Effects of ND + PPV (100 µM) on the mitochondrial membrane potential of MCF-7 and MDA-MB-231 cells. (A) JC-1 chemical structure and principle of assay. JC-1 accumulates in mitochondria based on membrane potential, emitting green fluorescence (JC-1 monomer) at low ΔψM and at higher ΔψM emits red fluorescence (J1-aggregates). (B) Two-parameter (dual-color fluorescence) density plot of MCF-7 cells, showing JC-1 green (fluorescein isothiocyanate [FITC]) fluorescence on the X-axis and red (PE) fluorescence on the Y-axis. Quadrant one demonstrates cells with high ΔψM, while quadrant four demonstrates cells with low ΔψM. (C) Relative fold changes in the JC-1 red/green ratio of MCF-7 cells exposed to different experimental conditions. (D) Two-parameter density plot of MDA-MB-231 cells. (E) Relative fold changes in the JC-1 red/green ratio of MDA-MB-231 cells exposed to different experimental conditions. cells. The mean fluorescence intensity for all conditions was measured against CTR (0 µM PPV) to determine relative fold change values. Data are presented as the means ± SDs of three independent experiments, with statistical significance calculated using a one-way ANOVA. P values are represented as detailed in the statistical considerations section.*

Contrasting results were observed in the MDA-MB-231 cell line, where CTR + PPV, ND1 and ND2 did not lead to a significant change in JC-1 red fluorescence intensity in the two-parameter density plot, resulting in an insignificant fold change in the red/green ratio relative to CTR (0 µM PPV) (**Figure 14D and 14E**). Notably, the addition of PPV to ND1 and ND2 resulted in a prominent and significant increase in JC-1 red fluorescent intensity as depicted in the density plot, consequently contributing to a statistically significant ($P < 0.05$) fold increase to 2.65 and 4.02 relative to CTR (0 µM PPV), respectively. Moreover, the red/green ratio changes observed in ND1 + PPV and ND2 + PPV were statistically significant ($P < 0.05$) when compared to the respective ND medium controls. Lastly, both MCF-7 and MDA-MB-231 VT cells did not exhibit any statistically significant changes in red/green ratio compared to CTR (0 µM PPV), respectively.

The results obtained indicate that PPV alone, and in combination with ND, leads to the depolarization (decreased ΔψM) of the mitochondrial membrane in MCF-7 cells, with insignificant differences observed between the ND1 and ND2 groups. Similarly, in the MDA-MB-231 cell line, propagation in ND1 and ND2 resulted in a slight depolarization (decreased ΔψM) of the mitochondrial membrane. However, upon the addition of PPV to ND mediums, a significant increase in the red/green ratio was observed, indicating that ND + PPV causes hyperpolarization (increased ΔψM) of the mitochondrial membrane. Therefore, the JC-1 staining assay demonstrates that ND + PPV exerts diametrically opposing effects on ΔψM in MCF-7 and MDA-MB-231 cells. These findings highlight the distinct mitochondrial responses to ND + PPV treatment across different breast tumorigenic cell lines, suggesting that the underlying mechanisms may vary significantly depending on the breast cancer subtype and metabolic phenotype

5.7. AMPK and mTORC1 signalling: p-AMPKα1 (S487) and p-mTORC1 (S2448) expression

Previous literature has demonstrated that the combination of fasting and mitochondrial complex I inhibition reduces the proliferation of tumorigenic cells by activating AMPK and inhibiting mTORC1, two key signaling proteins involved in nutrient sensing and growth (53,65,181). Thus, to elucidate the cell signalling mechanism by which ND + PPV induces antiproliferative effects in breast tumorigenic cells, the expression of two key phosphorylation sites, namely p-S487 on AMPK and p-S2448 on mTORC1, were investigated. AMPK consists of three subunits, with AMPKα serving as the master regulator of cellular energy demands. In nutrient-rich conditions, the catalytic α1 subunit of AMPK is phosphorylated at S487 by AKT, which inhibits AMPK activity by preventing T172 phosphorylation by LKB1, a crucial step for AMPK activation (**Figure 15A**) (146,147). Therefore, S487 phosphorylation on AMPKα1 can serve as a valuable indicator of AMPK activity and was investigated through sandwich ELISA.

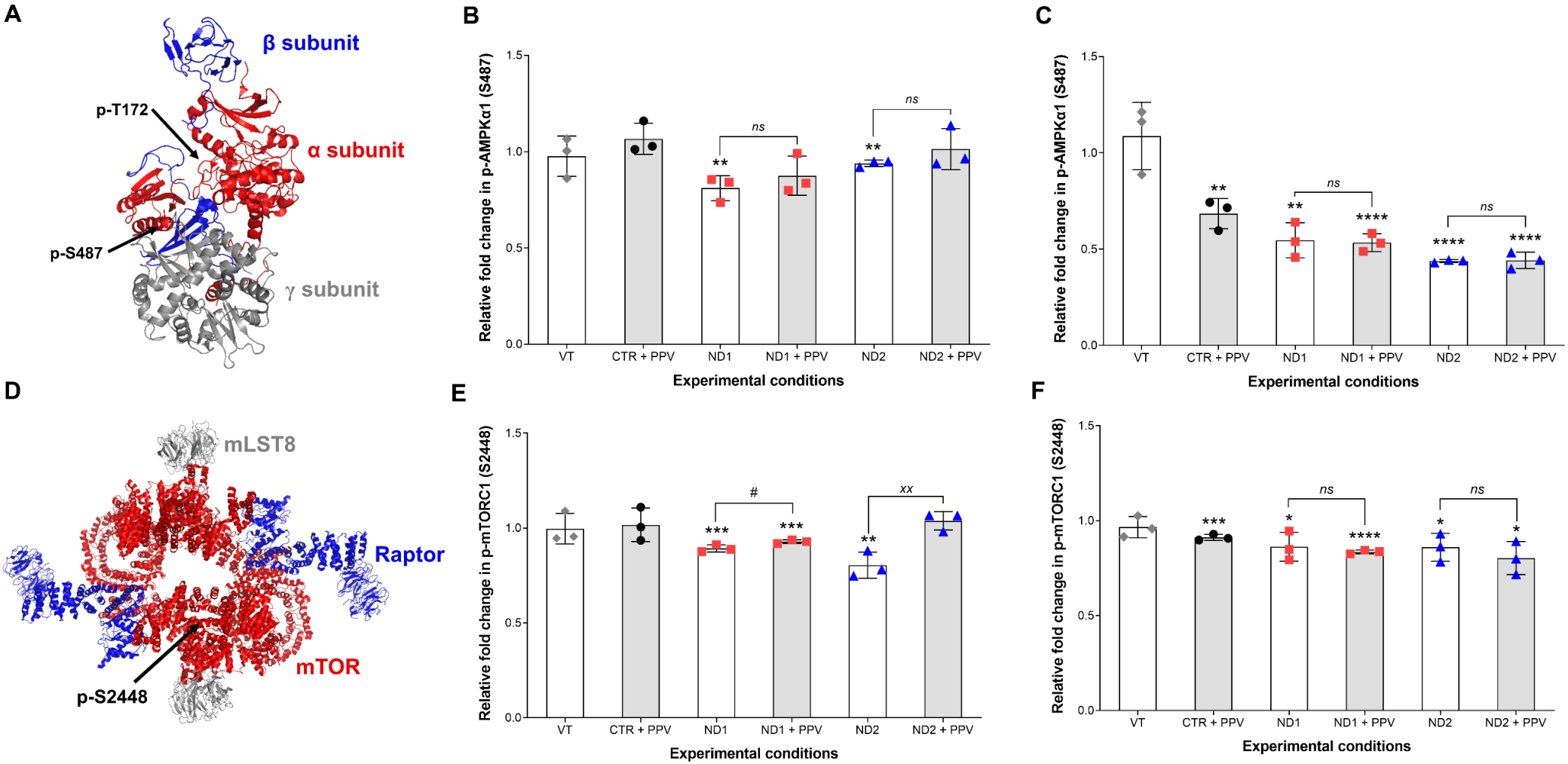

Figure 15. *Effects of ND + PPV (100 µM) on p-AMPKα1 (S487) and p-mTORC1 (S2448) expression. (A) Protein model of mammalian AMPK, created with PyMOL using crystal structure obtained from Protein Data Bank (PDB-4RER) as a template. (B) Relative fold changes in the expression of p-AMPKα1 (S487) in MCF-7 cells exposed to different experimental conditions. (C) Relative fold changes in the expression of p-AMPKα1 (S487) in MDA-MB-231 cells. (D) Protein model of mammalian mTORC1, created with PyMOL using crystal structure obtained from Protein Data Bank (PDB-5H64) as a template. (E) Relative fold changes in the expression of p-mTORC1 (S2448) in MCF-7 cells. (F) Relative fold changes in the expression p-mTORC1 (S2448) in MDA-MB-231 cells. All absorbencies and mean fluorescence intensities were measured against CTR (0 µM PPV) to determine relative fold change values. Data are presented as the means ± SDs of three independent experiments, with statistical significance calculated using a one-way ANOVA. P values are represented as detailed in the statistical considerations section.*

In the MCF-7 cell line, exposure to CTR + PPV did not result in a statistically significant change in p-AMPKα1 (S487) expression relative to CTR (0 µM PPV) (**Figure 15B**). However, propagation in ND1 and ND2 led to a statistically significant ($P < 0.01$) fold decrease in p-AMPKα1 (S487) expression to 0.81 and 0.94 relative to CTR (0 µM PPV), respectively. Although, the addition of PPV to both ND mediums did not result in statistically significant changes compared to CTR (0 µM PPV) and the respective ND controls. Contrary results were noted in the MDA-MB-231 cell line, where PPV alone, and in combination with ND resulted in significant decreases in p-AMPKα1 (**Figure 15C**) (S487). For instance, exposure to CTR + PPV led to a fold decrease to 0.68 ($P < 0.01$) relative to CTR (0 µM PPV). Propagation in ND1 and ND2 resulted in an even fold greater decrease to 0.55 ($P < 0.01$) and 0.43 ($P < 0.0001$) relative to CTR (0 µM PPV), respectively. Likewise, exposure to ND1 + PPV and ND2 + PPV led to a fold decrease in p-AMPKα1 (S487) expression to 0.53 ($P < 0.0001$) and 0.44 ($P < 0.0001$) relative to CTR (0 µM PPV), respectively. In comparison to their respective ND controls, no statistically significant changes were observed in both the ND1 + PPV and ND2 + PPV groups. Moreover, no statistically significant changes were noted in VT MCF-7 and MDA-MB-231 relative to CTR (0 µM PPV), respectively. Overall, these results demonstrate that ND + PPV exerts differential effects on p-AMPKα1 (S487) expression in both cell lines. Nutrient-deprived MCF-7 cells exhibited a decrease in p-AMPKα1 (S487) expression, indicative of increased AMPK activity, but this effect was reversed upon the addition of PPV. Similarly, nutrient-deprived MDA-MB-231 cells exhibited a substantial decrease in p-AMPKα1 (S487) expression, with non-statistically significant changes observed when combined with PPV compared to ND alone.

Owing to the decrease in p-AMPKα1 (S487) expression in the MDA-MB-231 cell line, which is indicative of an increase in AMPK activity, and given that AMPK can directly inhibit mTORC1, the effect of ND + PPV on mTORC1 activity was investigated by quantifying the expression of p-mTORC1 (S2448) (141). The multi-subunit heterotrimeric protein kinase mTORC1 consists of three core components: mTOR, mammalian lethal with SEC13 protein 8 (mLST8), and Raptor (**Figure 15D**) (222). The phosphorylation of mTORC1 at S2448 within the mTOR unit is crucial for activation and directly correlates with mTORC1 activity, making it a reliable indicator of mTORC1 activity (223). In the MCF-7 cell line, exposure to CTR + PPV did not statistically significantly alter p-mTORC1 (S2448) expression relative to CTR (0 µM PPV) (**Figure 15E**). The expression of p-mTORC1 (S2448) exhibited a significant fold decrease in MCF-7 propagated in ND1 and ND2 to 0.89 ($P < 0.001$) and 0.80 ($P < 0.01$), respectively. Exposure to ND1 + PPV led to a fold reduction in p-mTORC1 (S2448) expression to 0.93 ($P < 0.001$) relative to CTR (0 µM PPV), and this fold change was also statistically significant ($P < 0.05$) compared to ND1 alone. However, ND2 + PPV resulted in a non-statistically significant fold increase in p-mTORC1 (S2448) expression to 1.04 relative to CTR (0 µM PPV), but exhibited a statistically significant ($P < 0.01$) increase in expression compared to ND2 alone. Furthermore, MDA-MB-231 cells exposed to CTR + PPV exhibited a statistically significant fold decrease ($P < 0.001$) in

p-mTORC1 (S2448) expression to 0.91 relative to CTR (0 µM PPV) (**Figure 15F**). Propagation in ND1 and ND2 led to the same statistically significant ($P < 0.05$) fold decrease to 0.86 relative to CTR (0 µM PPV). Upon exposure to PPV, MDA-MB-231 cell propagated in ND1 exhibited a significant fold decrease to 0.84 ($P < 0.0001$); however, statistically insignificant to ND1 alone. Likewise, exposure to ND2 + PPV led to a significant decrease ($P < 0.05$) to 0.80 relative to CTR (0 µM PPV), but statistically insignificant compared ND2 alone.

Collectively, the results indicate a correlation between p-mTORC1 (S2448) expression and p-AMPKα1 (S487) expression. For example, in MCF-7 cells, ND2 + PPV led to a slight increase in both p-AMPKα1 (S487) and p-mTORC1 (S2448) expression, whereas ND1 resulted in a statistically significant decrease at both phosphorylation sites. This correlation was further corroborated in the MDA-MB-231 cell line, where ND1 and ND2, both alone and in combination with PPV, led to statistically significant decreases in p-AMPKα1 (S487) and p-mTORC1 (S2448) expression. Notably, cells propagated in ND2 alone and those exposed to ND2 + PPV showed the significant decreases in p-AMPKα1 (S487) and p-mTORC1 (S2448) expression in the MDA-MB-231 cell line. This suggests that reduced glucose- and glutamine concentrations, combined with PPV, increase AMPK activity while decreasing mTORC1 activity. Interestingly, the addition of PPV to nutrient-deprived MCF-7 cells appears to lead to a significant increase in mTORC1 activity compared to ND alone, an effect not observed in MDA-MB-231 cells. This ultimately demonstrates that ND + PPV exerts cell line-specific effects on both AMPK and mTORC1 activity.

6. Discussion

The current state of breast cancer treatment in SA reveals significant disparities compared to the USA, particularly regarding the access to affordable targeted therapies for financially constrained patients (1–3). This highlights an urgent need for cost-effective strategies that can be integrated into the existing breast cancer care framework in SA. An ideal therapeutic approach should minimize side effects, be widely accessible in the South African public health sector, be SAHPRA-approved, and have a well-established safety profile to maximize translational outcomes. Short-term fasting emerges as a promising lifestyle intervention, shown to impair tumor metabolism by reducing blood glucose and glutamine levels and to reduce chemotherapy-induced side effects (113,114,119-221). However, fasting alone has not demonstrated substantial improvements in tumor regression or overall survival *in vivo*, potentially owing to metabolic plasticity, which allows for cell survival through increased reliance on OXPHOS for ATP production (53,65). Therefore, inhibiting mitochondrial complex I during fasting could potentially exacerbate the bioenergetic stress in breast tumorigenic cell (53,65,162). In pursuit of an affordable and accessible mitochondrial complex I inhibitor for breast cancer patients, we explored repurposing PPV, a SAHPRA-approved drug for cerebral vasospasm.

However, the effects of physiological glucose- and glutamine concentrations, simulating fasting, combined with PPV on metabolically distinct breast tumorigenic cell lines remained to be explored. Thus, this study was the first to explore the *in vitro* effects of physiological glucose and glutamine deprivation and PPV (ND + PPV) on OXPHOS-dependent (MCF-7) and glycolysis-dependent (MDA-MB-231) cell lines.

To determine whether ND + PPV exerts antiproliferative effects, the crystal violet staining assay was utilized since this assay provides a more reliable measure of cell viability compared to resazurin assays, which can be confounded by changes in mitochondrial respiration induced by ND + PPV (181,212). The data obtained from the crystal violet staining assay demonstrated that ND significantly enhances the antiproliferative effects of PPV in both cell lines, especially under reduced glucose- and glutamine conditions, as noted in ND2. Notably, neither PPV nor ND alone significantly inhibited cell proliferation in either of the cell lines, indicating that ND sensitizes breast tumorigenic cells to the mitochondrial complex I inhibitory effects of PPV, although the degree of sensitization depends on the metabolic phenotypes of the cells. Furthermore, the most pronounced anti-proliferative effect was observed in the MDA-MB-231 cell line, likely due to its glycolytic phenotype and increased reliance on OXPHOS during ND, potentially contributing to the heightened PPV sensitivity (57–59). These findings align with previous literature reporting that nutrient-deprived MDA-MB-231 cells exhibit substantial metabolic plasticity under ND, as evident by a significant 40% increase ($P < 0.01$) in basal cellular oxygen consumption rate (key indicator of mitochondrial respiration), compared to the control glucose condition (25.52 mM) (66). In addition, further studies have demonstrated that MDA-MB-231 cells exhibit increased sensitivity to MET under glucose deprivation compared to MCF-7 cells, where the 24-hour IC_{50} of MET in MDA-MB-231 cells was 6.4 times higher than that of MCF-7 cells (224). Thus, the dual inhibition of glycolysis and glutaminolysis by ND and OXPHOS by PPV may potentially synergistically impair ATP production and redox balance in MDA-MB-231 cells, resulting in a more pronounced decrease in proliferation compared to that in MCF-7 cells. Previous literature has shown that MCF-7 cells exhibit increased glutamine synthetase expression, enabling *de novo* glutamine production under ND and sustaining their biosynthetic and redox demands (58,59). This mechanism may explain the reduced antiproliferative effects observed with ND + PPV in the MCF-7 cells. Furthermore, the potential reductions in ATP production leading to severe bioenergetic stress induced by ND + PPV may further explain the cell line-dependent decreases in proliferation observed with ND + PPV. Previous research has shown that ND significantly lowered steady-state ATP levels (~70%) in MDA-MB-231 cells, while only moderately inhibiting ATP production (~30%) in MCF-7 cells, an effect that, when combined with PPV, may lead to further decreases in ATP production (59). Nonetheless, the precise cell signalling mechanism through which ND + PPV exerts its antiproliferative effects remains to be elucidated. One potential mechanism could be the increased AMP/ATP ratio, reflecting bioenergetic stress, which consequently leads to the activation of LKB1 and phosphorylation of AMPK at T172, facilitating its activation (147). Activated AMPK then inhibits mTORC1, thereby limiting protein synthesis and

proliferation, as confirmed by previous studies exploring a combinational approach using ND + MET (53,64,141,181).

Since exposure to ND + PPV resulted in significant decreased proliferation, the prevalence of aberrant morphological changes was quantified in the same conditions. When propagated in ND1 and ND2, MCF-7 cells exhibited increased cell protrusions, where MDA-MB-231 cells exhibited a decrease. The decrease in cell protrusions observed in MDA-MB-231 cells may indicate a reduction in migratory capacity, supported by previous studies demonstrating that 24-hour glucose deprivation significantly decreases ($P < 0.05$) the migration of MDA-MB-231 cells compared to cells in control medium (225). However, ND + PPV led to an increase in cell protrusions in the MDA-MB-231 cell line, an effect potentially observed due to PPV's inhibitory effects on PDE10A, a cyclic adenosine monophosphate (cAMP) hydrolyzing enzyme (226,227). The inhibition of PDE10A results in an increase in cAMP, which could be further amplified by ND, leading to the hyperactivation of protein kinase A (PKA) (191). Furthermore, PKA is a tetramer comprising two regulatory subunits and two catalytic subunits, and it is activated upon the binding of cAMP to the regulatory subunits (228,229). In the absence of cAMP, PKA remains inactive because a constitutive regulatory subunit dimer forms, suppressing the activity of the two catalytic subunits (229). Upon cAMP binding, a conformational change occurs, exposing the catalytic subunits and restoring kinase activity. However, the precise mechanism underlying this release is still not fully understood. (230,231). Moreover, the proposed mechanism by which ND + PPV increases cell protrusions through the hyperactivation of PKA is supported by previous research demonstrating a strong correlation between PKA activity and protrusion formation, with PKA inhibition leading to a decrease in protrusion formation (232). However, previous studies have demonstrated that PPV alone significantly reduces the migration of MDA-MB-231 despite increased cell protrusions (233). The increased cell protrusions are likely due to mechanisms unrelated to migration, with macropinocytosis potentially being involved. Macropinocytosis, a nutrient-scavenging strategy employed by tumorigenic cells under nutrient stress, involves the uptake of extracellular proteins and subsequent degradation within endolysosomes, providing amino acids that fuel tumorigenic metabolism and growth (234,235). This process is closely linked to actin cytoskeleton dynamics, where membrane ruffles form via actin polymerization (234,235). Ultimately, this could aid in elucidating why MCF-7 cells exhibit fewer protrusions compared to MDA-MB-231 cells after exposure to ND + PPV, since MCF-7 cells possess increased rates of glutamine synthesis during ND (58,59). However, further research is needed to determine whether this is the mechanism by which MDA-MB-231 cells increase protrusions. Furthermore, AMPK has been shown to play a significant role in activating macropinocytosis, with Jayashankar et al. demonstrating that AMPK activation in nutrient-deprived TNBC cells (4T1 and MDA-MB-468) stimulates macropinocytosis, as evident by increased macropinosome formation (236). Moreover, ND + PPV led to an increase in enlarged morphologies in both cell lines, with the greatest increase observed in the MCF-7 and

MDA-MB-231 when exposed to ND1 + PPV and ND2 + PPV, respectively. The observed increase in enlarged cells may indicate the induction of oncosis-related cell death, as cellular swelling is a hallmark of oncosis, typically triggered by ATP depletion (237,238). The significant decrease in ATP leads to the disruption of the inner mitochondrial membrane barrier, resulting in the collapse of ion gradients and loss of mitochondrial membrane potential (237). This further exacerbates the decline in cellular ATP levels leading to membrane ion pumps failing culminating in the cell swelling (237). Lastly, both MCF-7 and MDA-MB-231 cells exhibited an increased prevalence of shrunken rounded morphology when exposed to ND + PPV, suggesting the induction of apoptotic cell death (239). This is corroborated by studies involving ND and MET, where the combination significantly increased ($P < 0.001$) both early and late apoptosis in MDA-MB-231 cells compared to the control medium and MET alone (224). Nonetheless, the mechanism by which ND + PPV potentially induces oncotic and apoptotic cell death still remains to be elucidated.

Given that ND + PPV induced significant reductions in the proliferation in both MCF-7 and MDA-MB-231 cell lines accompanied by aberrant morphology, further analysis was conducted to determine whether these antiproliferative effects were due to cell cycle arrest. In both MCF-7 and MDA-MB-231 cell lines, exposure to ND + PPV did not lead to significant alterations in cell cycle progression. However, both ND1 and ND2 alone significantly increased the percentage of MCF-7 and MDA-MB-231 cells in the S phase, suggesting a promotion of DNA synthesis. This data is corroborated by previous studies which demonstrated that MCF-7 and MDA-MB-231 cells propagated in glucose and/or glutamine deprived mediums have an increased percentage of cells in the occupying the S phase, although the reasoning behind this is not entirely understood (18). Nonetheless, these results suggest that the antiproliferative effects of ND + PPV on both cell lines are not due to cell cycle arrest. This finding aligns with the work of Ferretti et al., who demonstrated that glucose deprivation combined with MET did not induce cell cycle arrest, although their study was conducted using hepatocellular carcinoma cells (HepG2) (181). Furthermore, mostly insignificant changes were observed, with no exposure group exceeding 2% in the percentage of cells in the sub-G_1 phase in either cell line. The absence of noteworthy changes in the sub-G_1 fractions may be attributed to the 24-hour exposure period of PPV. Previous studies have demonstrated that exposing MD-MB-231 cells to 100 µM PPV for 48 hours and 72 hours resulted in 7.36% ($P < 0.05$) and 11.25% ($P < 0.05$) of cells in the sub-G_1 phase, respectively, highlighting a time-dependent response (196). Furthermore, previous research by Visagie et al. demonstrated that as little as 6 hours of exposure to ND significantly increased the percentage of cells in the sub-G_1 phase to 21% ($P < 0.05$) (18). However, the effects of ND at 24 hours was not investigated, leaving the lack of notable changes in sub-G_1 observed after 24-hour exposure to ND1 and ND2 unexplained and to be further elucidated. Based on previous findings, it would be expected that the combination of ND and PPV would significantly increase the sub-G_1 fractions; however, this was not observed in the current study. A proposed mechanism for the lack of change in sub-G_1 fractions is the hyperactivation of PKA, supported by previous

research showing that ND activates PKA in MDA-MB-231 cells, thereby protecting against cell death (240). Activated PKA indirectly activates the anti-apoptotic protein B-cell lymphoma 2 (BCL-2) by inhibiting BCL2-associated agonist of cell death (BAD), a protein that suppresses BCL-2 (241). The addition of PPV to nutrient-deprived breast tumorigenic cells may further activate PKA by increasing cAMP levels as previously discussed, thereby reducing cell death and, consequently, the proportion of cells in the sub-G_1 phase. Nevertheless, the propidium iodide staining assay shows that ND + PPV does not induce cell cycle arrest or apoptotic-like cell death in either cell line, suggesting that alternative mechanisms, such as oxidative stress, may be involved.

Excessive mitochondrial ROS results in oxidative stress, which is known to impede cell proliferation (21). Therefore, we aimed to determine if the combination of ND and PPV resulted in oxidative stress that correlated with the antiproliferative effects of ND + PPV. The quantification of O_2^- production was initially conducted since mitochondrial complex I is a major O_2^- source, making it a useful marker for oxidative stress and mitochondrial complex I activity (242). Propagation in nutrient-deprived media significantly increased O_2^- production in both cell lines, especially when utilizing the lower glucose- and glutamine concentrations present in ND2. These findings align with literature reporting that nutrient-deprived MDA-MB-231 cells exhibited a 40% increase in mitochondrial respiration, suggesting increased mitochondrial complex I activity following ND (66). However, ND + PPV led to a significant reduction in O_2^-, compared with CTR + PPV, indicating enhanced inhibition of mitochondrial complex I with ND, especially within MDA-MB-231 cells. The findings from the current study is contraindicatory with previous research on ND + MET, where mitochondrial complex I inhibition by MET in TNBCs did not differ between cells cultured in nutrient-deprived compared to CTR medium (53). The reduction in O_2^- following ND + PPV may be attributed to enhanced mitophagy, potentially driven by ATP depletion (243). Elevated AMP/ATP ratios result in the phosphorylation of AMPK at T172, mediated by LKB1 (147). Subsequently, AMPK can activate ULK1, an upstream kinase critical for initiating mitophagy, leading to mitochondrial degradation and a consequent decrease in O_2^- (244). ULK1 is the catalytic component of the autophagy pre-initiation complex and has been shown to stimulate mitophagy by phosphorylating BCL2-interacting protein 3 (BNIP3) at the serine residue 17 (S17) (244). Phosphorylation of BNIP3 at S17 by ULK1 promotes its interaction with microtubule-associated protein 1A/1B light chain 3 (LC3), thereby targeting mitochondria to autophagosomes (245,246). However, further studies are necessary to confirm whether mitophagy contributes to the observed reduction in O_2^- mediated through ND + PPV in both cell lines.

In light of the decreased O_2^- presence after exposure to ND + PPV in both cell lines, the quantification of H_2O_2 was conducted. Significant increases in H_2O_2 production was noted after ND + PPV in both cell lines, with insignificant differences between ND alone and in combination with PPV, consistent with findings from research involving ND + MET research (53). The MCF-7 cell line exhibited a more prominent increase in

H_2O_2 levels compared to the MDA-MB-231 cell line, which is consistent with previous findings in that catalase activity is significantly lower in MCF-7 cells than in MDA-MB-231 cells (59). Moreover, the increase in H_2O_2 in both cell lines propagated in ND1 and ND2 alone and in combination with PPV may be mediated by glutamine deprivation, which disrupts the synthesis of GSH, a crucial component of the GPx enzyme, leading to H_2O_2 accumulation (247). However, this does not account for the simultaneous decrease in O_2^- and increase in H_2O_2 observed with ND + PPV. Thus, subsequent analyses were conducted to determine whether the differential effects on ROS were due to increased SOD activity. Although both cell lines exhibited only slight and negligible changes, with no statistically significant differences observed in the MCF-7 cell line across all treatment groups, a statistically significant decrease in SOD activity was noted in the MDA-MB-231 cell line following exposure to ND2 + PPV. However, although SOD1 expression (as determined through the GEO RNA-sequencing data set [GSE100878]) does not significantly differ between the two cell lines, MDA-MB-231 cells possess a two-fold higher expression of SOD2 (59). Thus, the data obtained herein may not fully elucidate which SOD subtype has been affected, potentially influencing the observed decrease in SOD activity. Collectively, the data obtained in this current study suggests that ND + PPV alters O_2^- and H_2O_2 levels in a manner potentially independent of SOD, suggesting that ND + PPV decreases O_2^- levels by possibly disrupting its production through mitochondrial complex I inhibition or the induction of mitophagy. Furthermore, the increase in H_2O_2 may involve other factors, including reduced GPx and catalase activity, necessitating the need for further investigation. Overall, this data suggests that ND + PPV may exert antiproliferative effects in both cell lines through a mechanism that does not appear to be directly related to changes in O_2^- and H_2O_2 levels. Although H_2O_2 levels increased consistently across experimental conditions, only ND + PPV, and not ND alone, significantly reduced proliferation, which could indicate a mechanism independent of mitochondrial H_2O_2 production. This suggests that alternative mitochondrial mechanisms, particularly $\Delta\psi M$, may be involved in mediating the antiproliferative effects of ND + PPV.

In light of the fact that mitochondrial complex I is the central OXPHOS enzyme targeted in this study, the effects of ND + PPV were assessed on $\Delta\psi M$, which serves a universal indicator of mitochondrial health and activity. The inhibition of mitochondrial complex I has been widely demonstrated to lead to reduced $\Delta\psi M$, and similar results were anticipated following ND + PPV exposure in both cell lines (248). However, opposing results were obtained, with ND + PPV leading to a significant reduction in $\Delta\psi M$ in the MCF-7 cell line and a substantial increase in the MDA-MB-231 cell line. Firstly, considering the MCF-7 cell line, only the PPV-treated groups showed significant changes, with ND1 + PPV and ND2 + PPV showing the most prominent decreases. This is likely due to PPV's inhibition of mitochondrial complex I, disrupting the ETC and reducing $\Delta\psi M$ and ATP production. Moreover, the increased reliance on OXPHOS in the MCF-7 cell line may contribute to the significant decrease in $\Delta\psi M$ following exposure to ND + PPV. Furthermore, mitochondrial complex I activity has been shown to be approximately 60% higher in MCF-7 cells compared to MDA-MB-

231 cells (59). Therefore, PPV-mediated inhibition of mitochondrial complex I in MCF-7 cells could result in a more pronounced decrease in ΔψM due to their greater dependency on mitochondrial complex I and OXPHOS. Furthermore, a potential reason for the mitochondrial membrane depolarization in the MCF-7 cell line compared to the MDA-MB-231 may be the significant increase in H_2O_2 levels in MCF-7 cells, since increased H_2O_2 levels have been shown to lead to decreased ΔψM (249). Although a decrease in ΔψM is associated with the induction of apoptosis, MCF-7 cells did not exhibit a significant increase (<2%) in the percentage of cells in the sub-G_1 phase, as indicated by the propidium iodide staining assay. This suggests that MCF-7 cells may be in the early phase of apoptosis, with prolonged exposure to PPV potentially increasing the percentage of cells in the sub-G_1 phase, as demonstrated by Gomes et al., who showed a time-dependent rise in sub-G_1 cells in breast tumorigenic cells exposed to PPV (196). Thus, future research should focus on investigating the effects of ND + PPV using Annexin V and propidium iodide staining to confirm the early induction of apoptosis.

On the other hand, the significant mitochondrial membrane hyperpolarization in MDA-MB-231 cells was observed only in ND + PPV-treated groups, with the greatest increase occurring under lower glucose- and glutamine concentrations (ND2). This finding is unique since mitochondrial complex I inhibition typically leads to depolarization, indicating that ND + PPV induces distinct alterations in mitochondrial function in MDA-MB-231 cells. Interestingly, Bhat et al. demonstrated that PPV is capable of increasing ΔΨM in human cortical neurons and this was accompanied by a decrease in ROS production (250). However, this effect was not observed in the CTR + PPV groups, suggesting that PPV's hyperpolarization effect on the mitochondrial membrane is dependent on ND in MDA-MB-231 cells. Although an increase in ΔΨM typically indicates improved mitochondrial activity, the hyperpolarization observed after ND2 + PPV exposure may also suggest the early induction of mitochondria-dependent apoptosis. However, the semi-quantitative morphological analysis conducted in this study revealed that the most prominent aberrant change in MDA-MB-231 cells exposed to ND2 + PPV was an increase in enlarged morphology, indicative of cell swelling and potentially the induction of oncosis-related cell death (237,238). Oncosis is frequently triggered by ATP depletion and thus, an additional cell signalling mechanism may also contribute to the hyperpolarization of the mitochondrial membrane, namely the LKB1-AMPK pathway (237,238). A recent study conducted by Wang et al. demonstrated that MET increases ΔΨM though the activation of AMPK, which directly phosphorylates the outer mitochondrial membrane protein, A-Kinase Anchoring Protein 1 (AKAP1), that is essential in maintaining ΔΨM (251,252). AKAP1 anchors PKA near the mitochondria, where it is capable of directly phosphorylating dynamin-related protein 1 (DRP1) ultimately leading to increased ΔΨM. Thus, the simultaneous activation of PKA and AMPK induced by ND + PPV in MDA-MB-231 cells may be a key mechanism driving mitochondrial membrane hyperpolarization, in contrast to the depolarization observed in MCF-7 cells (253).

The relationship between PKA and AMPK remains unclear; however, studies have demonstrated that PKA inhibits AMPK activation by phosphorylating AMPKα1 at S487, which blocks upstream kinases including LKB1 from phosphorylating T172 (254). Hence, owing to PPVs ability to activate PKA, the effects of ND + PPV were investigated on p-AMPKα1 (S487) expression. The data obtained in this study indicates that ND + PPV has cell line specific effects on p-AMPKα1 (S487) expression. In the MCF-7 cell line, there was no significant change in expression, whereas MDA-MB-231 cells exhibited a significant decrease in p-AMPKα1 (S487) expression upon exposure to ND + PPV. Furthermore, the lack of changes observed in MCF-7 cells exposed to ND + PPV may possibly be mediated by AKT and PKA activation, both of which are known to phosphorylate this amino acid residue (146,254). Previous genomic analyses have shown that MCF-7 cells possess an *AKT1* mutation, leading to increased expression, which may explain why the effects of ND + PPV did not result in significant decreases as seen in MDA-MB-231 cells (59). Moreover, the addition of PPV to nutrient deprived-MCF-7 cells slightly reversed the decrease in p-AMPKα1 (S487) expression, potentially due to PPV-mediated PKA activation. These results are supported by Sprengler et al., who demonstrated that the addition of 3-isobutyl-1-methylxanthine (IBMX), an inhibitor of PDE10A, triggers PKA-mediated phosphorylation of AMPKα1 at S487 (254). In contrast, MDA-MB-231 cells exhibited decreased p-AMPKα1 (S487) expression, raising questions about the relationship between PKA activation and AMPK activity, as previous findings indicate that PKA activation increases S487 expression, thereby reducing AMPK activity. However, further research is required to determine the effects of ND + PPV on PKA activity and p-AMPKα1 (T172). Lastly, the decrease in p-AMPKα1 (S487) expression in MDA-MB-231 cells may further explain the increased presence of cell protrusions after exposure to ND + PPV compared to MCF-7 cells. Increased AMPK activation likely enhances macropinocytosis in MDA-MB-231 cells compared to MCF-7 cells. This is supported by findings from Jayashankar et al., who showed that AMPK activation in nutrient-deprived TNBC cells (4T1 and MDA-MB-468) promotes macropinocytosis, as indicated by increased macropinosome formation (236).

Given that previous literature has demonstrated that tumorigenic cells exposed to ND + MET exhibit increased activation of AMPK via LKB1, ultimately leading to the inhibition of mTORC1, we next explored the effects of ND + PPV on mTORC1 activity. When ATP levels drop, mTORC1 signalling is decreased, resulting in the activation of 4EBP and ULK1, as well as the inhibition of S6K1, which consequently reduces protein synthesis and cellular proliferation (131,132,153). Hence, owing to the decrease in p-AMPKα1 (S487), indicating an increase in AMPK activity, the effects of ND + PPV were investigated on a key phosphorylation site known to lead to the activation of mTORC1, namely p-mTORC1 (S2448). The results demonstrate that in MCF-7 cells, the greatest decrease in p-mTORC1 (S2448) expression was observed in the ND1 and ND2 groups. Notably, the addition of PPV to ND2 resulted in a statistically significant increase in expression, indicating that the inhibitory effects of ND2 on mTORC1 are reversed by PPV. However, it is important to note that

S2448 is only one of several key phosphorylation sites involved in mTORC1 activation. Other sites, such as those on mTORC1 subunits like Raptor, may also be affected (255). For instance, Jewell et al. showed that S791 on Raptor is phosphorylated by PKA, leading to mTORC1 inhibition in an AMPK-independent manner (255). Moreover, in MDA-MB-231, both ND alone and in combination PPV led to a statistically significant decrease in p-mTORC1 (S2448) expression, although this was insignificant compared to their respective ND medium controls. The most prominent decrease (>20%) was observed after exposure to ND2 + PPV, suggesting that this combination inhibits mTORC1 activity. However, further research is needed to determine whether this translates to functional inhibition of mTORC1. Future studies should focus on analysing the phosphorylation status of downstream mTORC1 targets (e.g., 4E-BP1, S6K) to confirm functional inhibition and further assess its impact on protein synthesis and cell growth. The MDA-MB-231 cell data suggests that ND + PPV downregulates AMPK activity by decreasing S487 phosphorylation, leading to reduced mTORC1 activity via lower S2448 phosphorylation. Overall, this data suggests that ND + PPV exerts stimulatory effects on AMPK and inhibitory effects on mTORC1 primarily in glycolysis-dependent TNBC cells. These findings support the initially proposed cell signaling mechanism underlying the antiproliferative effects of ND + PPV; however, further research is needed to clarify the role of the AMPK/mTOR pathway in this context.

Overall, the data obtained in this study contribute valuable insights into the fields of cancer systems biology and targeted drug repurposing by harnessing metabolic plasticity for therapeutic intervention in breast tumorigenic cells using PPV, a SAHPRA-approved small-molecule drug. Specifically, it provides further knowledge of how starvation-induced metabolic stress, combined with increased mitochondrial complex I activity, exposes a metabolic vulnerability that could be exploited for therapeutic purposes. Overall, these findings suggest that the combination of fasting and PPV may represent a viable, cost-effective approach for treating breast cancer, particularly, TNBC. However, further *in vitro* and *in vivo* studies are needed to fully elucidate the biochemical pathways altered by ND + PPV and to assess the effects on tumor growth and volume. Ideally, these studies should be conducted using patient-derived xenograft mouse models with TNBC tumors from women of African descent. Lastly, it is important to note that the potential impact of this study extends beyond its immediate findings; it aims to contribute to the ongoing efforts to address the unmet need for affordable and accessible breast cancer therapies for patients in SA, with implications that also extend to the broader sub-Saharan Africa region. This study underscores the importance of integrating geographical, economic, and accessibility considerations in the development of new metabolic cancer therapies.

7. Study limitations and future perspectives

This study provides valuable insights into the combined effects of fasting-mimetic ND and PPV on proliferation, morphology, cell cycle progression, oxidative stress, SOD activity, ΔΨM, and AMPK/mTOR

signaling in metabolically distinct breast tumorigenic cell lines. However, several limitations should be acknowledged along with considerations for future research. One key limitation is that ND was restricted to the deprivation of glucose and glutamine, without considering essential growth factors such as insulin and IGF-1. Both are known to activate pro-survival and proliferative signaling pathways, including the PI3K/AKT/mTOR pathway. Thus, future studies should investigate the effects of insulin and IGF-1 deprivation alongside ND to provide a more comprehensive understanding of the antiproliferative effects observed in both MCF-7 and MDA-MB-231 cell lines. Furthermore, owing to PPV's polypharmacological properties, it remains unclear whether the antiproliferative effects observed were solely due to mitochondrial complex I inhibition or whether PPV's effects on cAMP and PKA signaling also played a role. PPV is known to increase intracellular cAMP levels, leading to PKA activation, which may influence cell survival and proliferation independently of mitochondrial complex I inhibition. Future studies should therefore investigate the contribution of cAMP/PKA signaling to the observed effects, helping to elucidate whether these pathways act synergistically with mitochondrial complex I inhibition or drive distinct cellular responses.

This study was conducted exclusively on breast tumorigenic cell lines without assessing potential differential responses in non-tumorigenic cells. Including non-tumorigenic cells, such as human breast epithelial cells (MCF10A), in future studies would help determine whether the observed antiproliferative effects are selective for breast tumorigenic cells. Additionally, while the study provides insights into ND-induced metabolic shifts, further validation using metabolic respiration assays (such as Seahorse XF analysis) is needed. These assays would provide a real-time functional assessment of oxygen consumption rate (OCR) and extracellular acidification rate (ECAR), helping to elucidate how ND + PPV impacts mitochondrial respiration and glycolytic activity. Lastly, these findings were generated in vitro, which presents inherent limitations in predicting clinical relevance. To assess the therapeutic potential and safety of ND + PPV, further studies should evaluate in vivo efficacy using murine xenograft models. Such studies will be critical in determining whether this combination therapy effectively reduces tumor volume while minimizing systemic side effects. Overall, by addressing these limitations, future research can strengthen the translational potential of ND combined with PPV-mediated mitochondrial complex I inhibition as a cost-effective therapeutic strategy for breast cancer.

8. Conclusion

In this study the impact of physiologically relevant ND mediums and PPV-mediated mitochondrial complex I inhibition on metabolically distinct breast tumorigenic cells was investigated. The results demonstrate that ND sensitizes both MCF-7 and MDA-MB-231 breast tumorigenic cells to PPV, leading to a significant decrease in proliferation, an increase in morphologies indicative of oncotic cell death, no induction of cell

cycle arrest, and differential effects on O_2^- and H_2O_2 levels indicative of oxidative stress, potentially independent of SOD. Cell line-dependent results were obtained when investigating ΔΨM, with ND + PPV leading to significant depolarization of the mitochondrial membrane in MCF-7 cells and hyperpolarization in MDA-MB-231 cells, respectively. Lastly, only MDA-MB-231 cells exhibited a decrease in p-AMPKα1 (S487) and reduced p-mTORC1 (S2448), ultimately indicating activation of the AMPK pathway and inhibition of mTORC1 signaling. Through the combination of the above biochemical- and functional studies, this study demonstrates that MDA-MB-231 cells exhibited the most prominent changes, suggesting that inducing a shift from aerobic glycolysis to OXPHOS mediated through ND, notably sensitizes glycolysis-dependent breast tumorigenic cells to PPV-mediated mitochondrial complex I inhibition. Overall, these findings suggest that the combination of fasting and PPV could pave the way for a cost-effective and accessible therapeutic strategy for breast cancer, offering significant promise, especially in the treatment of TNBC.

9. Ethical considerations

The project received ethical approval (30/2024) from the Research Ethics Committee of the Faculty of Health Sciences (University of Pretoria, Pretoria, Gauteng, South Africa).

10. Funding

This research was funded by grants from the Cancer Association of South Africa (A0V741, A0W228) and the Medical Research Council (A0W110), awarded to A.M. Joubert. Additional support was received from the Struwig Germeshuysen Trust (AON074), the School of Medicine Research Committee of the University of Pretoria (AOR984), and the South African National Research Foundation (N00375, N0059).

11. Acknowledgements

Statistical support was obtained from P.J. Becker, Research Office, Health Sciences Faculty, University of Pretoria, South Africa. Access to the CytoFLEX flow cytometer (Beckman Coulter, Inc., Brea, California, USA) was facilitated by the Institute for Cellular and Molecular Medicine (ICMM), University of Pretoria, South Africa. Finally, to my supervisors, Dr Visagie, Professor Lee and Professor Joubert for their unwavering support and guidance throughout this project. Their mentorship has been instrumental in advancing our shared goal of developing accessible and effective breast cancer treatments for underserved populations in Africa.

12. References

1. Bray F, Laversanne M, Sung H, Ferlay J, Siegel RL, Soerjomataram I, et al. Global cancer statistics 2022: GLOBOCAN estimates of incidence and mortality worldwide for 36 cancers in 185 countries. CA Cancer J Clin. 2024 May 1;74(3):229–63. Available from: https://doi.org/10.3322/caac.21834
2. Mattila PO, Babar ZUD, Suleman F. Assessing the prices and affordability of oncology medicines for three common cancers within the private sector of South Africa. BMC Health Serv Res. 2021;21(1):661. Available from: https://doi.org/10.1186/s12913-021-06627-6
3. Sung H, Ferlay J, Siegel RL, Laversanne M, Soerjomataram I, Jemal A, et al. Global Cancer Statistics 2020: GLOBOCAN Estimates of Incidence and Mortality Worldwide for 36 Cancers in 185 Countries. CA Cancer J Clin. 2021 May 1;71(3):209–49. Available from: https://doi.org/10.3322/caac.21660
4. Breast cancer [Internet]. Who.int. 2022 [cited 2023 Aug 17]. Available from: https://www.who.int/news-room/fact-sheets/detail/breast-cancer
5. Li Y, Tang XQ, Bai Z, Dai X. Exploring the intrinsic differences among breast tumor subtypes defined using immunohistochemistry markers based on the decision tree. Sci Rep. 2016;6(1):35773. Available from: https://doi.org/10.1038/srep35773
6. Schettini F, Brasó-Maristany F, Kuderer NM, Prat A. A perspective on the development and lack of interchangeability of the breast cancer intrinsic subtypes. NPJ Breast Cancer. 2022;8(1):85. Available from: https://doi.org/10.1038/s41523-022-00451-9
7. Cejalvo JM, Martínez de Dueñas E, Galván P, García-Recio S, Burgués Gasión O, Paré L, et al. Intrinsic Subtypes and Gene Expression Profiles in Primary and Metastatic Breast Cancer. Cancer Res. 2017 Apr 30;77(9):2213–21. Available from: https://doi.org/10.1158/0008-5472.CAN-16-2717
8. Mthembu J, Bhuiyan M. Profile of molecular subtyping of breast cancer and clinicopathological features in Mankweng Hospital breast oncology clinic, Limpopo Province, South Africa. S Afr Med J. 2021 Dec 1;111(11b):1132-1135. Available from: https://doi.org/10.7196/SAMJ.2021.v111i11b.16104
9. Acheampong T, Kehm R, Terry M, Argov E, Tehranifar P. Incidence Trends of Breast Cancer Molecular Subtypes by Age and Race/Ethnicity in the US From 2010 to 2016. JAMA Netw. 2020 Aug 17;3(8):e2013226–e2013226. Available from: https://doi.org/10.1001/jamanetworkopen.2020.13226
10. Hendricks CL, Alessandrini M, Pepper MS. Equitable access to cell and gene therapies in South Africa: opportunities and hurdles. Gene Ther. 2023;30(1):180–6. Available from: https://doi.org/10.1038/s41434-021-00309-y
11. M MB, R BS. Health and Health Care in South Africa — 20 Years after Mandela. N Engl J Med. 2014 Oct 2;371(14):1344–53. Available from: https://doi.org/10.1056/NEJMsr1405012

12. Vanderpuye V, Dadzie MA, Huo D, Olopade OI. Assessment of Breast Cancer Management in Sub-Saharan Africa. JCO Glob Oncol. 2021 Nov 29;(7):1593–601. Available from: https://doi.org/10.1200/GO.21.00282
13. Osei Afriyie D, Krasniq B, Hooley B, Tediosi F, Fink G. Equity in health insurance schemes enrollment in low and middle-income countries: A systematic review and meta-analysis. Int J Equity Health. 2022;21(1):21. Available from: https://doi.org/10.1186/s12939-021-01608-x
14. Health insurance coverage in the United States: 2022 [Internet]. Census.gov. 2023 [cited 2024 May 24]. Available from: https://www.census.gov/library/publications/2023/demo/p60-281.html
15. DeBerardinis RJ, Chandel NS. Fundamentals of cancer metabolism. Sci Adv. 2023 Aug 20;2(5):e1600200. Available from: https://doi.org/10.1126/sciadv.1600200
16. Sainero-Alcolado L, Liaño-Pons J, Ruiz-Pérez MV, Arsenian-Henriksson M. Targeting mitochondrial metabolism for precision medicine in cancer. Cell Death Differ. 2022;29(7):1304–17. Available from: https://doi.org/10.1038/s41418-022-01022-y
17. Pavlova NN, Thompson CB. The Emerging Hallmarks of Cancer Metabolism. Cell Metab. 2016 Jan 12;23(1):27–47. Available from: https://doi.org/10.1016/j.cmet.2015.12.006
18. Visagie MH, Mqoco TV, Liebenberg L, Mathews EH, Mathews GE, Joubert AM. Influence of partial and complete glutamine-and glucose deprivation of breast-and cervical tumorigenic cell lines. Cell Biosci. 2015;5(1):37. Available from: https://doi.org/10.1186/s13578-015-0030-1
19. Seth Nanda C, Venkateswaran SV, Patani N, Yuneva M. Defining a metabolic landscape of tumours: genome meets metabolism. Br J Cancer. 2020;122(2):136–49. Available from: https://doi.org/10.1038/s41416-019-0663-7
20. Altman BJ, Stine ZE, Dang C V. From Krebs to clinic: glutamine metabolism to cancer therapy. Nat Rev Cancer. 2016;16(10):619–34. Available from: https://doi.org/10.1038/nrc.2016.71
21. Scialò F, Fernández-Ayala DJ, Sanz A. Role of Mitochondrial Reverse Electron Transport in ROS Signaling: Potential Roles in Health and Disease. Front Physiol. 2017;8. Available from: https://doi.org/10.3389/fphys.2017.00428
22. Peng Y, Wang Y, Zhou C, Mei W, Zeng C. PI3K/Akt/mTOR Pathway and Its Role in Cancer Therapeutics: Are We Making Headway? Front Oncol. 2022;12. Available from: https://doi.org/10.3389/fonc.2022.819128
23. Tian Y, Zhao L, Gui Z, Liu S, Liu C, Yu T, et al. PI3K/AKT signaling activates HIF1α to modulate the biological effects of invasive breast cancer with microcalcification. NPJ Breast Cancer. 2023;9(1):93. Available from: https://doi.org/10.1038/s41523-023-00598-z
24. Deng H, Chen Y, Li P, Hang Q, Zhang P, Jin Y, et al. PI3K/AKT/mTOR pathway, hypoxia, and glucose metabolism: Potential targets to overcome radioresistance in small cell lung cancer. Cancer pathog ther. 2023;1(1):56–66. Available from: https://doi.org/10.1016/j.cpt.2022.09.001

25. Li X, Hu S, Cai Y, Liu X, Luo J, Wu T. Revving the engine: PKB/AKT as a key regulator of cellular glucose metabolism. Front Physiol.2024;14.Available from: https://doi.org/10.3389/fphys.2023.1320964.
26. Fontana F, Giannitti G, Marchesi S, Limonta P. The PI3K/Akt Pathway and Glucose Metabolism: A Dangerous Liaison in Cancer. Int J Biol Sci. 2024;20(8):3113–25. Available from: https://doi.org/10.7150/ijbs.89942
27. Szwed A, Kim E, Jacinto E. Regulation and metabolic functions of mTORC1 and mTORC2. Physiol Rev. 2021 Feb 18;101(3):1371–426. Available from: https://doi.org/10.1152/physrev.00026.2020
28. Kim J, Tchernyshyov I, Semenza GL, Dang C. HIF-1-mediated expression of pyruvate dehydrogenase kinase: A metabolic switch required for cellular adaptation to hypoxia. Cell Metab. 2006;3(3):177–85. Available from: https://doi.org/10.1016/j.cmet.2006.02.002
29. Jha MK, Suk K. Pyruvate Dehydrogenase Kinase as a Potential Therapeutic Target for Malignant Gliomas. Brain Tumor Res Treat. 2013 Oct 31;1(2):57–63. Available from: https://doi.org/10.14791/btrt.2013.1.2.57
30. Jang M, Kim SS, Lee J. Cancer cell metabolism: implications for therapeutic targets. Exp Mol Med. 2013;45(10):e45–e45. Available from: https://doi.org/10.1038/emm.2013.85
31. Li B, Simon MC. Molecular Pathways: Targeting MYC-induced Metabolic Reprogramming and Oncogenic Stress in Cancer. Clin Cancer Res. 2013 Oct 31;19(21):5835–41. Available from: https://doi.org/10.1158/1078-0432.CCR-12-3629
32. Papa S, Choy PM, Bubici C. The ERK and JNK pathways in the regulation of metabolic reprogramming. Oncogene. 2019;38(13):2223–40. Available from: https://doi.org/10.1038/s41388-018-0582-8
33. Bott AJ, Peng IC, Fan Y, Faubert B, Zhao L, Li J, et al. Oncogenic Myc Induces Expression of Glutamine Synthetase through Promoter Demethylation. Cell Metab. 2015 Dec 1;22(6):1068–77. Available from: https://doi.org/10.1016/j.cmet.2015.09.025
34. Ko YH, Domingo-Vidal M, Roche M, Lin Z, Whitaker-Menezes D, Seifert E, et al. TP53-inducible Glycolysis and Apoptosis Regulator (TIGAR) Metabolically Reprograms Carcinoma and Stromal Cells in Breast Cancer. J Biol Chem. 2016 Dec 16;291(51):26291–303. Available from: https://doi.org/10.1074/jbc.M116.740209
35. Glaviano A, Foo ASC, Lam HY, Yap KCH, Jacot W, Jones RH, et al. PI3K/AKT/mTOR signaling transduction pathway and targeted therapies in cancer. Mol Cancer. 2023;22(1):138. Available from: https://doi.org/10.1186/s12943-023-01827-6
36. Wang H, Guo M, Wei H, Chen Y. Targeting p53 pathways: mechanisms, structures, and advances in therapy. Signal Transduct Target Ther. 2023;8(1):92. Available from: https://doi.org/10.1038/s41392-023-01347-1

37. Li C, Zhang G, Zhao L, Ma Z, Chen H. Metabolic reprogramming in cancer cells: glycolysis, glutaminolysis, and Bcl-2 proteins as novel therapeutic targets for cancer. World J Surg Oncol. 2016;14(1):15. Available from: https://doi.org/10.1186/s12957-016-0769-9
38. Tan Y, Li J, Zhao G, Huang KC, Cardenas H, Wang Y, et al. Metabolic reprogramming from glycolysis to fatty acid uptake and beta-oxidation in platinum-resistant cancer cells. Nat Commun. 2022;13(1):4554. Available from: https://doi.org/10.1038/s41467-022-32101-w
39. Desbats MA, Giacomini I, Prayer-Galetti T, Montopoli M. Metabolic Plasticity in Chemotherapy Resistance. Front Oncol. 2020;10. Available from: https://doi.org/10.3389/fonc.2020.00281
40. Burgess DJ. Choose your carbon source. Nat Rev Cancer. 2011;11(2):81. Available from: https://doi.org/10.1038/nrc3009
41. Pavlova NN, Zhu J, Thompson CB. The hallmarks of cancer metabolism: Still emerging. Cell Metab. 2022;34(3):355–77. Available from: https://doi.org/10.1016/j.cmet.2022.01.007
42. Fadaka A, Ajiboye B, Ojo O, Adewale O, Olayide I, Emuowhochere R. Biology of glucose metabolization in cancer cells. J Oncol Sci. 2017;3(2):45–51. Available from: https://doi.org/10.1016/j.jons.2017.06.002
43. Yoshida GJ. Metabolic reprogramming: the emerging concept and associated therapeutic strategies. J Exp Clin Cancer Res. 2015;34(1):111. Available from: https://doi.org/10.1186/s13046-015-0221-y
44. Li X, Yang Y, Zhang B, Lin X, Fu X, An Y, et al. Lactate metabolism in human health and disease. Signal Transduct Target Ther. 2022;7(1):305. Available from: https://doi.org/10.1038/s41392-022-01151-3
45. Otto AM. Warburg effect(s)—a biographical sketch of Otto Warburg and his impacts on tumor metabolism. Cancer Metab. 2016;4(1):5. Available from: https://doi.org/10.1186/s40170-016-0145-9
46. Liberti M V, Locasale JW. The Warburg Effect: How Does it Benefit Cancer Cells? Trends Biochem Sci. 2016 Mar 1;41(3):211–8. Available from: https://doi.org/10.1016/j.tibs.2015.12.001
47. Xie J, Wu H, Dai C, Pan Q, Ding Z, Hu D, et al. Beyond Warburg effect – dual metabolic nature of cancer cells. Sci Rep. 2014;4(1):4927. Available from: https://doi.org/10.1038/srep04927
48. Leone RD, Powell JD. Metabolism of immune cells in cancer. Nat Rev Cancer. 2020;20(9):516–31. Available from: https://doi.org/10.1038/s41568-020-0273-y
49. Gao M, Huang J, Jiang X, Yuan Y, Pang H, Luo S, et al. Regulation of aerobic glycolysis to decelerate tumor proliferation by small molecule inhibitors targeting glucose transporters. Protein Cell. 2020;11(6):446–51. Available from: https://doi.org/10.1007/s13238-020-00725-7
50. Feng J, Li J, Wu L, Yu Q, Ji J, Wu J, et al. Emerging roles and the regulation of aerobic glycolysis in hepatocellular carcinoma. J Exp Clin Cancer Res. 2020;39(1):126. Available from: https://doi.org/10.1186/s13046-020-01629-4
51. Vasan K, Werner M, Chandel NS. Mitochondrial Metabolism as a Target for Cancer Therapy. Cell Metab. 2020 Sep 1;32(3):341–52. Available from: https://doi.org/10.1016/j.cmet.2020.06.019

52. Chen X, Qian Y, Wu S. The Warburg effect: Evolving interpretations of an established concept. Free Radic Biol Med. 2015;79:253–63. Available from: https://doi.org/0.1016/j.freeradbiomed.2014.08.027
53. Marini C, Bianchi G, Buschiazzo A, Ravera S, Martella R, Bottoni G, et al. Divergent targets of glycolysis and oxidative phosphorylation result in additive effects of metformin and starvation in colon and breast cancer. Sci Rep. 2016;6(1):19569. Available from: https://doi.org/10.1038/srep19569
54. Miki K, Yagi M, Yoshimoto K, Kang D, Uchiumi T. Mitochondrial dysfunction and impaired growth of glioblastoma cell lines caused by antimicrobial agents inducing ferroptosis under glucose starvation. Oncogenesis. 2022;11(1):59. Available from: https://doi.org/10.1038/s41389-022-00437-z
55. Mathews EH, Visagie MH, Meyer AA, Joubert AM, Mathews GE. In vitro quantification: Long-term effect of glucose deprivation on various cancer cell lines. Nutrition. 2020;74:110748. Available from: https://doi.org/10.1016/j.nut.2020.110748.
56. Raut GK, Chakrabarti M, Pamarthy D, Bhadra MP. Glucose starvation-induced oxidative stress causes mitochondrial dysfunction and apoptosis via Prohibitin 1 upregulation in human breast cancer cells. Free Radic Biol Med. 2019;145:428–41. Available from: https://doi.org/10.1016/j.freeradbiomed.2019.09.020
57. Reda A, Refaat A, Abd-Rabou AA, Mahmoud AM, Adel M, Sabet S, et al. Role of mitochondria in rescuing glycolytically inhibited subpopulation of triple negative but not hormone-responsive breast cancer cells. Sci Rep. 2019;9(1):13748. Available from: https://doi.org/10.1038/s41598-019-50141-z
58. Lehuédé C, Dupuy F, Rabinovitch R, Jones R, Siegel M. Metabolic plasticity as a determinant of tumor growth and metastasis. Cancer Res. 2016 Sep 15;76(18):5201-8. Available from: https://doi.org/10.1158/0008-5472.CAN-16-0266
59. Lunetti P, Giacoma M, Vergara D, Deomenico S, Maffia M, Zara V, et al. Metabolic reprogramming in breast cancer results in distinct mitochondrial bioenergetics between luminal and basal subtypes. FEBS J. 2019 Feb;286(4):688-709. Available from: https://doi.org/10.1111/febs.14756
60. Sun S, Sun Y, Rong X, Bai L. High glucose promotes breast cancer proliferation and metastasis by impairing angiotensinogen expression. Biosci Rep. 2019 Jun 14;39(6):BSR20190436. Available from: https://doi.org/10.1042/BSR20190436
61. Marambio P, Toro B, Sanhueza C, Troncoso R, Parra V, Verdejo H, et al. Glucose deprivation causes oxidative stress and stimulates aggresome formation and autophagy in cultured cardiac myocytes. Biochim Biophys Acta. 2010;1802(6):509–18. Available from: https://doi.org/10.1016/j.bbadis.2010.02.002.
62. Ren Y, Shen HM. Critical role of AMPK in redox regulation under glucose starvation. Redox Biol. 2019;25:101154. Available from: https://doi.org/10.1016/j.redox.2019.101154
63. Li R, Kato H, Taguchi Y, Umeda M. Intracellular glucose starvation affects gingival homeostasis and autophagy. Sci Rep. 2022;12(1):1230. Available from: https://doi.org/10.1038/s41598-022-05398-2

64. Jin J, Byun JK, Choi YK, Park KG. Targeting glutamine metabolism as a therapeutic strategy for cancer. Exp Mol Med. 2023;55(4):706–15. Available from: https://doi.org/10.1038/s12276-023-00971-9
65. Elgendy M, Cirò M, Hosseini A, Weiszmann J, Mazzarella L, Ferrari E, et al. Combination of Hypoglycemia and Metformin Impairs Tumor Metabolic Plasticity and Growth by Modulating the PP2A-GSK3β-MCL-1 Axis. Cancer Cell. 2019;35(5):798-815.e5. Available from: https://doi.org/10.1016/j.ccell.2019.03.007
66. Palorini R, Simonetto T, Cirulli C, Chiaradonna F. Mitochondrial Complex I Inhibitors and Forced Oxidative Phosphorylation Synergize in Inducing Cancer Cell Death. Cerella C, editor. Int J Cell Biol. 2013;2013:243876. Available from: https://doi.org/10.1155/2013/243876
67. Lin Q, He Y, Wang X, Zhang Y, Hu M, Guo W, et al. Targeting Pyruvate Carboxylase by a Small Molecule Suppresses Breast Cancer Progression. Adv Sci. 2020 May 1;7(9):1903483. Available from: https://doi.org/10.1002/advs.201903483
68. Cappel DA, Deja S, Duarte JAG, Kucejova B, Iñigo M, Fletcher JA, et al. Pyruvate-Carboxylase-Mediated Anaplerosis Promotes Antioxidant Capacity by Sustaining TCA Cycle and Redox Metabolism in Liver. Cell Metab. 2019 Jun 4;29(6):1291-1305.e8. Available from: https://doi.org/10.1016/j.cmet.2019.03.014
69. Wang L, Li J jing, Guo L yu, Li P, Zhao Z, Zhou H, et al. Molecular link between glucose and glutamine consumption in cancer cells mediated by CtBP and SIRT4. Oncogenesis. 2018;7(3):26. Available from: https://doi.org/10.1038/s41389-018-0036-8
70. Yang L, Venneti S, Nagrath D. Glutaminolysis: A Hallmark of Cancer Metabolism. Annu Rev Biomed Eng. 2017 Jun 20;19(1):163–94. Available from: https://doi.org/10.1146/annurev-bioeng-071516-044546
71. Yoo HC, Yu YC, Sung Y, Han JM. Glutamine reliance in cell metabolism. Exp Mol Med. 2020;52(9):1496–516. Available from: https://doi.org/10.1038/s12276-020-00504-8
72. Bernfeld E, Foster DA. Glutamine as an Essential Amino Acid for KRas-Driven Cancer Cells. Trends Endocrinol Metab. 2019 Jun 1;30(6):357–68. Available from: https://doi.org/10.1016/j.tem.2019.03.003
73. He Y, Hakvoort TBM, Köhler SE, Vermeulen JLM, de Waart DR, de Theije C, et al. Glutamine Synthetase in Muscle Is Required for Glutamine Production during Fasting and Extrahepatic Ammonia Detoxification. J Biol Chem. 2010;285(13):9516–24. Available from: https://doi.org/10.1074/jbc.M109.092429
74. Cluntun AA, Lukey MJ, Cerione RA, Locasale JW. Glutamine Metabolism in Cancer: Understanding the Heterogeneity. Trends Cancer. 2017 Mar 1;3(3):169–80. Available from: https://doi.org/10.1016/j.trecan.2017.01.005
75. Yang WH, Qiu Y, Stamatatos O, Janowitz T, Lukey MJ. Enhancing the Efficacy of Glutamine Metabolism Inhibitors in Cancer Therapy. Trends Cancer. 2021 Aug 1;7(8):790–804. Available from: https://doi.org/10.1016/j.trecan.2021.04.003

76. Wise DR, Thompson CB. Glutamine addiction: a new therapeutic target in cancer. Trends Biochem Sci. 2010 Aug 1;35(8):427–33. Available from: https://doi.org/10.1016/j.tibs.2010.05.003
77. Suzuki S, Tanaka T, Poyurovsky M V, Nagano H, Mayama T, Ohkubo S, et al. Phosphate-activated glutaminase (GLS2), a p53-inducible regulator of glutamine metabolism and reactive oxygen species. Proc Natl Acad Sci USA. 2010 Apr 20;107(16):7461–6. Available from: https://doi.org/10.1073/pnas.1002459107
78. Wang R, Cao L, Thorne RF, Zhang XD, Li J, Shao F, et al. LncRNA GIRGL drives CAPRIN1-mediated phase separation to suppress glutaminase-1 translation under glutamine deprivation. Sci Adv. 2023 Aug 20;7(13):eabe5708. Available from: https://doi.org/10.1126/sciadv.abe5708
79. Scopelliti AJ, Font J, Vandenberg RJ, Boudker O, Ryan RM. Structural characterisation reveals insights into substrate recognition by the glutamine transporter ASCT2/SLC1A5. Nat Commun. 2018;9(1):38. Available from: https://doi.org/10.1038/s41467-017-02444-w
80. Franklin CC, Backos DS, Mohar I, White CC, Forman HJ, Kavanagh TJ. Structure, function, and post-translational regulation of the catalytic and modifier subunits of glutamate cysteine ligase. Mol Aspects Med. 2009;30(1):86–98. Available from: https://doi.org/10.1016/j.mam.2008.08.009
81. Kang YP, Mockabee-Macias A, Jiang C, Falzone A, Prieto-Farigua N, Stone E, et al. Non-canonical Glutamate-Cysteine Ligase Activity Protects against Ferroptosis. Cell Metab. 2021 Jan 5;33(1):174-189.e7. Available from: https://doi.org/10.1016/j.cmet.2020.12.007
82. Gwangwa MV, Joubert AM, Visagie MH. Effects of glutamine deprivation on oxidative stress and cell survival in breast cell lines. Biol Res. 2019;52(1):15. Available from: https://doi.org/10.1186/s40659-019-0224-9
83. Lampa M, Arlt H, He T, Ospina B, Reeves J, Zhang B, et al. Glutaminase is essential for the growth of triple-negative breast cancer cells with a deregulated glutamine metabolism pathway and its suppression synergizes with mTOR inhibition. PLoS One. 2017 Sep 26;12(9):e0185092-. Available from: https://doi.org/10.1371/journal.pone.0185092
84. Demas DM, Demo S, Fallah Y, Clarke R, Nephew KP, Althouse S, et al. Glutamine Metabolism Drives Growth in Advanced Hormone Receptor Positive Breast Cancer. Front Oncol. 2019;9. Available from: https://www.frontiersin.org/articles/10.3389/fonc.2019.00686
85. Stine ZE, Schug ZT, Salvino JM, Dang C V. Targeting cancer metabolism in the era of precision oncology. Nat Rev Drug Discov. 2022;21(2):141–62. Available from: https://doi.org/10.1038/s41573-021-00339-6
86. Méndez-Lucas A, Lin W, Driscoll PC, Legrave N, Novellasdemunt L, Xie C, et al. Identifying strategies to target the metabolic flexibility of tumours. Nat Metab. 2020;2(4):335–50. Available from: https://doi.org/10.1038/s42255-020-0195-8

87. Wu Q, Ba-alawi W, Deblois G, Cruickshank J, Duan S, Lima-Fernandes E, et al. GLUT1 inhibition blocks growth of RB1-positive triple negative breast cancer. Nat Commun . 2020 Aug 21;11(1):4205. Available from: https://doi.org/10.1038/s41467-020-18020-8
88. Kraus D, Reckenbeil J, Veit N, Kuerpig S, Meisenheimer M, Beier I, et al. Targeting glucose transport and the NAD pathway in tumor cells with STF-31: a re-evaluation. Cell Oncol (Dordr). 2018 Oct;41(5):485-494. Available from: https://doi.org/10.1007/s13402-018-0385-5
89. Li R, Mei S, Ding Q, Wang Q, Yu L, Zi F. A pan-cancer analysis of the role of hexokinase II (HK2) in human tumors. Sci Rep . 2022 Nov 5;12(1):18807. Available from: https://doi.org/10.1038/s41598-022-23598-8
90. Da Q, Huang L, Huang C, Chen Z, Jiang Z, Huang F, et al. Glycolytic regulatory enzyme PFKFB3 as a prognostic and tumor microenvironment biomarker in human cancers. Aging (Albany NY). 2023 May 30;15(10):4533-4559. Available from: https://doi.org/10.18632/aging.204758
91. Li L, Ai L, Jia L, Zhang L, Lei B, Zhang Q. High score of LDH plus dNLR predicts poor survival in patients with HER2-positive advanced breast cancer treated with trastuzumab emtansine. BMC Cancer. 2022 Jan 3;22(1):29. Available from: https://doi.org/10.1186/s12885-021-09131-6
92. Singh R, Gupta V, Kumar A, Singh K. 2-Deoxy-D-Glucose: A Novel Pharmacological Agent for Killing Hypoxic Tumor Cells, Oxygen Dependence-Lowering in Covid-19, and Other Pharmacological Activities. Adv Pharmacol Pharm Sci. 2023 Mar 2;2023:9993386. Available from: https://doi.org/10.1155/2023/9993386
93. Zheng M, Wu C, Yang K, Yang Y, Liu Y, Gao S, et al. Novel selective hexokinase 2 inhibitor Benitrobenrazide blocks cancer cells growth by targeting glycolysis. Pharmacol Res. 2021 Feb:164:105367. Available from: https://doi.org/10.1016/j.phrs.2020.105367
94. Clem B, Telang S, Clem A, Yalcin A, Meier J, Simmons A, et al. Small-molecule inhibition of 6-phosphofructo-2-kinase activity suppresses glycolytic flux and tumor growth. Mol Cancer Ther. 2008 Jan;7(1):110-20. Available from: https://doi.org/10.1158/1535-7163
95. Kashyap A, Umar S, Dev A, Mathur S, Gogia A, Batra A, et al. Combination of 3PO analog PFK15 and siPFKL efficiently suppresses the migration, colony formation ability, and PFK-1 activity of triple-negative breast cancers by reducing the glycolysis. J Cell Biochem. 2023 Sep;124(9):1259-1272. Available from: https://doi.org/10.1002/jcb.30443
96. Cruz-Lopez K, Catsro-Munoz L, Hernandes D, Carranca A, Merino J. Lactate in the Regulation of Tumor Microenvironment and Therapeutic Approaches. Front Oncol. 2019 Nov 1;9:1143. Available from: https://doi.org/10.3389/fonc.2019.01143
97. Du M, Yu T, Zhan Q, Li H, Zou Y, Geng M, et al. Development of a novel lactate dehydrogenase A inhibitor with potent antitumor activity and immune activation. Cancer Sci. 2022 Sep;113(9):2974-2985. Available from: https://doi.org/10.1111/cas.15468

98. Sonveux P, Copetti T, Saedeleer C, Vegran F, Verrax J, Kenndey K. Targeting the Lactate Transporter MCT1 in Endothelial Cells Inhibits Lactate-Induced HIF-1 Activation and Tumor Angiogenesis. PLoS One. 2012;7(3):e33418. Available from: https://doi.org/10.1371/journal.pone.0033418
99. Halford S, Veal G, Wedge S, Payne G, Bacon C, Sloan P, et al. A Phase I Dose-escalation Study of AZD3965, an Oral Monocarboxylate Transporter 1 Inhibitor, in Patients with Advanced Cancer. Clin Cancer Res. 2023 Apr 14;29(8):1429-1439. Available from: https://doi.org/ 10.1158/1078-0432.CCR-22-2263
100. Babari M, Galobart T, Goni T, Wantuch S, Parkes H, Tandy D, et al. Monocarboxylate transporter 1 blockade with AZD3965 inhibits lipid biosynthesis and increases tumour immune cell infiltration. Br J Cancer. 2020 Mar;122(6):895-903. Available from: https://doi.org/10.1038/s41416-019-0717-x
101. Geldermalsen M, Wang Q, Bailey G, Toole S, Rasko J, Holst J, et al. Targeting the ASCT2 glutamine uptake and metabolism pathway in triple-negative breast cancer. Ann Oncol. 2015;29(9):1878-1886. Available from: https://doi.org/10.1093/annonc/mdv121.04
102. Schulte M, Fu A, Zhao P, Li J, Geng L, Smith S, et al. Pharmacological Blockade of ASCT2-dependent Glutamine Transport Leads To Anti-tumor Efficacy in Preclinical Models. Nat Med. 2018 Feb;24(2):194-202. Available from: https://doi.org/10.1038/nm.4464
103. Li Q, Zhong X, Yao W, Yu J, Wang C, Li Z, et al. Inhibitor of glutamine metabolism V9302 promotes ROS-induced autophagic degradation of B7H3 to enhance antitumor immunity. J Biol Chem. 2022 Apr;298(4):101753. Available from: https://doi.org/10.1016/j.jbc.2022.101753
104. Koppula P, Zhuang L, Gan B. Cystine transporter SLC7A11/xCT in cancer: ferroptosis, nutrient dependency, and cancer therapy. Protein Cell. 2021 Aug;12(8):599-620. Available from: https://doi.org/10.1007/s13238-020-00789-5
105. Nath P, Alarsi L, El-Ansari R, Masisi B, Erkan B, Fakroun A, et al. The amino acid transporter SLC7A11 expression in breast cancer. Cancer Biol Ther. 2024 Dec 31;25(1):2291855. Available from: https://doi.org/10.1080/15384047.2023.2291855
106. Long Y, Xu Z, Yu J, Hu X, Xie Y, Duan X, et al. Targeting xCT with sulfasalazine suppresses triple-negative breast cancer growth via inducing autophagy and coordinating cell cycle and proliferation. Anticancer Drugs. 2024 Oct 1;35(9):830-843. https://doi.org/10.1097/CAD.0000000000001630.
107. Anthony J, Varalakshmi S, Sekar A, Devarajan N, Janakiraman B, Peramaiyan R, et al. Glutaminase - A potential target for cancer treatment. Biomedicine (Taipei). 2024 Jun 1;14(2):29-37. Available from: https://doi.org/10.37796/2211-8039.1445
108. Novotna K, Tenora L, Slusher B, Rais R. Therapeutic resurgence of 6-diazo-5-oxo-l-norleucine (DON) through tissue-targeted prodrugs. Adv Pharmacol. 2024:100:157-180. Available from: https://doi.org/10.1016/bs.apha.2024.04.003. Available from: https://doi.org/

109. Lemberg K, Vornov J, Rais R, Slusher B. We're Not "DON" Yet: Optimal Dosing and Prodrug Delivery of 6-Diazo-5-oxo-L-norleucine. Mol Cancer Ther. 2018 Sep;17(9):1824-1832. Available from: https://doi.org/10.1158/1535-7163.MCT-17-1148

110. Tannir N, Agarwal N, Porta C, Lawrence N, Motzer R, McGrego B, et al. Efficacy and safety of telaglenastat plus cabozantinib vs placebo plus cabozantinib in patients with advanced renal cell carcinoma. JAMA Oncol. 2022 Sep 1;8(10):1411–1418. Available from: https://doi.org/10.1001/jamaoncol.2022.3511

111. Luengo A, Gui DY, Vander Heiden MG. Targeting Metabolism for Cancer Therapy. Cell Chem Biol. 2017 Sep 21;24(9):1161–80. Available from: https://doi.org/10.1016/j.chembiol.2017.08.028

112. Wouters O, McKee, Luyten J. Estimated research and development investment needed to bring a new medicine to market, 2009-2018. JAMA. 2020 Mar 3;323(9):844-853. Available from: https://doi.org/10.1001/jama.2020.1166

113. Lee C, Raffaghello L, Brandhorst S, Safdie FM, Bianchi G, Martin-Montalvo A, et al. Fasting Cycles Retard Growth of Tumors and Sensitize a Range of Cancer Cell Types to Chemotherapy. Sci Transl Med. 2012 Mar 7;4(124):124ra27-124ra27. Available from: https://doi.org/10.1126/scitranslmed.3003293

114. Nencioni A, Caffa I, Cortellino S, Longo VD. Fasting and cancer: molecular mechanisms and clinical application. Nat Rev Cancer. 2018;18(11):707–19. Available from: https://doi.org/10.1038/s41568-018-0061-0

115. Diabetes Mellitus, Fasting Glucose, and Risk of Cause-Specific Death. N Engl J Med. 2011 Mar 3;364(9):829–41. Available from: https://doi.org/10.1056/NEJMoa1008862

116. Cruzat V, Rogero M, Keane J, Curi R, Newsholme P. Glutamine: Metabolism and Immune Function, Supplementation and Clinical Translation. Nutrients. 2018 Oct 23;10(11):1564. Available from: https://doi.org/10.3390/nu10111564

117. Rui L. Energy Metabolism in the Liver. Compr Physiol. 2014 Jan;4(1):177–197. Available from: https://doi.org/10.1002/cphy.c130024

118. Zhang J, Deng Y, Khoo BL. Fasting to enhance Cancer treatment in models: the next steps. J Biomed Sci. 2020;27(1):58. Available from: https://doi.org/10.1186/s12929-020-00651-0

119. Buono R, Longo V. Starvation, Stress Resistance, and Cancer. Trends Endocrinol Metab. 2018 Feb 17;29(4):271–280. Available from: https://doi.org/10.1016/j.tem.2018.01.008

120. de Groot S, Vreeswijk M, Welters M, Gravesteijn G, Boei J, Jochems A, et al. The effects of short term fasting on tolerance to (neo) adjuvant chemotherapy in HER2- negative breast cancer patients: a randomised pilots study. BMC Cancer. 2015 Oct 5:15:652. Available from: https://doi.org/10.1186/s12885-015-1663-5

121. Dorff T, Groshen S, Garcia A, Shah M, Tsoa-Wei D, Pham H, et al. Safety and feasibility of fasting in combination with platinum-based chemotherapy. BMC Cancer. 2016 Jun 10:16:360. Available from: https://doi.org/10.1186/s12885-016-2370-6

122. Attina A, Leggeri C, Paroni R, Pivari F, Cas M, Mingione A, et al. Fasting: How to Guide. Nutrients. 2021 May 7;13(5):1570. Available from: https://doi.org/10.3390/nu13051570

123. Cheng C, Adams GB, Perin L, Wei M, Zhou X, Lam BS, et al. Prolonged Fasting Reduces IGF-1/PKA to Promote Hematopoietic-Stem-Cell-Based Regeneration and Reverse Immunosuppression. Cell Stem Cell. 2014 Jun 5;14(6):810–23. Available from: https://doi.org/10.1016/j.stem.2014.04.014

124. Feng Z, Levine AJ. The regulation of energy metabolism and the IGF-1/mTOR pathways by the p53 protein. Trends Cell Biol. 2010 Jul 1;20(7):427–34. Available from: https://doi.org/10.1016/j.tcb.2010.03.004

125. Weng M lin, Chen W kun, Chen X yuan, Lu H, Sun Z rong, Yu Q, et al. Fasting inhibits aerobic glycolysis and proliferation in colorectal cancer via the Fdft1-mediated AKT/mTOR/HIF1α pathway suppression. Nat Commun. 2020;11(1):1869. Available from: https://doi.org/10.1038/s41467-020-15795-8

126. Zhao R, Zhao X, Wang X, Liu Y, Yang J, Jiang S, et al. Fasting promotes acute hypoxic adaptation by suppressing mTOR-mediated pathways. Cell Death Dis. 2021;12(11):1045. Available from: https://doi.org/10.1038/s41419-021-04351-x

127. Marques-Ramos A, Cervantes R. Expression of mTOR in normal and pathological conditions. Mol Cancer. 2023;22(1):112. Available from: https://doi.org/10.1186/s12943-023-01820-z

128. Zou Z, Tao T, Li H, Zhu X. mTOR signaling pathway and mTOR inhibitors in cancer: progress and challenges. Cell Biosci. 2020;10(1):31. Available from: https://doi.org/10.1186/s13578-020-00396-1

129. Fernandes SA, Demetriades C. The Multifaceted Role of Nutrient Sensing and mTORC1 Signaling in Physiology and Aging. Front Aging. 2021;2. Available from: https://doi.org/10.3389/fragi.2021.707372

130. Simcox J, Lamming DW. The central moTOR of metabolism. Dev Cell. 2022;57(6):691–706. Available from: https://doi.org/10.1016/j.devcel.2022.02.024

131. Dibble CC, Cantley LC. Regulation of mTORC1 by PI3K signaling. Trends Cell Biol. 2015 Sep 1;25(9):545–55. Available from: https://doi.org/10.1016/j.tcb.2015.06.002

132. Zhang S, Lin X, Hou Q, Hu Z, Wang Y, Wang Z. Regulation of mTORC1 by amino acids in mammalian cells: A general picture of recent advances. Anim Nutr. 2021;7(4):1009–23. Available from: https://doi.org/10.1016/j.aninu.2021.05.003

133. He Y, Sun MM, Zhang GG, Yang J, Chen KS, Xu WW, et al. Targeting PI3K/Akt signal transduction for cancer therapy. Signal Transduct Target Ther. 2021;6(1):425. Available from: https://doi.org/10.1038/s41392-021-00828-5

134. Gombos A, Metzger-Filho O, Dal Lago L, Awada-Hussein A. Clinical development of insulin-like growth factor receptor—1 (IGF-1R) inhibitors: At the crossroad? Invest New Drugs. 2012;30(6):2433–42. Available from: https://doi.org/10.1007/s10637-012-9811-0

135. Jiang Q, Zhang X, Dai X, Han S, Wu X, Wang L, et al. S6K1-mediated phosphorylation of PDK1 impairs AKT kinase activity and oncogenic functions. Nat Commun. 2022;13(1):1548. Available from: https://doi.org/10.1038/s41467-022-28910-8

136. Gómez-Suárez M, Gutiérrez-Martínez IZ, Hernández-Trejo JA, Hernández-Ruiz M, Suárez-Pérez D, Candelario A, et al. 14-3-3 Proteins regulate Akt Thr308 phosphorylation in intestinal epithelial cells. Cell Death Differ. 2016;23(6):1060–72. Available from: https://doi.org/10.1038/cdd.2015.163

137. Memmott RM, Dennis PA. Akt-dependent and -independent mechanisms of mTOR regulation in cancer. Cell Signal. 2009;21(5):656–64. Available from: https:/doi.org/10.1101/gad.1662308

138. Zhou X, Zhong Y, Molinar-Inglis O, Kunkel MT, Chen M, Sun T, et al. Location-specific inhibition of Akt reveals regulation of mTORC1 activity in the nucleus. Nat Commun. 2020;11(1):6088. Available from: https://doi.org/10.1038/s41467-020-19937-w

139. Steinberg GR, Carling D. AMP-activated protein kinase: the current landscape for drug development. Nat Rev Drug Discov. 2019;18(7):527–51. Available from: https://doi.org/10.1038/s41573-019-0019-2

140. González A, Hall MN, Lin SC, Hardie DG. AMPK and TOR: The Yin and Yang of Cellular Nutrient Sensing and Growth Control. Cell Metab. 2020 Mar 3;31(3):472–92. Available from: https://doi.org/10.1016/j.cmet.2020.01.015

141. Ling NXY, Kaczmarek A, Hoque A, Davie E, Ngoei KRW, Morrison KR, et al. mTORC1 directly inhibits AMPK to promote cell proliferation under nutrient stress. Nat Metab. 2020;2(1):41–9. Available from: https://doi.org/10.1038/s42255-019-0157-1

142. Liu X, Chhipa RR, Pooya S, Wortman M, Yachyshin S, Chow LML, et al. Discrete mechanisms of mTOR and cell cycle regulation by AMPK agonists independent of AMPK. Proceedings of the National Academy of Sciences. 2014 Jan 28;111(4):E435–44. Available from: https://doi.org/10.1073/pnas.1311121111

143. Lin SC, Hardie DG. AMPK: Sensing Glucose as well as Cellular Energy Status. Cell Metab. 2018;27(2):299–313. Available from: https://doi.org/10.1016/j.cmet.2017.10.009

144. Wang W, Yang X, López de Silanes I, Carling D, Gorospe M. Increased AMP:ATP Ratio and AMP-activated Protein Kinase Activity during Cellular Senescence Linked to Reduced HuR Function. J Biol Chem. 2003;278(29):27016–23. Available from: https://doi.org/10.1074/jbc.M300318200.

145. Garcia D, Shaw RJ. AMPK: Mechanisms of Cellular Energy Sensing and Restoration of Metabolic Balance. Mol Cell. 2017;66(6):789–800. Available from: https://doi.org/10.1016/j.molcel.2017.05.032

146. Hawley SA, Ross FA, Gowans GJ, Tibarewal P, Leslie NR, Hardie DG. Phosphorylation by Akt within the ST loop of AMPK-α1 down-regulates its activation in tumour cells. Biochemical Journal. 2014 Mar 28;459(2):275–87. Available from: https://doi.org/10.1042/BJ20131344

147. Jeon SM. Regulation and function of AMPK in physiology and diseases. Exp Mol Med. 2016;48(7):e245–e245. Available from: https://doi.org/10.1038/emm.2016.81

148. Willows R, Sanders MJ, Xiao B, Patel BR, Martin SR, Read J, et al. Phosphorylation of AMPK by upstream kinases is required for activity in mammalian cells. Biochem J. 2017 Aug 22;474(17):3059–73. Available from: https://doi.org/10.1042/BCJ20170458

149. Bujak AL, Crane JD, Lally JS, Ford RJ, Kang SJ, Rebalka IA, et al. AMPK Activation of Muscle Autophagy Prevents Fasting-Induced Hypoglycemia and Myopathy during Aging. Cell Metab. 2015 Jun 2;21(6):883–90. Available from: https://doi.org/10.1016/j.cmet.2015.05.016

150. Bianchi G, Martella R, Ravera S, Marini C, Capitanio S, Orengo A, et al. Fasting induces anti-Warburg effect that increases respiration but reduces ATP-synthesis to promote apoptosis in colon cancer models. Oncotarget . 2015 May 20;6(14):11806-19. Available from: https://doi.org/10.18632/oncotarget.3688

151. Leprivier G, Rotblat B. How does mTOR sense glucose starvation? AMPK is the usual suspect. Cell Death Discov. 2020;6(1):27. Available from: https://doi.org/10.1038/s41420-020-0260-9

152. Inoki K, Zhu T, Guan KL. TSC2 Mediates Cellular Energy Response to Control Cell Growth and Survival. Cell. 2003;115(5):577–90. Available from: https://doi.org/10.1016/s0092-8674(03)00929-2

153. Clohessy JG, Reschke M, Pandolfi PP. Found in translation of mTOR signaling. Cell Res. 2012;22(9):1315–8. Available from: https://doi.org/10.1038/cr.2012.85

154. Kim J, Kundu M, Viollet B, Guan KL. AMPK and mTOR regulate autophagy through direct phosphorylation of Ulk1. Nat Cell Biol. 2011;13(2):132–41. Available from: https://doi.org/10.1038/ncb2152

155. Mizushima N, Komatsu M. Autophagy: Renovation of Cells and Tissues. Cell. 2011 Nov 11;147(4):728–41. Available from: https://doi.org/10.1016/j.cell.2011.10.026

156. Yim W, Mizushima N. Lysosome biology in autophagy. Cell Discov. 2020;6(1):6. Available from: https://doi.org/10.1038/s41421-020-0141-7

157. Feng Y, He D, Yao Z, Klionsky DJ. The machinery of macroautophagy. Cell Res. 2014;24(1):24–41. Available from: https://doi.org/10.1038/cr.2013.168

158. Lim SM, Mohamad Hanif EA, Chin SF. Is targeting autophagy mechanism in cancer a good approach? The possible double-edge sword effect. Cell Biosci. 2021;11(1):56. Available from: https://doi.org/10.1186/s13578-021-00570-z

159. Liu Y, Levine B. Autosis and autophagic cell death: the dark side of autophagy. Cell Death Differ. 2015;22(3):367–76. Available from: https://doi.org/10.1038/cdd.2014.143

160. Kravchuk V, Petrova O, Kampjut D, Wojciechowska-Bason A, Breese Z, Sazanov L. A universal coupling mechanism of respiratory complex I. Nature. 2022;609(7928):808–14. Available from: https://doi.org/10.1038/s41586-022-05199-7

161. Saura P, Kaila VRI. Energetics and Dynamics of Proton-Coupled Electron Transfer in the NADH/FMN Site of Respiratory Complex I. J Am Chem Soc. 2019 Apr 10;141(14):5710–9. Available from: https://doi.org/10.1021/jacs.8b11059

162. Birsoy K, Possemato R, Lorbeer FK, Bayraktar EC, Thiru P, Yucel B, et al. Metabolic determinants of cancer cell sensitivity to glucose limitation and biguanides. Nature. 2014;508(7494):108–12. Available from: https://doi.org/10.1038/nature13110

163. Masoud R, Castellanos G, Lac S, Garcia S, Garcia J, Dou S, et al. Targeting Mitochondrial Complex I Overcomes Chemoresistance in High OXPHOS Pancreatic Cancer. Cell Rep Med. 2020 Nov 17;1(8):100143. Available from: https://doi.org/10.1016/j.xcrm.2020.100143

164. Zhou Y, Zou J, Xu J, Zhou Y, Cen X, Zhao Y. Recent advances of mitochondrial complex I inhibitors for cancer therapy: Current status and future perspectives. Eur J Med Chem . 2023 May 5:251:115219. Available from: https://doi.org/10.1016/j.ejmech.2023.115219

165. Assi A, Posty A, Lamarche F, Chebel A, Guitton J, Rousselle C, et al. A novel inhibitor of the mitochondrial respiratory complex I with uncoupling properties exerts potent antitumor activity. Cell Death Dis . 2024 May 2;15(5):311. Available from: https://doi.org/10.1038/s41419-024-06668-9.

166. Martin M, Belaid A, Bost S, Kahi M, Peraldi P, Rouleau M, et al. Targeting cancer and immune cell metabolism with the complex I inhibitors metformin and IACS-010759. Mol Oncol . 2024 Jul;18(7):1719-1738. Available from: https://doi.org/10.1002/1878-0261.13583.

167. Yap T, Daver N, Mahendra M, Zhang J, Matsuoka C, Bernstam F, et al. Complex I inhibitor of oxidative phosphorylation in advanced solid tumors and acute myeloid leukemia: phase I trials. Nat Med. 2023 Jan;29(1):115-126. Available from: https://doi.org/10.1038/s41591-022-02103-8

168. Yap T, Ahnert J, Paul S, Fu S, Janku F, Karp D, et al. Phase I trial of IACS-010759 (IACS), a potent, selective inhibitor of complex I of the mitochondrial electron transport chain, in patients (pts) with advanced solid tumors. 2019;37: 3014-3014. Available from: https://doi.org/10.1200/JCO.2019.37.15_suppl.3014

169. Rha S, Beom S, Shin Y, Yim D, Moon Y, Kim T, et al. Phase I study of IM156, a novel potent biguanide oxidative phosphorylation (OXPHOS) inhibitor, in patients with advanced solid tumors. 2020;38:3590-3590. Available from: https://doi.org/10.1200/JCO.2020.38.15_suppl.3590

170. Rha S, Beom S, Moon Y, Kim T, Shin Y, Yim D, et al. First-in-human study of IM156, a novel potent biguanide oxidative phosphorylation (OXPHOS) inhibitor, in patients with advanced solid tumors. Invest New Drugs . 2022 Oct;40(5):1001-1010. Available from: https://doi.org/10.1007/s10637-022-01277-9.

171. Baccelli I, Gareau Y, Lehnertz B, Gingras S, Spinella J, Corneau S, et al. Mubritinib Targets the Electron Transport Chain Complex I and Reveals the Landscape of OXPHOS Dependency in Acute Myeloid Leukemia. Cancer Cell. 2019 Jul 8;36(1):84-99.e8. Available from: https://doi.org/10.1016/j.ccell.2019.06.003

172. Kwong S, Brubacher J. Phenformin and lactic acidosis: a case report and review. J Emerg Med. 1998 Nov-Dec;16(6):881-6. Available from: https://doi.org/10.1016/s0736-4679(98)00103-6

173. Yu O, Suissa S. Metformin and Cancer: Solutions to a Real-World Evidence Failure. Diabetes Care. 2023 May 1;46(5):904-912. Available from: https://doi.org/10.2337/dci22-0047

174. Lord S, Harri A. Is it still worth pursuing the repurposing of metformin as a cancer therapeutic? Br J Cancer. 2023 Apr;128(6):958-966. Available from: https://doi.org/10.1038/s41416-023-02204-2

175. Goodwin P, Chen B, Gelmon K, Whelan T, Ennis M, Lemieux J, et al. Effect of Metformin Versus Placebo on New Primary Cancers in Canadian Cancer Trials Group MA.32: A Secondary Analysis of a Phase III Randomized Double-Blind Trial in Early Breast Cancer. J Clin Oncol. 2023 Dec 10;41(35):5356-5362. Available from: https://doi.org/10.1200/JCO.23.00296

176. Benej M, Hong X, Vibhute S, Scott S, Wu J, Graves E, et al. Abstract 2927: Papaverine and its novel derivatives radiosensitize solid tumors by inhibiting mitochondrial metabolism. Cancer Res. 2019 July 1;79:2927. Available from: https://doi.org/10.1158/1538-7445.AM2019-2927

177. Gomes DA, Joubert AM, Visagie MH. The Biological Relevance of Papaverine in Cancer Cells. Cells. 2022 Oct 26;11(21):3385. Available from: https://doi.org/10.3390/cells11213385

178. Benej M, Hong X, Vibhute S, Scott S, Wu J, Graves E, et al. Papaverine and its derivatives radiosensitize solid tumors by inhibiting mitochondrial metabolism. Proc Natl Acad Sci USA. 2018 Oct 16;115(42):10756-10761. Available from: https://doi.org/10.1073/pnas.1808945115

179. Xia Y, Sun M, Huang H, Jin WL. Drug repurposing for cancer therapy. Signal Transduct Target Ther . 2024 Apr 19;9(1):92. Available from: https://doi.org/10.1038/s41392-024-01808-1

180. Pushpakom S, Iorio F, Eyers P, Escott J, Hopper S, Wells A, et al. Drug repurposing: progress, challenges and recommendations. Nat Rev Drug Discov. 2019 Jan;18(1):41-58. Available from: https://doi.org/10.1038/nrd.2018.168

181. Ferretti AC, Hidalgo F, Tonucci FM, Almada E, Pariani A, Larocca MC, et al. Metformin and glucose starvation decrease the migratory ability of hepatocellular carcinoma cells: targeting AMPK activation to control migration. Sci Rep. 2019;9(1):2815. Available from: https://doi.org/10.1038/s41598-019-39556-w

182. Alhourani AH, Tidwell TR, Bokil AA, Røsland G V, Tronstad KJ, Søreide K, et al. Metformin treatment response is dependent on glucose growth conditions and metabolic phenotype in colorectal cancer cells. Sci Rep. 2021;11(1):10487. Available from: https://doi.org/10.1038/s41598-021-89861-6

183. Goodwin P, Chen B, Gelmon K, Whelan T, Ennis M, Lemieux, et al. Effect of Metformin vs Placebo on Invasive Disease–Free Survival in Patients With Breast Cancer. JAMA. 2022 May 24;327(20):1963-1973. Available from: https://doi.org/10.1001/jama.2022.6147

184. Anemoulis M, Vlastos A, Kachtsidis V, Karras S. Intermittent Fasting in Breast Cancer: A Systematic Review and Critical Update of Available Studies. Nutrients. 2023 Jan 19;15(3):532. Available from: https://doi.org/10.3390/nu15030532

185. Coyle C, Cafferty FH, Vale C, Langley RE. Metformin as an adjuvant treatment for cancer: a systematic review and meta-analysis. Ann Oncol. 2016 Dec 1;27(12):2184–95. Available from: https://doi.org/10.1093/annonc/mdw410

186. Vial G, Detaille D, Guigas B. Role of Mitochondria in the Mechanism(s) of Action of Metformin. Front Endocrinol. 2019;10. Available from: https://doi.org/10.3389/fendo.2019.00294.

187. Triggle CR, Mohammed I, Bshesh K, Marei I, Ye K, Ding H, et al. Metformin: Is it a drug for all reasons and diseases? Metabolism. 2022;133:155223. Available from: https://doi.org/10.1016/j.metabol.2022.155223

188. Wen J, Yi Z, Chen Y, Huang J, Mao X, Zhang L, et al. Efficacy of metformin therapy in patients with cancer: a meta-analysis of 22 randomised controlled trials. BMC Med. 2022;20(1):402. Available from: https://doi.org/10.1186/s12916-022-02599-4

189. Lord SR, Harris AL. Is it still worth pursuing the repurposing of metformin as a cancer therapeutic? Br J Cancer. 2023;128(6):958–66. Available from: https://doi.org/10.1038/s41416-023-02204-2

190. Cai H, Everett RS, Thakker DR. Efficacious dose of metformin for breast cancer therapy is determined by cation transporter expression in tumours. Br J Pharmacol. 2019 Aug 1;176(15):2724–35. Available from: https://doi.org/10.1111/bph.14694

191. Lee YY, Park JS, Leem YH, Park JE, Kim DY, Choi YH, et al. The phosphodiesterase 10 inhibitor papaverine exerts anti-inflammatory and neuroprotective effects via the PKA signaling pathway in neuroinflammation and Parkinson's disease mouse models. J Neuroinflammation. 2019;16(1):246. Available from: https://doi.org/10.1186/s12974-019-1649-3

192. Marciano R, Prasad M, Ievy T, Tzadok S, Leprivier G, Elkabets M, et al. High-Throughput Screening Identified Compounds Sensitizing Tumor Cells to Glucose Starvation in Culture and VEGF Inhibitors In Vivo. Cancers (Basel). 2019 Jan 30;11(2):156. Available from: https://doi.org/10.3390/cancers11020156

193. Subik K, Lee JF, Baxter L, Strzepek T, Costello D, Crowley P, et al. The Expression Patterns of ER, PR, HER2, CK5/6, EGFR, Ki-67 and AR by Immunohistochemical Analysis in Breast Cancer Cell Lines. Breast Cancer (Auckl). 2010 Jan 1;4:117822341000400000. Available from: https://doi.org/10.1177/117822341000400004

194. Holliday DL, Speirs V. Choosing the right cell line for breast cancer research. Breast Cancer Res. 2011;13(4):215. Available from: https://doi.org/10.1186/bcr2889

195. Tsai P, Lee MM, Jadhav U, Naqvi I, Madha S, Adler A, et al. Adaptation of pancreatic cancer cells to nutrient deprivation is reversible and requires glutamine synthetase stabilization by mTORC1. Proc Natl Acad Sci USA. 2021;118(10):e2003014118. Available from: https://doi.org/10.1073/pnas.2003014118

196. Gomes DA, Joubert AM, Visagie MH. In Vitro Effects of Papaverine on Cell Proliferation, Reactive Oxygen Species, and Cell Cycle Progression in Cancer Cells. Molecules. 2021 Oct 22;26(21):6388. Available from: https://doi.org/10.3390/molecules26216388

197. Śliwka L, Wiktorska K, Suchocki P, Milczarek M, Mielczarek S, Lubelska K, et al. The Comparison of MTT and CVS Assays for the Assessment of Anticancer Agent Interactions. PLoS One. 2016 May 19;11(5):e0155772. Available from: https://doi.org/10.1371/journal.pone.0155772

198. Visagie MH, Joubert AM. The in vitro effects of 2-methoxyestradiol-bis-sulphamate on cell numbers, membrane integrity and cell morphology, and the possible induction of apoptosis and autophagy in a non-tumorigenic breast epithelial cell line. Cell Mol Biol Lett. 2010;15(4):564–81. Available from: https://doi.org/10.2478/s11658-010-0030-4

199. Visagie MH, Joubert AM. In vitro effects of 2-methoxyestradiol-bis-sulphamate on reactive oxygen species and possible apoptosis induction in a breast adenocarcinoma cell line. Cancer Cell Int. 2011;11(1):43. Available from: https://doi.org/10.1186/1475-2867-11-43

200. Plesca D, Mazumder S, Almansa A. DNA Damage Response and Apoptosis. Methods Enzymol. 2008;446:107–122. Available from: https://doi.org/10.1016/S0076-6879(08)01606-6

201. Chen J, Rogers SC, Kavdia M. Analysis of Kinetics of Dihydroethidium Fluorescence with Superoxide Using Xanthine Oxidase and Hypoxanthine Assay. Ann Biomed Eng. 2013;41(2):327–37. Available from: https://doi.org/10.1007/s10439-012-0653-x

202. Visagie MH, van den Bout I, Joubert AM. A bis-sulphamoylated estradiol derivative induces ROS-dependent cell cycle abnormalities and subsequent apoptosis. PLoS One. 2017 Apr 14;12(4):e0176006-. Available from: https://doi.org/10.1371/journal.pone.0176006

203. Visagie MH, Jaiswal SR, Joubert AM. In vitro assessment of a computer-designed potential anticancer agent in cervical cancer cells. Biol Res. 2016;49(1):43. Available from: https://doi.org/10.1186/s40659-016-0104-5

204. Kalyanaraman B, Darley-Usmar V, Davies KJA, Dennery PA, Forman HJ, Grisham MB, et al. Measuring reactive oxygen and nitrogen species with fluorescent probes: challenges and limitations. Free Radic Biol Med. 2012;52(1):1–6. Available from: https://doi.org/10.1016/j.freeradbiomed.2011.09.030

205. Kim H, Xue X. Detection of Total Reactive Oxygen Species in Adherent Cells by 2',7'-Dichlorodihydrofluorescein Diacetate Staining. JoVE. 2020;(160):e60682. Available from: https://doi.org/10.3791/60682

206. Visagie M, Theron A, Mqoco T, Vieira W, Prudent R, Martinez A, et al. Sulphamoylated 2-Methoxyestradiol Analogues Induce Apoptosis in Adenocarcinoma Cell Lines. PLoS One. 2013 Sep 5;8(9):e71935. Available from: https://doi.org/10.1371/journal.pone.0071935

207. Bakavayex S, Chetrit N, Zvagelsky T, Mansour R, Vyazmensky M, Barak Z, et al. Cu/Zn-superoxide dismutase and wild-type like fALS SOD1 mutants produce cytotoxic quantities of H2O2 via cysteine-dependent redox short-circuit. Sci Rep. 2019 Jul 25;9(1):10826. Available from: https://doi.org/10.1038/s41598-019-47326-x

208. Lebelo M, Joubert AM, Visagie MH. Dysregulation of Catalase by a Sulphamoylated Estradiol Analogue Culminates in Antimitotic Activity and Cell Death Induction in Breast Cancer Cell Lines. Molecules. 2021 Jan 25;26(3):622. Available from: https://doi.org/10.3390/molecules26030622

209. Sivandzade F, Bhalerao A, Cucullo L. Analysis of the Mitochondrial Membrane Potential Using the Cationic JC-1 Dye as a Sensitive Fluorescent Probe. Bio Protoc. 2019 Jan 5;9(1):e3128. Available from: https://doi.org/10.21769/BioProtoc.3128

210. Hua H, Kong Q, Zhang H, Wang J, Luo T, Jiang Y. Targeting mTOR for cancer therapy. J Hematol Oncol. 2019;12(1):71. Available from: https://doi.org/10.1186/s13045-019-0754-1

211. Liu Y, Azizian N, Sullivan D, Li Y. mTOR inhibition attenuates chemosensitivity through the induction of chemotherapy resistant persisters. Nat Commun. 2022 Nov 17;13(1):7047. Available from: https://doi.org/10.1038/s41467-022-34890-6

212. Aslanturk OS. In Vitro Cytotoxicity and Cell Viability Assays: Principles, Advantages, and Disadvantages. 2017 Dec 20. Available from: https://doi.org/10.5772/intechopen.71923

213. Clifton KK, Ma CX, Fontana L, Peterson LL. Intermittent fasting in the prevention and treatment of cancer. CA Cancer J Clin. 2021 Nov 1;71(6):527–46. Available from: https://doi.org/10.3322/caac.21694

214. Caino MC, Chae Y, Vaira V, Ferrero S, Nosotti M, Martin N, et al. stress regulates cytoskeletal dynamics and metastasis of cancer cells. J Clin Invest. 2013 Jun 10;123(7):2907–2920. Available from: https://doi.org/10.1172/JCI67841

215. Babes R, Tofolean I, Sandu R, Baran O, Cosoreanu V. Simple discrimination of sub-cycling cells by propidium iodide flow cytometric assay in Jurkat cell samples with extensive DNA fragmentation. Cell Cycle. 2018;17(6):766-779. Available from: https://doi.org/10.1080/15384101.2018.1426415

216. Zorov D, Juhaszova M, Sollot SJ. Mitochondrial ROS and ROS-Induced ROS Release. Physiol Rev. 2014 Jul;94(3):909–950. Available from: https://doi.org/10.1152/physrev.00026.2013

217. Robb E, Hall AR, Primer T, Eaton S, Szibor M, Viscomi C, et al. Control of mitochondrial superoxide production by reverse electron transport at complex I. J Biol Chem. 2018 Jun 22;293(25):9869-9879. Available from: https://doi.org/10.1074/jbc.RA118.003647

218. Millare B, O'Rourke B, Trayanova N. Hydrogen peroxide diffusion and scavenging shapes mitochondrial network instability and failure by sensitizing ROS-induced ROS release. Sci Rep. 2020 Sep 25;10(1):15758. Available from: https://doi.org/10.1038/s41598-020-71308-z

219. Hewitt OH, Degnan SM. Antioxidant enzymes that target hydrogen peroxide are conserved across the animal kingdom, from sponges to mammals. Sci Rep. 2023;13(1):2510. Available from: https://doi.org/10.1038/s41598-023-29304-6

220. Wang Y, Branicky R, Noë A, Hekimi S. Superoxide dismutases: Dual roles in controlling ROS damage and regulating ROS signaling. J Cell Biol. 2018 Jun 4;217(6):1915-1928. Available from: https://doi.org/10.1083/jcb.201708007

221. Elafantova K, Lakatos B, Kubickova J, Sulova Z, Breier A. Detection of the Mitochondrial Membrane Potential by the Cationic Dye JC-1 in L1210 Cells with Massive Overexpression of the Plasma Membrane ABCB1 Drug Transporter. Int J Mol Sci. 2018 Jul 7;19(7):1985. Available from: https://doi.org/10.3390/ijms19071985

222. Saxton R, Sabatini D. mTOR Signaling in Growth, Metabolism, and Disease. Cell. 2017 Mar 9;168(6):960–976. Available from: https://doi.org/10.1016/j.cell.2017.02.004

223. Min W, Qin L, Zhang H, Giraldes FL, Jiang N, Kim Y, et al. mTORC1 Signaling in Brain Endothelial Progenitors Contributes to CCM Pathogenesis. Circ Res. 2024 Aug 2;135(4):e94-e113. Available from: https://doi.org/10.1161/CIRCRESAHA.123.324015

224. Li Y, Zhang Q, Yang J, He W, Jiang Y, Chen Y, et al. Metformin combined with glucose starvation synergistically suppress triple-negative breast cancer by enhanced unfolded protein response. Biochem Biophys Res Commun. 2023;675:146–54. Available from: https:/doi.org/10.1016/j.bbrc.2023.07.029.

225. Prasad A, Roy AC, Priya K, Meena R, Ghosh I. Effect of differential deprivation of nutrients on cellular proliferation, oxidative stress, mitochondrial function, and cell migration in MDA-MB-231, HepG2, and HeLa cells. 3 Biotech. 2023;13(10):339. Available from: https://doi.org/10.1007/s13205-023-03759-w

226. Layton ME, Kern J, Hartingh TJ, Shiper W, Raheem I, Kandebo M, et al. Discovery of MK-8189, a Highly Potent and Selective PDE10A Inhibitor for the Treatment of Schizophrenia. J Med Chem. 2023 Jan 26;66(2):1157-117. Available from: https:/doi.org/10.1021/acs.jmedchem.2c01521

227. Delhaye S, Bardoni B. Role of phosphodiesterases in the pathophysiology of neurodevelopmental disorders. Mol Psychiatry . 2021 Sep;26(9):4570-4582. Available from: https:/doi.org/10.1038/s41380-020-00997-9

228. Xiong W, Qin M, Zhong H. PKA regulation of neuronal function requires the dissociation of catalytic subunits from regulatory subunits. Elife. 2024 Nov 7:13:RP93766. Available from: https:/doi.org/10.7554/eLife.93766

229. Das R, Esposito V, Abu-Abed M, Anand G, Taylor S, Melacini G. AMP activation of PKA defines an ancient signaling mechanism. Proc Natl Acad Sci USA. 2007 Jan 2;104(1):93-8. Available from: https:/doi.org/10.1073/pnas.0609033103

230. Walker-Gray R, Stengel F, Gold MG. Mechanisms for restraining cAMP-dependent protein kinase revealed by subunit quantitation and cross-linking approaches. Proc Natl Acad Sci USA. 2017 Sep 26;114(39):10414-10419. Available from: https:/doi.org/10.1073/pnas.1701782114

231. Lefkimmiatis K, Zaccolo M. cAMP signaling in subcellular compartments. Pharmacol Ther. 2014 Apr 1;143(3):295–304. Available from: https:/doi.org/10.1016/j.pharmthera.2014.03.008

232. Newell-Litwa KA, Horwitz AR. Cell Migration: PKA and RhoA Set the Pace. Current Biology. 2011 Aug 9;21(15):R596–8. Available from: https://doi.org/10.1016/j.cub.2011.06.032

233. Gomes DA, Joubert AM, Visagie MH. In Vitro Effects of Papaverine on Cell Migration and Vascular Endothelial Growth Factor in Cancer Cell Lines. Int J Mol Sci. 2022 Apr 22;23(9):4654. Available from: https://doi.org/10.3390/ijms23094654

234. Recourvreux M, Commisso C. Macropinocytosis: A Metabolic Adaptation to Nutrient Stress in Cancer. Front Endocrinol (Lausanne). 2017 Sep 29:8:261. Available from: https://doi.org/10.3389/fendo.2017.00261

235. Florey O, Overholtzer M. Macropinocytosis and autophagy crosstalk in nutrient scavenging. Philos Trans R Soc Lond B Biol Sci. 2018 Dec 17;374(1765):20180154. Available from: https://doi.org/10.1098/rstb.2018.0154

236. Jayashankar V, Edinger A. Macropinocytosis confers resistance to therapies targeting cancer anabolism. Nat Commun . 2020 Feb 28;11(1):1121. Available from: https://doi.org/10.1038/s41467-020-14928-3

237. Guo J, Yang WT, Mai F, Liang FY, Luo J, Zhou M, et al. Unravelling oncosis: morphological and molecular insights into a unique cell death pathway. Front Immunol. 2024 Aug 29:15:1450998. Available from: https://doi.org/10.3389/fimmu.2024.1450998

238. Fang C, Li W, Yin R, Zhu D, Liu X, Wang Q, et al. Potent antitumor activity of a glutamyltransferase-derived peptide via an activation of oncosis pathway. Sci Rep. 2021 Aug 13;11:16507. Available from: https://doi.org/10.1038/s41598-021-93055-5

239. Nunez R, Martinez SM, Novoa J, Hernandez F. Apoptotic volume decrease as a geometric determinant for cell dismantling into apoptotic bodies. Cell Death Differ. 2010 Nov;17(11):1665-7. Available from: https://doi.org/10.1038/cdd.2010.96

240. Palorini R, Votta G, Pirola Y, De Vitto H, De Palmer S, Airoldi C, et al. Protein Kinase A Activation Promotes Cancer Cell Resistance to Glucose Starvation and Anoikis. PLoS Genet. 2016 Mar 15;12(3):e1005931. Available from: https://doi.org/10.1371/journal.pgen.1005931

241. Harada H, Becknell B, Wilm M, Huang L, Talor S, Scott D, et al. Phosphorylation and inactivation of BAD by mitochondria-anchored protein kinase A. Mol Cell. 1999 Apr;3(4):413-22. Available from: https://doi.org/10.1016/s1097-2765(00)80469-4

242. Kussmaul L, Hirst J. The mechanism of superoxide production by NADH:ubiquinone oxidoreductase (complex I) from bovine heart mitochondria. Proc Natl Acad Sci USA. 2006 May 16;103(20):7607–12. Available from: https://doi.org/10.1073/pnas.0510977103

243. Wang S, Long H, Hou L, Feng B, Ma Z, Wu Y, et al. The mitophagy pathway and its implications in human diseases. Signal Transduct Target Ther. 2023 Aug 16;8(1):304. Available from: https://doi.org/10.1038/s41392-023-01503-7

244. Herzig S, Shaw RJ. AMPK: guardian of metabolism and mitochondrial homeostasis. Nat Rev Mol Cell Biol. 2018;19(2):121–35. Available from: https://doi.org/10.1038/nrm.2017.95

245. Poole L,, Bock-Hughes A, Beradi D, Macleod KF. ULK1 promotes mitophagy via phosphorylation and stabilization of BNIP3. Sci Rep. 2021 Oct 15;11(1):20526. Available from: https://doi.org/10.1038/s41598-021-00170-4

246. Shi RY, Zhu S, Li V, Gibson S,Xu X, Kong J. BNIP3 Interacting with LC3 Triggers Excessive Mitophagy in Delayed Neuronal Death in Stroke. CNS Neurosci Ther. 2014 Dec;20(12):1045-55 Available from: https://doi.org/10.1111/cns.12325.

247. Byun JK, Park M, Lee S, Yun JW, Lee J, Kim JS, et al. Inhibition of Glutamine Utilization Synergizes with Immune Checkpoint Inhibitor to Promote Antitumor Immunity. Mol Cell. 2020 Nov 19;80(4):592-606.e8. Available from: https://doi.org/10.1016/j.molcel.2020.10.015

248. Basit F, van Oppen LM, Schockel L, Bossenbroek HM , Emst-de Vries S, Hermeling J, et al. Mitochondrial complex I inhibition triggers a mitophagy-dependent ROS increase leading to necroptosis and ferroptosis in melanoma cells. Cell Death Dis. 2017 Mar 30;8(3):e2716. Available from: https://doi.org/10.1038/cddis.2017.133

249. Park WH. Effects of antioxidants and MAPK inhibitors on cell death and reactive oxygen species levels in H2O2-treated human pulmonary fibroblasts. Oncol Lett. 2013 May;5(5):1633-1638. Available from: https://doi.org/10.3892/ol.2013.1216

250. Bhat A, Tan V, Heng B, Chow S, Basappa S, Essa MM, Cidambaram SB, et al. Papaverine, a Phosphodiesterase 10A Inhibitor, Ameliorates Quinolinic Acid-Induced Synaptotoxicity in Human Cortical Neurons. Neurotox Res. 2021 Aug;39(4):1238-1250. Available from: https://doi.org/10.1007/s12640-021-00368-4

251. Wang Y, An H, Liu T, Qin C, Sesaki H, Guo S, et al. Metformin Improves Mitochondrial Respiratory Activity through Activation of AMPK. Cell Rep. 2019 Nov 5;29(6):1511–1523.e5. Available from: https://doi.org/10.1016/j.celrep.2019.09.070

252. Hoffman NJ, Parker BL, Chaudhuri R, Wellman KH, Kleinhert M, Humphrey SJ, et al. Global Phosphoproteomic Analysis of Human Skeletal Muscle Reveals a Network of Exercise-Regulated Kinases and AMPK Substrate. Cell Metab. 2015 Nov 3;22(5):922-35. Available from: https://doi.org/10.1016/j.cmet.2015.09.001

253. Monterisi S, Lobo MJ, Livie C, Castle JC, Weinberger M, Baillie H, et al. PDE2A2 regulates mitochondria morphology and apoptotic cell death via local modulation of cAMP/PKA signalling. Elife. 2017 May 2:6:e21374. Available from: https://doi.org/10.7554/eLife.21374

254. Sprengler K, Zibrova D, Woods A, Langerndorf CG, Scott JW, Carling D, et al. Protein kinase A negatively regulates VEGF-induced AMPK activation by phosphorylating CaMKK2 at serine 495. Biochem J . 2020 Sep 18;477(17):3453-3469. Available from: https://doi.org/10.1042/BCJ20200555

255. Jewell JL, Fu V, Hong AW, Yu F, Meng D, Melick CH, et al. GPCR signaling inhibits mTORC1 via PKA phosphorylation of Raptor. Elife. 2019 May 21:8:e43038. Available from: https://doi.org/10.7554/eLife.43038